Studies on the physical stability of a C-terminally amidated variant of GLP-1

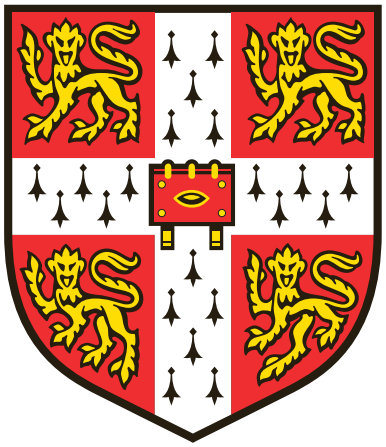

Eva Brichtová
Girton College
Department of Chemistry
University of Cambridge

This dissertation is submitted for the degree of
Master of Philosophy
August 2019

Declaration

This dissertation is the result of my own work and includes nothing which is the outcome of work done in collaboration except where specifically indicated in the text. It does not exceed the 15 000 word limit, as imposed by the Physics and Chemistry Degree Committee.

Eva Brichtová
August 2019

Summary

The phenomenon of peptide and protein aggregation is of great biochemical importance. Not only is it a key feature of numerous neurodegenerative diseases such as Alzheimer's, Parkinson's or Huntington's disease, but it also plays a significant role in the manufacturing and processing of therapeutic peptides. In the process of producing pharmaceutical peptides, molecules are exposed to a wide variety of conditions, some of which enhance aggregation, such as high peptide concentrations. In addition, the long-term physical stability of therapeutic peptides is essential for storage and use of these drugs, and also influences their half-lives *in vivo*. Therefore, aggregation of peptide-based therapeutics remains a great challenge for the pharmaceutical industry.

Aggregation is typically defined as a process involving the non-covalent association of polypeptide chains, however, in some cases aggregates can also be linked covalently. The process of aggregation proceeds via a multi-step mechanism: First, the monomeric peptide self-associates to oligomeric structures, and these can form nucleating species which then further elongate to form amyloid fibrils. When a peptide aggregates, it leads not only to the loss of its biological activity but it can also give rise to other critical problems, e.g. toxicity and immunogenicity, associated with the formation of intermediate oligomeric species.

This work is focused on the C-terminal amidated analogue of the commonly used peptide therapeutic, glucagon-like peptide 1 (GLP-1). This peptide is responsible for many regulatory mechanisms affecting the level of glucose in the bloodstream. Unfortunately, it was shown that GLP-1 has a great propensity to aggregate over a wide pH range that inhibits its function. The studies presented here establish that C-terminal amidation of this peptide hormone significantly slows its fibril formation at neutral and basic pH. It was found that during the significantly prolonged lag times, small stable soluble peptide oligomers start to form. These oligomers, which were characterised using a number of different biophysical techniques, may be off-pathway species of amyloid fibril formation or products of partial peptide degradation. The aggregation kinetics were shown to differ below and above pH 8. However, it was demonstrated that oligomers formed during the process have similar structural characteristics. While amyloid fibrils have a characteristic cross β-sheet structure, the structure of small oligomers formed mainly during the lag and elongation and growth phases is highly disordered. Surprisingly, these small oligomers show a great stability. The exact role of these small, soluble disordered aggregates in fibrillation processes requires further investigation.

These results contribute to the understanding of a complex pathway of aggregation and misfolding processes by providing size and structural characterization of oligomeric species formed during the lag, elongation and growth phases.

Acknowledgement

First and foremost, I would like to thank Prof. Sophie Jackson for her guidance and support during this project and for providing me with the opportunity to perform research in her group.

I would also like to thank all my colleagues from the Jackson group and Lab 290 for creating a friendly work atmosphere. Special thanks go to Frederik Becher and Carolina Orozco for their valuable advice and help.

Finally, I am very grateful to my family for their support throughout my studies, and to my boyfriend Adam Přáda for his not only personal but also academic encouragement.

Abbreviations

a. u.	arbitrary units
A_{280}	absorbance at the wavelength of 280 nm
Aβ	amyloid-β peptide
ACN	acetonitrile
ANS	8-anilinonaphtalene-1-sulfonic acid
APR	aggregation prone region
CD	circular dichroism (spectroscopy)
ddH_2O	distilled deionized water
GLP-1	Glucagon-like peptide 1
GLP-1-Am	Glucagon-like peptide 1 amide
MES	2-(*N*-morpholino)ethanesulfonic acid
MW	molecular weight
MWCO	molecular weight cut-off
NMR	nuclear magnetic resonance
PES	polyethersulfone
pI	isoelectric point
PVDF	polyvinylidene fluoride
rpm	revolutions per minute
SDS	sodium dodecyl sulfate
SDS-PAGE	SDS polyacrylamide gel electrophoresis
SEC	size-exclusion chromatography
SEM	scanning electron microscopy
ThT	thioflavin T
Tris	tris(hydroxymethyl)aminomethane
UV	ultraviolet
UV-Vis	ultraviolet-visible (spectroscopy)

Contents

List of Figures

Chapter 1
Introduction

Aggregation is one of the most common forms of peptide and protein degradation. Extensive research has been undertaken on peptide and protein aggregation associated with numerous neurodegenerative diseases including Alzheimer's, Parkinson's and Huntington's disease.[1–5] Another field where the stability and aggregation of peptides and proteins plays a key role is in the manufacturing and processing of therapeutic peptide drugs. During drug processing, peptides are exposed to a wide range of conditions that can enhance their propensity to aggregate. This includes high peptide concentrations, extreme pH values, high temperatures etc. Moreover, the long-term stability of peptides is essential for drug storage (shelf life) and it can also influence the drug's half-life *in vivo*.[6]

The term aggregation refers to many different processes during which peptide or protein monomers self-assemble into larger species. These processes can be either reversible or irreversible. Having complex structural landscapes, peptides and proteins may transform into a wide range of species, such as various insoluble aggregates, amyloid fibrils or small soluble oligomers.[7,8] The nature of the aggregates formed can differ greatly and depends critically on many different factors. Aggregates can be amorphous or highly structured, and may consist of different numbers of monomer units, starting with dimers all the way to amyloid fibrils that consist of many hundreds, if not thousands, of monomer units.

In this Thesis, the aggregation properties of a polypeptide hormone glucagon-like peptide 1 (GLP-1) and its C-terminal amidated analogue (GLP-1-Am) were investigated. This peptide hormone is involved in many regulatory mechanisms affecting the blood glucose level in humans. It is able to reduce hyperglycemia in type 2 diabetic patients and therefore it is used for type 2 diabetes mellitus treatment.[9–11] Unfortunately, GLP-1 aggregates into amyloid fibrils over a wide range of pH.[12] However, C-terminal amidation of GLP-1 was recently shown to significantly slow down the fibrillation at neutral and basic pH.[13] There are already a number of C-terminally modified GLP-1 analogues on the market. For example, the C-terminus has been used as a linkage site in commercially available GLP-1 active analogues that are fused with an antibody fragment (dulaglutide — Trulicity™).[14] The main focus of this Thesis is an investigation of the aggregation behaviour of GLP-1-Am at neutral (Chapter 3) and basic (Chapter 4) pH values.

1.1 Therapeutic peptides

Peptide therapeutics history goes back to the 1920s, when insulin therapy was developed. Since then, peptide-based drugs have played an important role in medicinal practice. Many peptides in the human body serve as hormones having a signalling role in physiological functions. Some of the peptide drugs are used in replacement therapies, where a shortage of a naturally secreted hormone is compensated for.[10] At the beginning of the peptide therapeutics era, peptide drugs were isolated from natural sources, e.g. insulin or the adrenocorticotropic hormone. Nowadays, peptide drugs are either produced using recombinant DNA technology or by solid-phase peptide synthesis.[9] Over seven thousand naturally occurring peptides have already been characterized, many of which play an essential role in human physiology. More than 80 approved peptide drugs are currently on the market and hundreds of others are currently in the process of development and in clinical trials or preclinical phases.[11] Peptide drug development focuses mainly on metabolic and cardiovascular diseases, and oncology. Currently, the majority of peptide therapeutics are given in the form of injections, however, alternative administration routes are under extensive development, for instance, a transbuccal delivery system that uses insulin-passivated gold glyconanoparticles[15] or oral delivery where peptides are directly expressed in the gastrointestinal tract by engineered bacterial strains.[16]

Since 2005, the market of injectable GLP-1 agonists as a treatment for type 2 diabetes mellitus has continuously grown. Nowadays, GLP-1 agonists belong among the peptide drugs with the greatest financial turnover. In 2017, 47 peptide drugs that target the GLP-1 receptor entered clinical testing, five of which have already been approved.[10]

1.1.1 Peptide therapeutics: stability

The peptide therapeutics industry faces many challenges due to limitations in peptide drug stability. Among these, poor chemical and physical stability, and short plasma half-life are generally the most problematic. Short plasma half-lives are usually due to the natural presence of various peptidases that regulate hormone levels in the plasma to maintain homeostasis. These regulatory mechanisms are often inconvenient for the use of therapeutic peptide drugs.

In terms of chemical and physical stability, the aggregation of peptides is one of the most common problems. Peptide aggregates can be both non-covalent assemblies or covalently linked peptide chains depending on the chemical and physical stability of the specific peptide. When a peptide drug aggregates, it leads to a loss of its biological activity and other critical

problems, e.g. potential toxicity and immunogenicity of aggregated species. The mechanism(s) of peptide aggregation are described in more detail in Section 1.2.4.

Peptide therapeutics are also prone to chemical degradation. There are many types of chemical degradation, such as isomerisation, deamidation[17], racemisation, β-elimination, oxidation,[18,19] hydrolysis, formation or breakage of disulphide bonds, succinimidation[20] or the Maillard reaction. These processes often change not only the chemical properties but also the physical properties of the peptide (e.g. hydrophobicity, net charge, secondary and/or tertiary structure) and therefore can significantly alter the peptide's behaviour including an enhancement of its aggregation propensity.

To overcome the obstacles associated with the intrinsic instability of peptide drugs, various synthetic strategies have been developed. These include direct modification of the peptide backbone, incorporation of non-natural amino acids, amino-acid side chain modification or conjugation to different moieties (e.g. lipidation, glycosylation or antibody fragment conjunction[21]) that improve solubility, administration or stability of the peptide. For instance, a peptide can be protected against enzymatic cleavage by the inclusion of lactam bridges, by cyclisation, or by stapling of the peptide sequence.[22,23] Examples of peptide modifications used to improve stability and half-lives include peptide acylation, amidation or lipidation (e.g. liraglutide — a lipidated form of GLP-1,[24] and insulin detemir — a lipidated form of insulin[25]).

For some peptides, it has been shown that such modifications often suppress fibrillation but increase the rate of oligomer formation.[6,26] Lipidated analogues of GLP-1 were shown to form oligomers of various sizes depending on the pH. [26,27] Similar effects have been observed after phosphorylation, citrullination or nitration of the Aβ peptide, where fibrillation processes were suppressed, but the formation of oligomers increased.[4,28–31] For α-synuclein, whose aggregation is associated with Parkinson's disease, the same trends were observed as well.[32,33]

1.1.2 Factors affecting the stability of peptide therapeutics

The effect of peptide sequence

The propensity towards chemical or physical degradation is to a large extent determined by the amino-acid sequence of the peptide or protein. Some amino-acid residues are more prone to chemical degradation such as oxidation (Met, Trp, Tyr, His, Phe), hydrolysis (Trp, Asp), deamidation (Gln, Asn) or disulphide bridge formation (Cys).[6] The propensity to self-assemble is, in part, also governed by the overall intrinsic properties of the amino-acid residues. This has been subject of extensive studies, and a range of software packages for the prediction of the

aggregation-prone regions (APR) in peptides and proteins have been developed (Section 1.3.3).[34–39]

The effect of pH and net charge

The pH and therefore the net charge of the peptide determine the electrostatic interactions between the peptide monomers, which can influence their self-assembly. A higher net charge is generally associated with slower aggregation since a greater electrostatic repulsion needs to be overcome for oligomers and larger aggregates to form. Usually, peptides and proteins show the greatest propensity to aggregate around their pI where their solubility is the lowest.[40–42] However, there are exceptions to this rule, e.g. GLP-1 and its amidated analogue show the slowest aggregation (i.e. the lowest fibrillation rate) around their pI values.[13] Some other peptides and proteins that can form amyloid fibrils still aggregate at their pI, but instead of highly regular fibrillary structures they form monodisperse and quasi-amorphous aggregates.[43]

The effect of buffers and ionic strength

Even though the main use of buffers is to modulate the pH, some buffers have a direct effect on the stability of peptides and proteins. The increase in stability in one buffer relative to a different one is usually explained by direct binding of the buffer molecules to the peptide or protein.[44] It was reported that the phosphate buffer can increase the stability of the native state of some proteins, thereby reducing aggregation propensity.[45,46] Several times, stabilisation has been observed with nitrogen-based buffers. For example, increased stability of antibodies has been reported in MES and histidine buffers.[47,48] Similarly, histidine was shown to stabilise interferon-tau[49] and recombinant human erythropoietin.[50] In the case of interferon-tau, Tris buffer was also found to be an effective stabilising agent.[49] In addition, citrate buffer has been shown to result in an increase in stability of antitrypsin[51] and of human interleukin-1 receptor antagonist.[52]

Various studies have shown that the ionic strength of the buffer can affect both the kinetics of aggregation and the structure of the resulting aggregates.[53–56] For example, hen egg white lysozyme was reported to form rigid fibrils at low salt concentrations, but oligomers and curvi-linear fibrils at higher salt concentrations. At pH 2 and 52 °C, a kinetic phase diagram was constructed for the fibril-to-oligomer transition as a function of protein concentration and ionic strength.[55,56]

The stability of peptides can also be significantly affected by the nature of ions in solution and it usually follows the Hofmeister series. This series, originally proposed in 1888, is a qualitative ordering of ions based on their ability to salt-out proteins from aqueous solutions.[57] Later, it

was discovered that many processes including enzymatic activity and protein folding also follow the same ordering.[54,58] A large effect of ions on the aggregation propensity of numerous peptides and proteins has been shown, e.g., for Aβ,[59] islet amyloid polypeptide[53] and the mouse prion protein.[60]

The effect of temperature and agitation

Temperature and agitation play an important role in the physical stability of numerous peptides and proteins. Raising the temperature induces aggregation in many peptide or protein systems. However, aggregation kinetics often show non-Arrhenius behaviour over the temperature ranges studied.[61] This makes it challenging to extrapolate aggregation kinetic data measured at higher temperatures to lower temperatures.

Various agitation methods are routinely used in peptide and protein aggregation studies.[62] Agitation and the effect of shear forces on peptides and proteins are of practical interest, as many peptide pharmaceuticals, e.g. insulin, are subject to shear during the syringe pump delivery as well as during processing. Shear forces alone are unlikely to cause structural changes (protein denaturation) to a sufficient extent to initiate aggregation, however, they increase interfacial interactions (particularly at liquid/air interface) that can lead to protein interactions and self-assembly.[63] Shear speeds up nucleation rates and protofibril formation but can, to some extent, limit the formation of mature fibrils, probably due to fibril fragmentation as has been shown for Aβ peptide.[64] Nevertheless, in some cases, breakage of fibrils may further speed up the aggregation process since fibril fragments may act as nucleation seeds.[8,65,66]

Different methods of agitation (shaking, stirring etc.) are common sources of inconsistencies in aggregation kinetic data obtained by different research groups and the lack of standardized aggregation protocols limits the comparison of kinetic data.[62]

1.2 Peptide and protein aggregation

In general, the amino-acid sequence of peptides and proteins with biological functions has coevolved with their physiological environments to maintain peptides and protein in their soluble states. However, under certain conditions, it is possible for many peptides and proteins to convert into non-functional and potentially damaging aggregates.[7,67] The aggregation process starts with the formation of small clusters of monomers (oligomers). These clusters are usually rather unstable with only relatively weak inter-molecular interactions. However, these clusters can undergo internal reorganization to form more stable species.[55,68] Sometimes, specific oligomers can act as nucleation species that, once formed, can further rapidly elongate to form

fibrils, which can coalesce to create large insoluble plaques such as those seen in some neurodegenerative diseases.

1.2.1 Amyloid fibril formation

Since amyloid fibrils are associated with a number of pathological conditions, including neurodegenerative diseases such as Alzheimer's and Parkinson's disease, they are perhaps the most studied form of protein aggregates. However, amyloid fibrils are not only a pathological phenomenon; functional amyloid structures exist in microorganisms and animals.[69–72] Also, many denatured proteins, not associated with any disease state, have also been shown to form amyloid fibrils.[73] These fibrils can have an even higher stability than the native state of the protein. This is true especially for shorter peptides that are able to generate highly ordered structures from relatively unfolded monomeric units. Interestingly, it was found that a large number of peptides and proteins with highly variable primary sequences are capable of forming fibrils with similar structural characteristics given the right conditions. The remarkable stability of fibrils can be attributed mainly to the complex arrangement of hydrogen-bonded β-sheets closely interacting with each other.

1.2.2 Fibril morphology and structure

Amyloid fibrils are thread-like structures usually about 7–13 nm in diameter. The length of fibrils varies greatly; usually fibrils are around 100 nm to 1000 nm long. Amyloid fibrils are typically composed of a number (usually 2 to 8) of protofilaments that twist around each other, however, the types of lateral association can significantly differ. Some fibrils are formed by just a single protofilament,[1,74,75] whereas other proteins can form highly associated fibrillar structures (**Figure 1**). The morphological types can also differ depending on the external conditions (pH, ionic strength, etc.).[55]

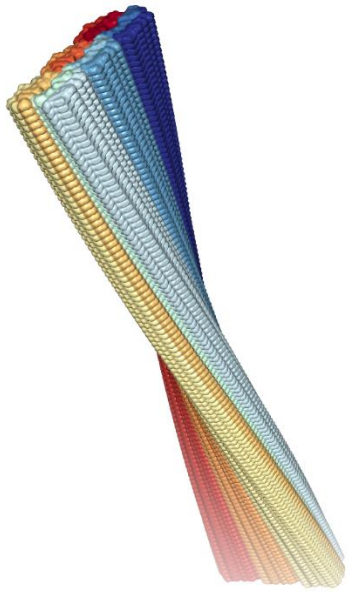

Figure 1: Morphology of an amyloid fibril of transthyretin(105-115) fragment. The fibril structure was obtained from solid-state NMR and cryo-electron microscopy data. The fibril consists of six protofilaments each shown in different colour. PDB ID: 2M5K, (Fitzpatrick 2013)[76]

Mature amyloid-like fibrils have a so-called 'cross β-sheet structure' composed of parallel, in-register β-strands. The peptide/protein backbone runs perpendicular to the fibre axis in each protofilament and forms a β-strand along the fibre. β-strands stack together by hydrogen bonding of their amide N-H and C=O groups forming a β-sheet. In contrast to the non-repetitive β-sheets seen in native proteins, amyloid β-sheets consist of multiple copies of identical polypeptide chains, which leads to symmetrical patterns in their assembly (**Figure 2**). The amide group in the side chains of glutamine and asparagine residues can also form in-register hydrogen bonds between different β-sheet layers, creating hydrogen-bonded ladders. Other side chains, such as tyrosine, serine and threonine, can also contribute to ladder formation. This cross-β structural motif can be detected by 'amyloid specific' fluorescent dyes, such as thioflavin T (ThT), Congo red or their derivatives. Structural models of amyloid fibrils suggest that ThT binds by aligning itself parallel to the long axis of the fibre and it intercalates into the repeating side chain interactions within a β-sheet layer.[8]

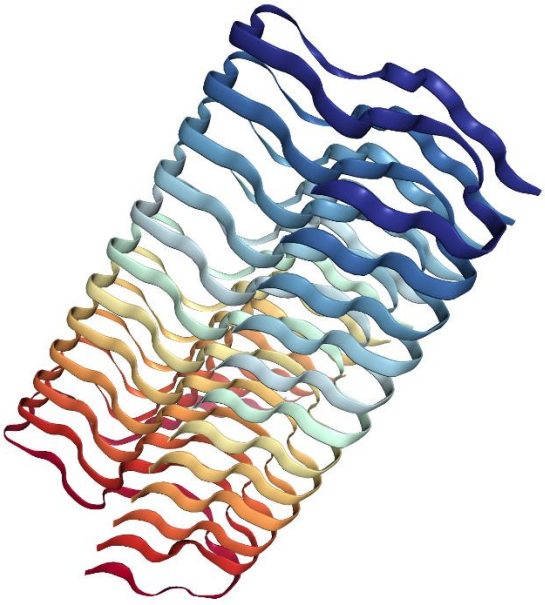

Figure 2: Protofilament of Aβ(1-42) peptide. An atomic model was obtained from solid-state NMR data. Each peptide chain is coloured differently. PDB ID: 2MXU (Xiao 2015)[77]

1.2.3 Intermediate species (oligomers) and their structures

In contrast to fibrils, which generally all have a similar cross-β structural motif, oligomers that are formed during the aggregation process vary widely in their size and structure. These oligomers can also have different roles in the aggregation process. They can be formed as on- or off-pathway intermediates either in the process of fibrillation and/or as a consequence of secondary nucleation on the surface of pre-formed fibrils.[78,79] Stable misfolded oligomers have been found during the aggregation of a variety of proteins,[55,80–82] yet it is not entirely clear whether these stable/metastable oligomers are obligatory or optional precursors of amyloid fibrils, or whether they are an alternative folding product competing with the fibrillation pathway.

Many independent studies have shown that the size of oligomers and the level of exposure of hydrophobic residues within them play an important role in their cytotoxicity.[1,83–85] It was found that toxicity generally decreases with increasing oligomer size and that oligomers with a higher percentage of solvent-exposed hydrophobic residues tend to have higher toxicity. This is mainly because of their interaction with the lipid bilayers of biological membranes.[1,5]

Oligomeric species populated during the aggregation process are often challenging to characterise due to their low abundance and transient nature. Moreover, depending on the experimental conditions, multiple types of oligomeric species are often formed, including possible polymorphisms of oligomers of the same size. In the case of intrinsically disordered

systems, e.g. the Aβ peptide or α-synuclein, oligomers formed early during aggregation have generally a disordered structure and more highly organised oligomers appear in the later stages of the reaction (**Figure 3**). Similarly, early aggregates in the fibrillation of initially globular proteins preserve a more native-like structure of the monomers that later converts to a β-sheet structure.[7,86–90] Early aggregates are typically of low molecular weight and do not bind ThT or Congo red dyes.

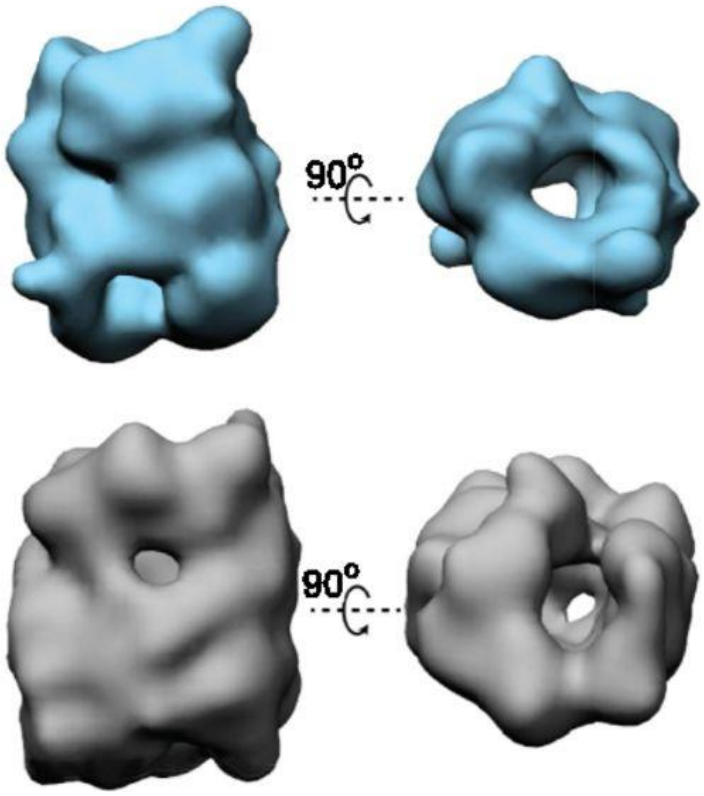

Figure 3: Three-dimensional reconstruction of oligomers isolated during α-synuclein aggregation. Oligomers are approximately 260 kDa and 420 kDa in size corresponding to circa 18-mer and 29-mer, respectively. Adapted from (Chen 2015).[68]

1.2.4 Kinetic models of fibrillation

In 1989, Naiki *et al.*[91] quantified amyloid fibrils *in vitro* by spectrophotometric detection of the fluorescence emission of thioflavin T using the linearity between the concentration of fibrils and the fluorescence emission intensity at 480 nm that ThT displays when bound to the β-sheet-rich structure of fibrils. Since then, ThT assays have been widely used for the investigation of the kinetics of amyloid fibril formation.

The fibrillation process generally proceeds *via* a multi-step mechanism: First, the monomeric peptides self-associate to oligomeric structures, and these further elongate to form amyloid fibrils. A classical fibrillation exhibits sigmoidal kinetics with three distinct phases — a lag phase (during which nucleation takes place), a growth phase (which consists of elongation and

secondary nucleation processes) and a plateau phase (where monomer is completely depleted or equilibrium is reached).[92–95] However, none of these phases can be ascribed to a single type of molecular event or microscopic process (e.g., nucleation, elongation, fragmentation etc.). All of the microscopic processes are present in all phases to some extent, although their prevalence can vary significantly with time. Monomeric species dominate in the lag phase and fibrils in the plateau phase, while during the growth phase their concentrations can be similar.[95] A typical sigmoidal ThT fluorescence aggregation profile assuming a nucleation-polymerization model is depicted in **Figure 4**, which also shows approximate boundaries of the individual phases and illustrates the meaning of the kinetic parameters. The slope of the apparent growth can vary depending on the dominant underlying secondary processes.

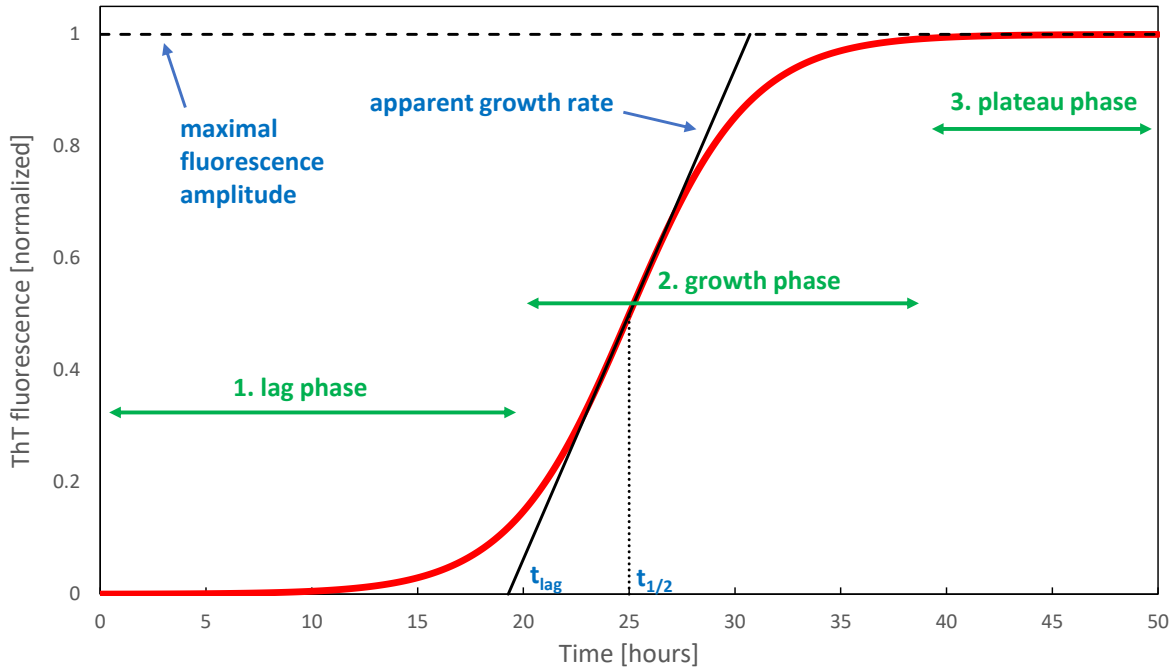

Figure 4: Sigmoidal aggregation kinetics and kinetic parameters.

The ThT aggregation curves can be empirically described by the equation 1.1:

$$Y = Y_0 + \frac{A}{1 + \mathrm{e}^{-k(t - t_{1/2})}} \tag{1.1}$$

,where Y_0 is the initial fluorescence, A is the maximal amplitude in the plateau phase relative to Y_0, $t_{1/2}$ is the half-time, which is defined as the time when ThT fluorescence has reached 50% of its maximal amplitude, k represents the apparent growth rate.[8,12,96] The lag time can be obtained from the kinetic parameters using equation 1.2:

$$t_{\mathrm{lag}} = t_{1/2} - \frac{2}{k} \tag{1.2}$$

Primary nucleation

The process during which new aggregates are formed directly from soluble monomers is known as primary nucleation (**Figure 5**). The rate-limiting step is the formation of a sufficient number of critical nuclei and the reaction is highly dependent on the monomer concentration. Primary nucleation is also usually very slow in the absence of extrinsic factors such as agitation.[97] Primary nucleation is the first process that proceeds at the onset of the lag phase, and it is usually accompanied by the secondary processes as soon as any fibrils are formed.

Secondary processes

The main characteristic of the secondary processes is the formation of new fibrils with the aid of the already existing ones. Therefore, the rate of fibril formation is proportional to the overall mass of fibrils in the sample. This leads to a rapid exponential growth following the lag phase, which is a typical behaviour of these processes. This growth is likely to play a significant role in spreading of amylogenic diseases within an organism.[1] There are several types of secondary processes and their occurrence and ratio depends on the system of interest and the exact conditions. Among the most common secondary processes are surface-catalysed secondary nucleation and fragmentation (**Figure 5**).

In a surface-catalysed secondary nucleation process, the fibrillation is catalysed by the surface of already existing fibrils. Since both monomers and fibrils are needed for this secondary nucleation process, its maximal rate occurs around the half time in the growth phase of the aggregation reaction, where both species are highly populated. New fibrils are formed from monomers and the process generates a positive feedback loop since increasing the number of fibrils also increases the available catalytic surface.[98,99] Moreover, it was reported that other biological surfaces are also able to catalyse the nucleation step in amyloid formation, e.g. cell membranes as in the case of α-synuclein aggregation.[100]

Fragmentation refers to the process in which a growing fibril breaks into smaller fragments, which increases the number of elongation sites, and the fibrillation process is, therefore, faster. This process often depends on external factors, such as sonication or stirring.[97] Fragmentation of fibrils has been observed in actin filaments,[101] and in both yeast and mammalian prions.[92,102]

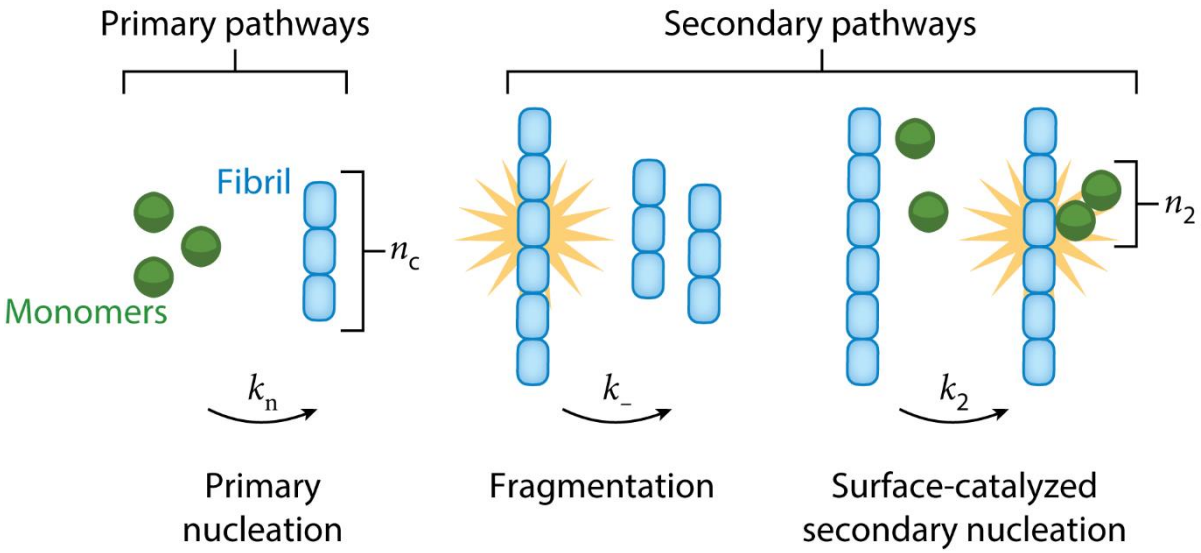

Figure 5: Fibrillation mechanisms — nucleation pathways. Adapted from (Dobson 2019).[2]

Off-pathway aggregation — Non-fibrillar oligomers in peptide and protein aggregation

Non-fibrillar aggregates have often been observed in fibrillation processes, populated both before and during fibril formation. So far, the exact effect of non-fibrillar species on the fibrillation process has not been fully explored. It is generally assumed that their effect on the fibrillation kinetics depends on their role in the mechanism and that non-fibrillar oligomers can be broadly divided into two categories.[67] Oligomers can be either on-pathway, which means that they are capable of directly converting to fibrils, or they can be off-pathway, i.e. incapable of direct conversion to fibrils (**Figure 6**).

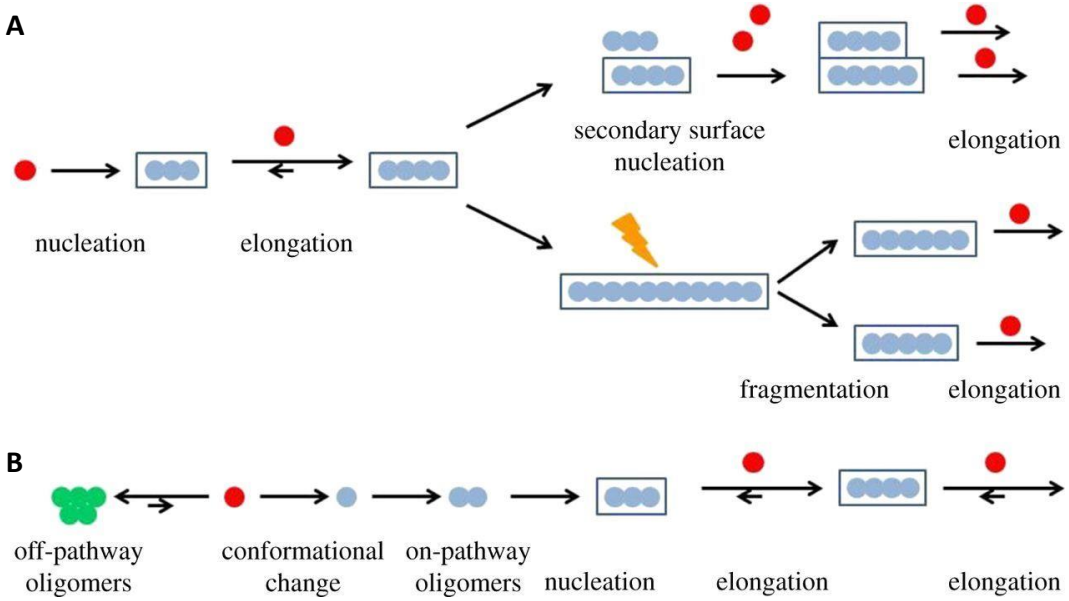

Figure 6: Nucleation-polymerization and off-pathway oligomer mechanism. Comparison of the on-pathway (**A**) and off-pathway (**B**) fibrillation mechanism. Adapted from (Zapadka 2017).[6]

Off-pathway aggregates affect fibrillation through their equilibrium with the monomer. They limit the concentration of the monomer available for fibril formation and as the monomer gets depleted by fibrillation, these aggregates release monomers back into the solution to preserve the equilibrium. This reduction in the available monomer concentration slows down the fibrillation process. For example, the formation of off-pathway oligomers was used to explain the unusual dependence of the aggregation kinetics on the peptide concentration observed for GLP-1[12] and liraglutide,[26] where in both cases the fibrillation process slows down with increasing peptide concentration. For some peptides, formation of off-pathway oligomers and even of off-pathway short curvi-linear fibrils was observed above a certain concentration threshold, called the critical oligomer concentration. It was also shown that these off-pathway species are not precursors of the classical late-stage rigid fibrils.[55]

1.3 Glucagon-like peptide 1 (GLP-1) and its aggregation properties

Nowadays, GLP-1 analogues are commonly used as drugs for type 2 diabetes treatment. However, there are many issues arising due to GLP-1 instability during the manufacturing process as well as *in vivo*. Therefore, pharmaceutical companies are trying to develop effective GLP-1 analogues with improved physical stability and long-acting effects. The main issues regarding GLP-1 stability are its high propensity to aggregate under a wide range of conditions and short plasma life-time due to enzymatic degradation. These issues are among the current challenges of the pharmaceutical industry.[103]

1.3.1 Physiological role of GLP-1

GLP-1 belongs to the incretins family of gastrointestinal peptide hormones.[104] This peptide hormone is responsible for many regulatory mechanisms affecting the glucose level in blood. In healthy patients, GLP-1 is secreted from intestinal endocrine L-cells, where the proglucagon gene is expressed and further processed,[105] and the secretion is stimulated by food ingestion. The full peptide has 37 amino acids, however, it becomes bioactive only after a cleavage of the first six N-terminal residues. The two major bioactive forms circulating in blood are GLP-1(7-37) and GLP-1(6-36)NH_2. The latter, GLP-1(6-36)NH_2, is the prevailing (about 80%) active form of the hormone in blood.[106] Naturally, GLP-1 stimulates meal-induced insulin release from the pancreas and inhibits glucagon release from the liver (**Figure 7**). Moreover, it positively influences all steps in insulin biosynthesis. Overall, GLP-1 is able to reduce

hyperglycemia in type 2 diabetic patients, and therefore GLP-1 analogues are considered to be promising candidates for type 2 diabetes mellitus treatment.

Recent studies have shown a potential use of GLP-1 in obesity treatment due to its ability to reduce appetite. It has been shown that GLP-1 administration inhibits food intake in rodents which suggests that GLP-1 may directly affect the brain. This is supported by the finding that GLP-1 circulating in blood can access GLP-1 receptors in certain brain areas that are involved in the regulation of appetite and in energy homeostasis.[106]

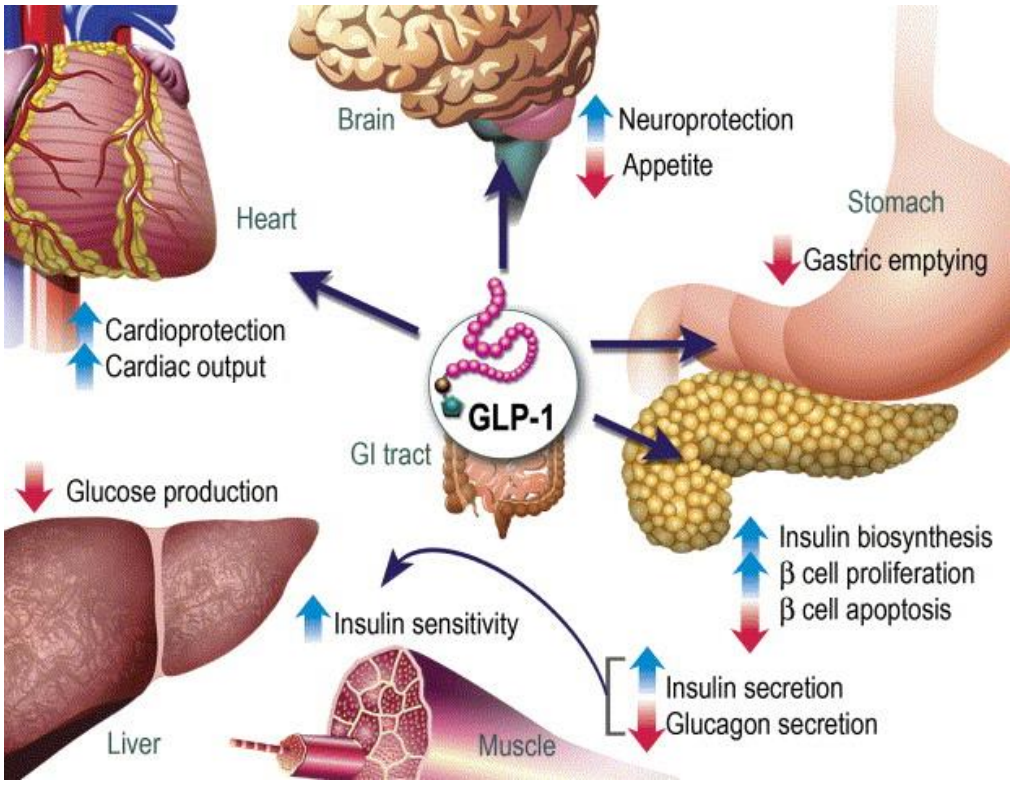

Figure 7: Functions of GLP-1 in humans. Adapted from (Drucker 2006).[106]

1.3.2 Analogues of GLP-1

To overcome the problem of GLP-1 instability, pharmaceutical companies are developing GLP-1 analogues with improved stability but similar therapeutic effects. The most promising strategies include lipidation, e.g.in liraglutide or semaglutide, which are shown in **Figure 8**, or antibody fragment conjugation like in dulaglutide. Many pharmaceutical companies are aiming to develop long-acting GLP-1 analogues with an easy way of administration (**Figure 9**).

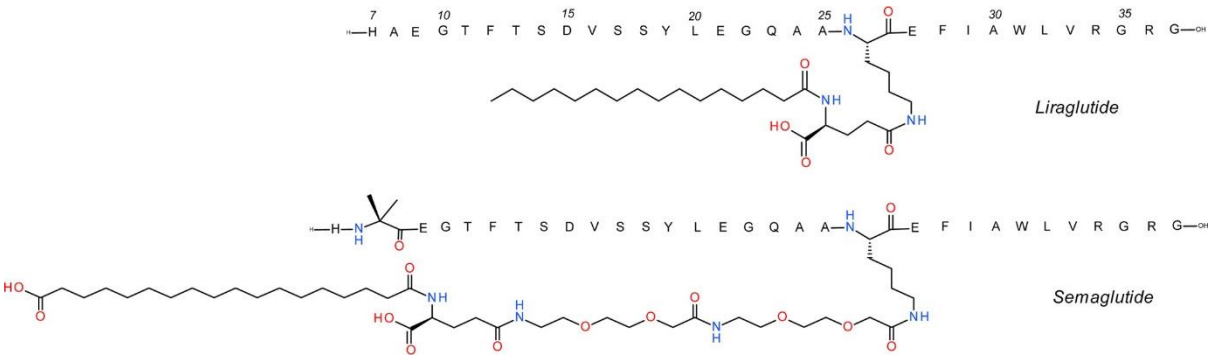

Figure 8: Lipidated GLP-1 analogues. Structure of liraglutide and semaglutide. Adapted from (Lau 2015).[107]

GLP-1 agonists currently in clinical or preclinical testing[a]				
Company	**Peptide name**	**Development stage**	**Target**	**Dosing regimen**
Lilly	Cpd86	Preclinical	GLP-1/GIP	SC, once daily
Zealand Pharma	ZPGG-72	Preclinical	GLP-1/GLP-2	SC, once daily
	ZP3022	Preclinical	GLP-1/CCKB	SC, once daily
Prolor (Opko Biologics)	MOD-6030	Preclinical	GLP-1/GCG	SC, once weekly
Zealand Pharma	ZP2929	Phase I	GLP-1/GCG	SC, once daily
Hamni Pharmaceuticals	HM12525A	Phase I	GLP-1/GCG	SC, once weekly
Diartis Pharmaceuticals	VSR859	Phase I	GLP-1	SC, once monthly
Novo Nordisk	NN9926	Phase I	GLP-1	Oral, long acting
TransTech Parma	TTP273/TTP054	Phase II	GLP-1	Oral
Zydus-Cadila	ZYOG1	Phase I	GLP-1	Oral
Roche	MAR709	Phase II	GLP-1/GIP	SC, once daily
Eli Lilly	TT401	Phase II	GLP-1/GCG	SC, once weekly
Hamni Pharmaceuticals	HM11260C	Phase II	GLP-1	SC, once weekly
PhaseBio Pharmaceuticals	PB1023	Phase II	GLP-1	SC, once weekly
Eli Lilly	Dulaglutide	Phase III	GLP-1	SC, once weekly
Novo Nordisk	Semaglutide	Phase III	GLP-1	SC, once weekly
Intarcia	ITCA	Phase III	GLP-1	SC, once yearly

[a] *Abbreviation*: SC subcutaneous.

Figure 9: GLP-1 analogues in clinical and preclinical testing. Adapted from (Fosgerau 2015).[10]

1.3.3 Aggregation propensity of GLP-1

It has been shown that GLP-1 forms amyloid fibrils under a wide range of conditions.[12,13] Previously, an unusual pH-dependent aggregation behaviour attributed to the formation of off-pathway aggregates was reported by our group.[12] Aggregation has also been observed for liraglutide.[26]

Prediction of the aggregation prone regions of GLP-1

Various algorithms have been developed to theoretically predict aggregation-prone regions (APRs) of peptides and proteins. Some examples of prediction software with a brief description of the methods are given in **Table 1**. Comparison of different APR predictions on GLP-1 peptide is shown in **Figure 10**.

Method	**Description**
TANGO[34]	Sequence-based statistical mechanics algorithm. The algorithm takes into account the hydrophobicity, solvation energies, electrostatic interactions and hydrogen bonding of each residue.
3D Profile Method[39]	Structure-based method. Each six-residue protein segment is mapped onto a set of templates generated from the crystal structure of a small NNQQNY peptide fibril. The energy of each mapping is evaluated using ROSETTADESIGN, and the lowest energy match for a given peptide is taken as the prediction. If the energy of the structure is lower than a threshold value, a prediction for fibrillation is made.
CamSol Intrinsic[38]	Sequence-based method focused on the solubility of peptide regions which correlates with the aggregation propensity. The score is given on the basis on the hydrophobicity, charge, α-helix and β-stand propensity of a residue taking into an account 7 neighbouring residues.

Table 1: Software for the prediction of aggregation prone regions in peptides and proteins.

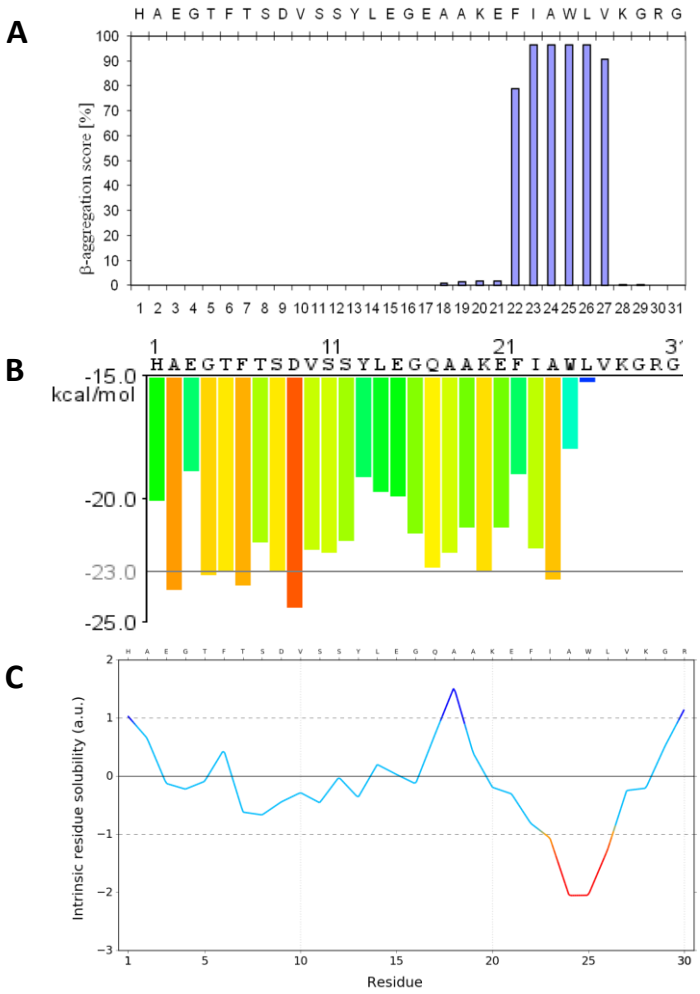

Figure 10: GLP-1 aggregation-prone region predictions. Comparison of TANGO algorithm (**A**) 3D Profile Method (**B**) and CamSol method (**C**). In TANGO algorithm and CamSol method prediction was done using a theoretical pH value of 8. The red colours in B and C indicate the highest propensity for fibrillation and the lowest solubility, respectively.

Predictions by both TANGO and CamSol methods show the GLP-1 fragment between the phenylalanine at position 22 and the valine at position 27 (i.e. the FIAWLV segment) has the highest propensity for fibrillation. However, the 3D Profile Method identified the region containing the aspartic acid (at position 9) and adjacent residues as the one with the highest propensity for aggregation (**Figure 10**).

1.4 Aims of the M.Phil. research

Studies previously conducted by our group have found that GLP-1 has a high propensity for fibrillation under a wide range of conditions.[12] However, under some conditions, the aggregation kinetics do not follow the classical nucleation-polymerization mechanism. Based on experimental kinetic data, a mechanism with a metastable off-pathway intermediate species was proposed for this system.[12]

The main aim of the research presented in this Thesis is to study the aggregation behaviour of a C-terminally amidated analogue of GLP-1, GLP-1-Am, at neutral and basic pH. Previous work conducted in our group showed that the C-terminal amidation of GLP-1 significantly slows the aggregation rate, however, it does not prevent it completely. Moreover, at basic pH values GLP-1-Am showed a large variance in aggregation kinetics.[13] The work presented here sets out to investigate the aggregation kinetics under these conditions and, as far as possible, identify and characterise the intermediate species populated during the aggregation process.

In the following chapters, the kinetics of fibrillation was investigated using thioflavin T binding assays. The formation of small soluble oligomers as well as depletion of the monomeric peptide during the aggregation was monitored by size-exclusion chromatography. Analytical size-exclusion chromatography was also used for size determination, separation and assessment of the stability of the oligomeric species. The stability of the oligomers was also tested using sodium dodecyl sulfate polyacrylamide gel electrophoresis. The structure of oligomers and fibrils formed was investigated using circular dichroism and fluorescence spectroscopies. The presence of fibrils was shown by scanning electron microscopy.

Chapter 2
Materials and methods

Peptide

The 31-residue GLP-1(7-37), HAEGTFTSDVSSYLEGQAAKEFIAWLVKGRG, and its C-terminally amidated version GLP-1-Am(7-37) were purchased from Bachem in the form of an acetate salt with 98.5% and 96.7% purity, respectively, and used without further purification. The molecular weight of both peptides is approximately 3355 Da.

Buffers

All buffers were prepared using the appropriate acids and salts of analytical grade purchased from Sigma-Aldrich or Fisher Chemicals with distilled deionized water (at a resistivity of 18.2 MΩ cm at 25 °C) in volumetric glassware and filtered through 0.22 µm pore size membrane (PES or PVDF membranes, Millex). All buffers were prepared gravimetrically without further pH adjustment. The pH of buffers was checked using a PHM210 pH meter (Radiometer Analytical).

Buffer acid and salt amounts were calculated using the Henderson-Hasselbalch equation and the conservation of molar amount:

$$\mathrm{pH} = \mathrm{p}K_\mathrm{a} + \log\left(\frac{[\mathrm{A}^-]}{[\mathrm{HA}]}\right) \tag{2.1}$$

$$[\mathrm{A}^-] + [\mathrm{HA}] = c_\mathrm{buffer} \tag{2.2}$$

where $[A^-]$ is the concentration of the basic buffer component, [HA] is the concentration of the acidic buffer component (dissociation in solution was neglected) and c_buffer is the total buffer concentration.

The ionic strength (I) of buffers was calculated using:

$$\mathrm{I} = \frac{1}{2}\sum_i c_i z_i^2 \tag{2.3}$$

where c_i is the molar concentration of ion i, z_i is the charge number of the ion i, and the sum is taken over all types of ions in the solution.

Composition of buffers for aggregation assays and biophysical measurement:

Sodium phosphate buffer, 25 mM at pH 8 (ionic strength ≈ 71 mM) was prepared by dissolving 0.638 g of $NaH_2PO_4 \cdot 2\ H_2O$ (MW: 156.01 g mol^{-1}) and 3.259 g of Na_2HPO_4 (MW: 141.96 g mol^{-1}) in distilled deionized water. The pK_a value was 6.95.

This buffer was used for sample incubation during aggregation reactions, analytical size-exclusion chromatography calibration curves and sample analysis on size-exclusion columns.

Tris buffer, 25 mM at pH 8.2 at 37 °C (ionic strength ≈ 7 mM) was prepared by dissolving 1.085 g of Trizma® hydrochloride (MW: 157.6 g mol^{-1}) and 2.194 g of Trizma® base (MW: 121.14 g mol^{-1}) (both SigmaAldrich). The pK_a at this temperature is 7.78 (37 °C). For experiments at 25 °C, where the pK_a is 8.12, buffer calculations were performed analogously (ionic strength of the resulting buffer ≈ 11 mM).

Tris buffer, 25 mM at pH 8.5 at 37 °C (ionic strength ≈ 4 mM) was prepared by dissolving 0.631 g of Trizma® hydrochloride (MW: 157.6 g mol^{-1}) and 2.544 g of Trizma® base (MW: 121.14 g mol^{-1}) (both SigmaAldrich). The pK_a of Tris is 7.78 (37 °C). For experiments at 25 °C, the pK_a of Tris is 8.12 and buffer calculations were performed analogously (ionic strength of the resulting buffer ≈ 7 mM).

Other chemicals

Thioflavin T (ThT) was purchased from Sigma-Aldrich. The dye content in the powder was ≥65%. A stock solution was prepared in distilled deionized water in 5 mM concentration. The ThT stock was filtered through a 0.22 µm filter (PES membrane, Millex) and stored at -20 °C.

8-Anilo-1-naphthalene-sulfonatic acid (ANS) was purchased from Sigma-Aldrich with ≥97% purity. A stock solution was prepared in distilled deionized water in 9.84 mM concentration. ANS stock was filtered through 0.22 µm filter (PES membrane, Millex) and stored at -20 °C. The concentration of ANS was determined spectrophotometrically using the absorbance at 350 nm and the extinction coefficient ε_{350} = 5000 cm^{-1} M^{-1}.[108]

Tween® 20, **polyoxyethylene(20)sorbitan monolaurate**, was purchased form Acros Organics. Phosphate buffer with 1% Tween (v/v) was prepared prior to the sample incubation/aggregation by pipetting corresponding volume of Tween® 20 to the 25 mM phosphate buffer at pH 8.

Peptide sample preparation and aggregation

The peptide powder was dissolved in 25 mM sodium phosphate buffer (pH 7–8) or 25 mM Tris buffer (pH 7.5–8.5). After peptide dissolution, the sample was filtered through a 0.22 µm filter (PES or PVDF membranes, Millex). The concentration of the peptide was determined photometrically on a Cary 60 UV-Vis spectrophotometer (Agilent Technologies) using the

Beer-Lambert law and a theoretical extinction coefficient of 6990 M^{-1} cm^{-1} at 280 nm. The extinction coefficients of GLP-1 and GLP-1-Am were calculated using the ExPASy Bioinformatics Resource Portal using:

$$\varepsilon_{280} = 5500\, n_{\mathrm{Trp}} + 1490\, n_{\mathrm{Tyr}} + 125\, n_{\mathrm{S\text{-}S}} \qquad (2.4)$$

where ε_{280} represents the extinction coefficient at 280 nm, n_{Trp} is the number of tryptophan residues in the peptide sequence, n_{Tyr} is the number of tyrosine residues in the peptide sequence and $n_{\mathrm{S\text{-}S}}$ is the number of disulfide bridges in the peptide sequence. Absorbance measurements were performed by scanning the sample between 200 and 400 nm and subtracting the absorption spectrum of the buffer measured in the same cuvette over the same wavelength range. For freshly prepared samples, no significant light scattering was observed (i.e. the absorbance at 320 nm was close to zero) and, therefore, peptide concentration was calculated directly using A_{280} without further correction.

Samples were incubated in 1.5 mL or 2.0 mL plastic microcentrifuge tubes (STARLAB) sealed and wrapped in aluminium foil to protect from sunlight. Incubation/aggregation was performed in an Incubator Shaker (Innova®43) at 37 °C at 80 rpm, 100 rpm or 180 rpm, or on a microplate reader FLUOstar Omega (BMG Labtech) plate (Corning 3881), sealed with tape (Costar Thermowell) at 37 °C, with 5 minutes of shaking every 30 minutes (orbital shaker mode at 600 rpm).

Oligomers were separated from the solution either by filtration though a 0.22 µm filter (PES or PVDF membranes, Millex) that removed all large insoluble aggregates or by size-exclusion chromatography where the oligomer-containing fractions were subsequently concentrated in 3 kDa MWCO cellulose Amicon® Ultra centrifugal filters 0.5 mL (Merck Millipore) or in Vivaspin 6, 3 kDa MWCO 3 mL (GE Healthcare).

Size-exclusion chromatography

Analytical size-exclusion chromatography was performed on an ÄKTA FPLC system (GE Healthcare), using a Superose 12 10/300 or a Superdex 75 10/300 column (both GE Healthcare). Samples were loaded using 100 µL or 200 µL loops. Prior to loading, the samples were filtered through a 0.45 µm filter. All samples were eluted at a flow rate of 0.75 mL min^{-1} at room temperature and UV absorbance detection at 280 nm through a 0.5 cm flow cell was used. Globular protein standards were used for column calibration under the same conditions as the experiments for the GLP-1-Am oligomers. The elution volume of each protein standard

was plotted against the logarithm of its molecular weight. A linear regression of this plot was used to determine the molecular weight of the observed GLP-1-Am oligomers.

Circular dichroism

Circular dichroism spectra were measured on a Chirascan CD spectrometer (Applied Photophysics). All measurements were performed with 1 nm step size and with 1 nm spectral bandwidth at room temperature. Far-UV CD spectra over the range 180–250 nm were measured in 1 mm or 0.1 mm pathlength cuvettes. Near-UV CD spectra over the range 250–350 nm were measured in 2 mm pathlength cuvettes. The resulting spectrum was obtained as an average of three identical scans and the spectrum of the pure buffer was subtracted.

Kinetics of aggregation — Thioflavin T binding assays

Fluorescence kinetic measurements were carried out using a microplate reader FLUOstar Omega (BMG Labtech). Peptide samples at a given concentration were incubated at 37 °C with 50 µM concentration of ThT. Peptide samples with ThT were pipetted into a 96-well half-area plate (Corning 3881) and sealed with tape (Costar Thermowell) to prevent samples from evaporation. The total volume of each sample in a well was 100 µL. Bottom reading of the plate was performed every 30 minutes with 5 minutes of shaking prior to each reading (orbital shaker mode at 600 rpm). ThT binding to fibrils was monitored by recording the fluorescence emission at 482 nm with an excitation filter at 448 nm. Fluorescence was measured at a gain of 500 with 8 flashes per well.

Thioflavin T and 8-anilo-1-naphthalene-sulfonic acid binding experiments

Binding of both 8-anilo-1-naphthalene-sulfonic acid (ANS) and ThT were measured using a Cary Eclipse Fluorescence Spectrophotometer (Agilent Technologies). For ThT binding experiments, spectra were obtained by excitation at 448 nm and emission was recorded in the range 460–600 nm with a step of 1 nm. The ThT concentration in the samples was 50 µM.

ANS fluorescence emission was recorded in the range from 400 to 600 nm after excitation at 350 nm. ANS concentration in all samples was 250 µM.

Intrinsic tryptophan fluorescence

Intrinsic tryptophan fluorescence spectra were measured on a Cary Eclipse Fluorescence Spectrophotometer (Agilent Technologies). Spectra were obtained using an excitation wavelength of 280 nm and emission spectra were recorded between 300 and 400 nm with a step of 1 nm. Emission and excitation band passes of 10 nm, and a voltage on the photomultiplier

tube of 550 V were used. Samples were measured in a 120 µL quartz cuvette (Hellma Analytics).

Denaturing protein gel electrophoresis

The non-covalent character of GLP-1-Am oligomers was assessed by sodium dodecyl sulfate-polyacrylamide gel electrophoresis (SDS-PAGE) using a pre-cast 4–12% Bis-Tris gels (Life Technologies) run in NuPAGE® MES SDS Running buffer (Life Technologies) for 35 minutes at a constant voltage of 200 V. Peptide samples were prepared in NuPAGE® LDS Sample buffer (Life Technologies), heated for 5 minutes to 95 °C and immediately loaded onto the gel. Protein and peptide standards, Mark 12 Unstained Standard and PageRuler Unstained Protein Ladder (both ThermoFisher Scientific), were run in parallel for size reference. Gels were stained with InstantBlue (Expedeon).

Scanning electron microscopy

A single drop of the sample was spread onto a microscope glass slide which was previously washed with isopropanol and acetone and then dried. The sample was left to dry and the excess salts were washed by rinsing the glass slide gently with 300 µL of distilled deionized water two times. Prior to the imaging, the samples were dried under a stream of nitrogen and coated with a 10 nm layer of platinum using a Quorum Technologies Q150T ES Turbo-Pumped Sputter Coater/Carbon Coater. Scanning electron microscopy (SEM) images were taken with a MIRA3 instrument (TESCAN) at 5.0 kV using an In-Beam Secondary Electron detector.

Assessment of oligomer stability

Oligomer stability testing was performed using size-exclusion analytical columns Superose 12 10/300 and Superdex 75 10/300. For elution at pH 8, a 25 mM sodium phosphate buffer was used and at pH 8.5 and 8.2, a 25 mM Tris buffer was used. Samples containing isolated oligomers or a mixture of the monomer and oligomeric species were either heated, sonicated or incubated with an organic solvent (20% isopropanol, 30% and 40% acetonitrile) for a specified time. Immediately after this, samples were run on a buffer-equilibrated SEC column at room temperature.

Chapter 3
GLP-1-Am aggregation at pH 7–8

In this Chapter the aggregation behaviour of glucagon-like peptide 1 amide (GLP-1-Am) at pH values from 7 to 8 is described. In this pH range, C-terminal amidation of GLP-1 was shown to have the greatest effect on the aggregation behaviour. Compared to non-amidated peptide, C-terminal amidation significantly slows fibrillation under these conditions, however, it cannot prevent it completely.[13] Most of the experiments in this Chapter were performed at pH 8 in 25 mM sodium phosphate buffer, however, a very similar behaviour was also observed at pH 7 and 7.5 (**Appendix A**).

3.1 GLP-1-Am shows significantly lower propensity to aggregate at pH 7–8 than GLP-1

To monitor and compare the aggregation behaviour of GLP-1 and GLP-1-Am, peptide samples were incubated with ThT at 37 °C for approximately one week with shaking at 600 rpm for 5 minutes prior to each fluorescence reading. During this time, ThT emission at 482 nm (after excitation at 448 nm) was monitored as a measure of fibril formation. In accordance with the previous study,[13] it was observed that in the range of pH between 7 and 8, the aggregation properties of GLP-1-Am differ greatly from those of GLP-1. This is apparent from the significantly prolonged lag times as well as the shape of the ThT fluorescence curve over time. Moreover, while GLP-1 shows a typical sigmoidal aggregation curve with a rapid elongation phase after a critical number of nuclei is formed, GLP-1-Am aggregation curves lack the rapid rise in fluorescence due to the elongation and growth phases, and the increase in fluorescence is rather slow and gradual when compared with GLP-1 at the same peptide concentration (**Figure 11**). Therefore, it is not possible to extract any kinetic parameters, e.g. k, $t_{1/2}$, for the aggregation of amidated GLP-1 at pH 8 over 145 hours. This suggests a significantly lower propensity to aggregate compared with GLP-1 under the same conditions.

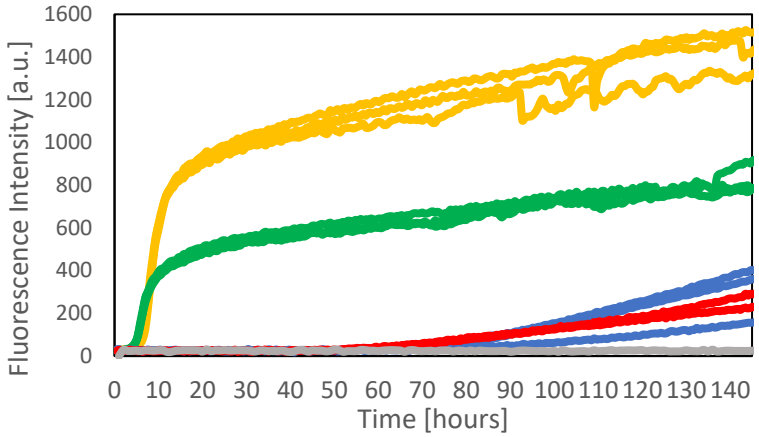

Figure 11: Aggregation of GLP-1 and GLP-1-Am at pH 8 in 25 mM sodium phosphate buffer monitored by ThT at 37 °C. Aggregation assay was performed using a microplate reader FLUOstar Omega. Runs in triplicate are shown. Yellow: GLP-1 85 µM; Green: GLP-1 42.5 µM; Blue GLP-1-Am 85 µM; Red: GLP-1-Am 42.5 µM.

3.2 GLP-1-Am forms small oligomers during the long lag phase

Samples of 85 µM GLP-1 and GLP-1-Am were analysed by SEC, during their incubation at 37 °C using constant double orbital shaking at 80 rpm. Before the SEC analysis, the sample was filtered through a 0.45 µm filter to remove fibrils and large insoluble aggregates which would block the filter of the SEC column. Using a Superose 12 SEC column, it was possible to monitor depletion of monomeric peptide during the aggregation reaction. Moreover, the column matrix was able to resolve the monomer from the peaks of small oligomers, which were formed during the aggregation, and thus monitor their formation over time.

Significant differences were observed between GLP-1 and GLP-1-Am in the monomer depletion rate. GLP-1 shows fast depletion of the monomer over time compared to GLP-1-Am. In addition, during the incubation/aggregation time oligomers were detected for GLP-1-Am but not for GLP-1. After 48 hours of incubation, oligomers of GLP-1-Am start to appear and gradually increase over time as shown in **Figure 12**. Presumably, for GLP-1, the monomer is quickly converted into the amyloid fibril or other large insoluble aggregates that are removed by filtration prior to the SEC analysis.

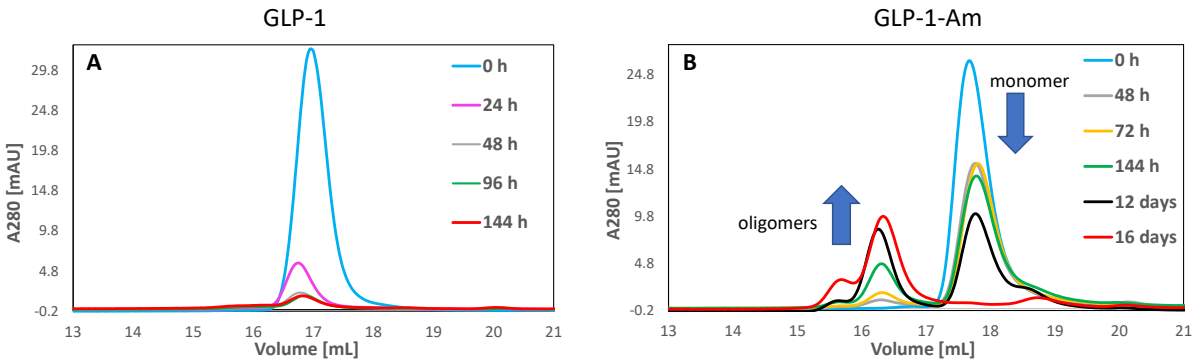

Figure 12: Size-exclusion chromatographic analysis of the population of the monomer and small oligomers during the aggregation of GLP-1 and GLP-1-Am. GLP-1 (**A**) and GLP-1-Am (**B**) monomer depletion and oligomer formation was monitored over time by SEC. Samples at an initial concentration 85 µM (both GLP-1 and GLP-1-Am) incubated at 37 °C with continuous shaking at 80 rpm were analysed on a Superose 12 10/300 size-exclusion column in 25 mM sodium phosphate buffer at pH 8 at room temperature. In the case of GLP-1, the only peak was eluted at approximately 16.9 mL corresponding to the monomer. For GLP-1-Am, there is only one peak, most likely monomeric, at the beginning of incubation (0 h) at approximately 17.7 mL. After 48 hours incubation, peaks with lower retention volumes (approximately 15.5 mL and 16.2 mL), corresponding to small oligomers, start to appear.

For GLP-1-Am the single peak at approximately 17.7 mL most probably corresponds to the monomeric peptide. The peaks at the lower elution volumes (approximately 15.5 and 16.2 mL) correspond to species with higher molecular masses compared to the monomer. This suggests that they are peptide oligomers that were formed during the aggregation process. It is important to note that under the conditions used, there were not only the monomer and the oligomers present but also amyloid fibrils and possibly other insoluble aggregates were formed as was shown by scanning electron microscopy (SEM) in **Figure 24** (this Chapter, section 3.7). These larger species were removed by the filtration step prior to the SEC and therefore are not observed in the SEC experiment.

3.3 Determination of the size of GLP-1-Am oligomers

In order to determine the size of the GLP-1-Am oligomers formed during the aggregation reaction, the calibration of two different SEC columns under the same conditions was performed using globular protein standards of a defined size in 25 mM sodium phosphate buffer at pH 8, 0.75 mL min^{-1} flow rate.

Calibration curve for Superose 12 10/300 in 25 mM sodium phosphate buffer at pH 8.

The void volume of the column was determined using Blue dextran 2000 and was 7.7 mL. A set of globular proteins (**Table 2**) was used for calibration (**Figure 13**). The total volume of a Superose 12 10/300 column is 19.7 mL. The elution volumes of protein standards were plotted

against the logarithm of their molecular weight and the correlation was described by a linear regression fit and its square of the correlation coefficient, where V_e is the protein elution volume measured from the centre of a peak.

Protein standard	MW [Da]	Elution volume [mL]
Aldolase	158,000	11.4
Conalbumin	75,000	12.2
Ovalbumin	44,000	12.6
carbonic anhydrase	29,000	13.9
Trypsinogen	24,000	14.5
ribonuclease A	13,700	15.1
chymotrypsin inhibitor 2	9,265	15.9
GLP-1-Am monomer	3,355	17.7

Table 2: Protein standards and their elution volumes on a Superose 12 10/300 in 25 mM sodium phosphate buffer at pH 8.

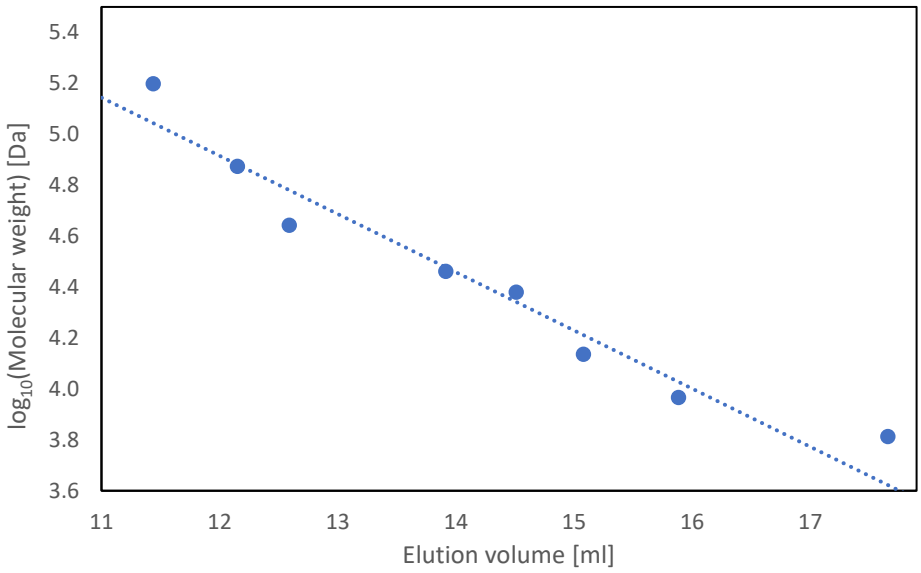

Figure 13: Superose 12 10/300 column calibration curve. Calibration performed in 25 mM sodium phosphate buffer at pH 8 on a set of protein standards (Table 2) at room temperature. Elution was performed with a flow rate 0.75 mL min^{-1} and 100 µL of approximately 100 µM of each protein was injected using a 200 µL injection loop. The blue dotted line is the linear regression fit, see below.

$$log_{10}(\mathrm{MW/Da}) = -0.2285 \cdot V_e + 7.6579$$
$$R^2 = 0.9565$$

The elution volumes of the GLP-1-Am oligomers (**Figure 14**) were 15.5 mL for oligomer A and 16.2 mL for oligomer B. Using the equation above, the size of oligomer A was calculated as 13 kDa and 9 kDa for oligomer B.

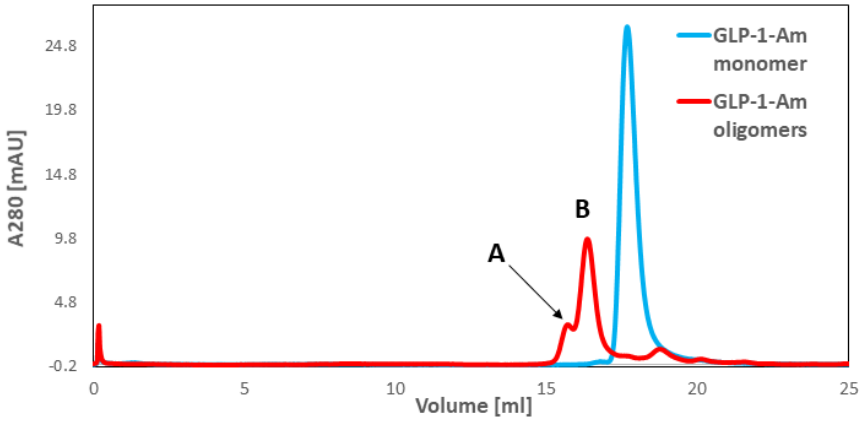

Figure 14: Elution profiles of the GLP-1-Am monomer and oligomers on a Superose 12 column. The sample was analysed prior to the incubation (0 h, blue line) and after 16 days (red line) of incubation at 37 °C with continuous shaking at 80 rpm. Elution conditions: 25 mM sodium phosphate buffer at pH 8, flow rate 0.75 mL min^{-1}, Superose 12 10/300.

Calibration curve for Superdex 75 10/300 in 25 mM sodium phosphate buffer at pH 8.

The void volume of the column was determined using Blue Dextran 2000 and was 8.2 mL. A set of globular proteins (**Table 3**) was used for calibration curve points (**Figure 15**). The total volume of the Superdex 75 10/300 column is 18.1 mL. The protein standards elution volumes were plotted against the logarithm of their molecular weight and the correlation is described by a linear regression fit and its square of the correlation coefficient, where V_e is the protein elution volume measured from the centre of a peak.

Protein standard	MW [Da]	Elution volume [mL]
Ovalbumin	44,000	9.8
carbonic anhydrase	29,000	11.4
Trypsinogen	24,000	12.1
ribonuclease A	13,700	13.3
chymotrypsin inhibitor 2	9,265	14.4
GLP-1-Am monomer	3,355	17.1

Table 3: Protein standards and their elution volumes on a Superdex 75 10/300 in 25 mM sodium phosphate buffer at pH 8.

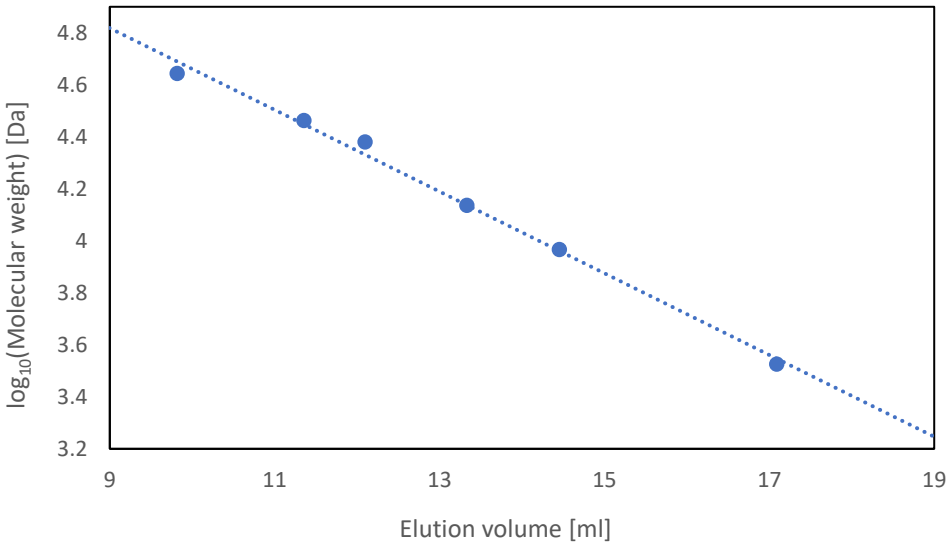

Figure 15: Superdex 75 10/300 calibration curve. Calibration performed in 25 mM sodium phosphate buffer at pH 8 on a set of protein standards (Table 3) at room temperature. Elution was performed at a flow rate of 0.75 mL·min^{-1} and 100 µL of approximately 100 µM of each protein was injected using a 200 µL injection loop. The blue dotted line is the linear regression fit, see below.

$$log_{10}(\mathrm{MW/Da}) = -0.1571 \cdot V_e + 6.232$$
$$R^2 = 0.9935$$

The elution volumes of the GLP-1-Am oligomers (**Figure 16**) were 14.4 mL for oligomer A and 15.3 mL for oligomer B. Using the equation above, the size of oligomer A was calculated as 9.3 kDa and 6.7 kDa for oligomer B.

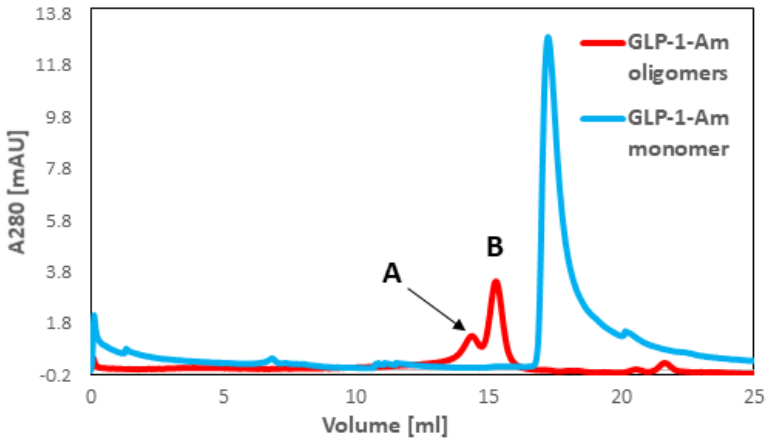

Figure 16: Elution profiles of GLP-1-Am monomer and oligomers on a Superdex 75 column. Samples were analysed prior to the incubation (0 h, blue line) and after 7 days (red line) of incubation at 37 °C with continuous shaking at 180 rpm. Elution conditions: 25 mM sodium phosphate buffer at pH 8, flow rate 0.75 mL min^{-1}, Superdex 75 10/300.

Molecular weights of oligomer A and B, which were calculated on the basis of the corresponding column calibrations, vary between the two SEC columns used. The difference is most probably given by the slightly different properties of the column matrices. Superose 12 matrix is composed of cross-linked agarose with an average matrix bead size of 8–12 µm and Superdex 75 is a composite of cross-linked agarose and dextran with an average matrix particle

size of 13 μm. The separation range of a Superose 12 column (1000–300000 Da) is also much broader than the separation range of a Superdex 75 column (3000–70000 Da). Therefore, the resolution of Superose 12 column may be less precise. However, results of both SEC columns indicate that eluted species are low molecular weight oligomers of a size range from 6.7 kDa to 13 kDa. These values correspond to a range of species from peptide dimers (6710 Da) to peptide tetramers (13 420 Da).

Although SEC data may provide a reasonable estimate of the size of the oligomeric species, further complementary size characterization techniques are needed. It is important to point out that calibration of the size-exclusion column is based on the separation of globular proteins according to their hydrodynamic radii. GLP-1-Am monomer and oligomers may not be fully globular and this could cause inaccuracies in the size estimates. Characterization by complementary techniques such as mass spectrometry will be subject of further research.

3.4 Stability of GLP-1-Am oligomers

In this Section, the stability of GLP-1-Am oligomers formed in 25 mM sodium phosphate buffer at pH 8 with continuous shaking at 180 rpm was investigated. Stability experiments were performed using analytical SEC and SDS-PAGE. Prior to the SEC, a sample containing either previously isolated oligomers or a mixture of the monomer and small oligomers was heated, sonicated or incubated with an organic solvent, followed by a SEC under the usual conditions (25 mM sodium phosphate buffer, pH 8) on buffer-equilibrated columns.

As was shown earlier in this Chapter, the amount of the oligomers steadily increases with time and then, after depletion of the monomer, remains constant, i.e. no backwards transformation into fibrils or monomers was observed (**Figure 12**). A series of stability experiments was performed using SEC (**Figure 17**).

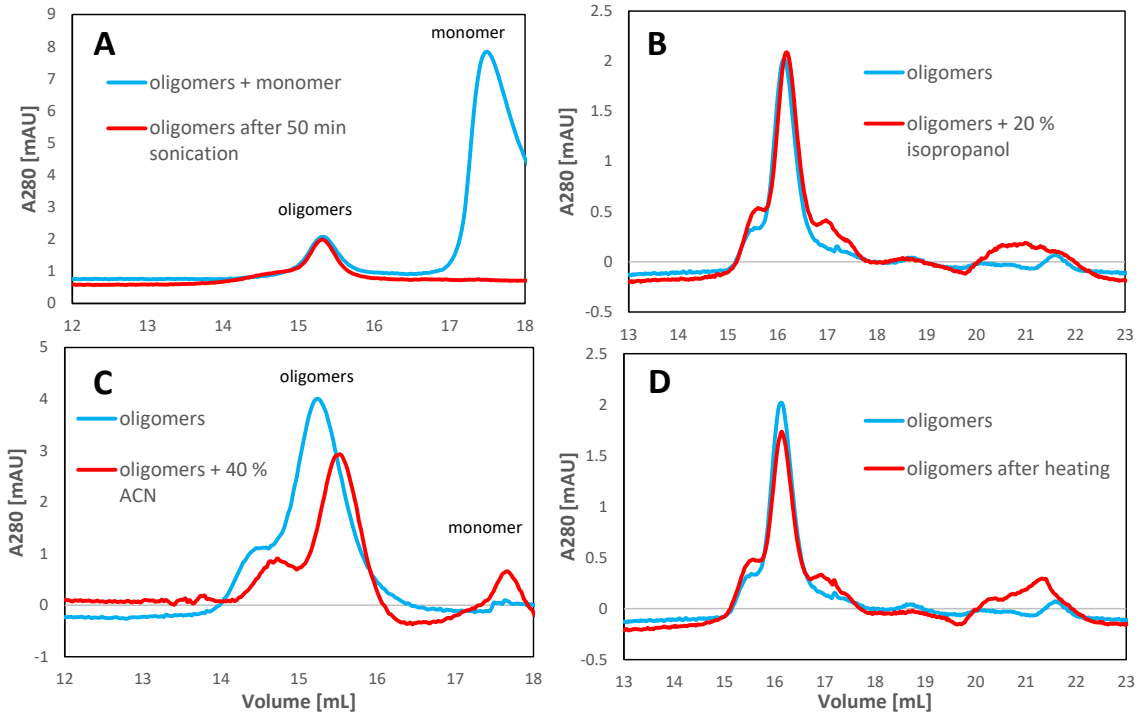

Figure 17: Stability of small oligomers formed by GLP-1-Am. SEC elution curves before (blue line) and after (red line) a stability test. Samples A and C were analysed on a Superdex 75 10/300 column, and B and D on a Superose 12 10/300 SEC column. After incubation (in 25 mM sodium phosphate buffer at pH 8 with continuous shaking at 180 rpm, for 3–9 days), oligomeric peaks were first separated by SEC (for B, C, D only) and after the particular stability test analysed on an SEC column in 25 mM sodium phosphate buffer at pH 8. The samples were: A mixture of the monomer and oligomers sonicated for 50 min (**A**). Isolated oligomers incubated in 20% isopropanol for 1 hour (**B**), incubated in 40% ACN for 2 hours (**C**), or heated to 95 °C for 10 min (**D**).

When the aggregating mixture containing both the monomer and small oligomers was sonicated for 50 min, the oligomeric peak remained unchanged, however, all the monomer was depleted, presumably converted into large aggregates (fibrils) as can be seen in **Figure 17A**. Therefore, sonication has the effect of intense agitation and speeds up fibrillation. Upon heating to 95 °C for 10 min, no significant change in the oligomeric peaks was observed (**Figure 17D**). Similarly, when small oligomers were incubated in 20% isopropanol for one hour, the oligomeric peaks were not significantly changed (**Figure 17B**). However, upon incubation in 40% acetonitrile (ACN) for 2 hours, the oligomeric peaks decreased and small new peak of higher retention volume appeared (**Figure 17C**). This may imply a partial denaturation of small oligomers back to the monomer.

Oligomeric fractions isolated using SEC were also tested by SDS-PAGE. Here, only one band corresponding to the molecular weight of the monomer was observed for the oligomeric samples (**Figure 18**). This suggests a complete denaturation of oligomers during SDS-PAGE.

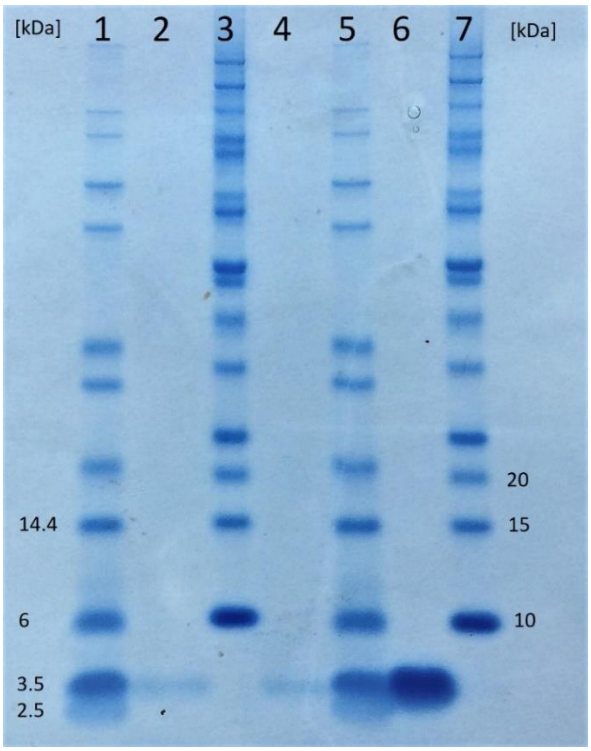

Figure 18: SDS-PAGE analysis of GLP-1-Am oligomers formed at pH 8 in 25 mM sodium phosphate buffer. The oligomers were isolated (by SEC) from the 130 μM GLP-1-Am aggregated mixture incubated in 25 mM sodium phosphate buffer at pH 7.5 for 5 days at 37 °C with continuous shaking at 180 rpm. Lanes 2 and 4: GLP-1-Am oligomers; lane 6: fresh (monomeric) GLP-1-Am sample; lanes 1, 3, 5 and 7: proteins reference ladders.

3.5 Structural characterization of GLP-1-Am oligomers

GLP-1-Am oligomers were characterized using fluorescence spectroscopy and circular dichroism spectroscopy in the far- and the near-UV range. First, a far-UV CD spectrum of the peptide powder freshly dissolved in 25 mM sodium phosphate buffer at pH 8 was recorded and it shows that the monomeric peptide has some secondary structure (α-helix and β-sheet) as well as some disordered regions (**Figure 19A**). The secondary structure was predicted to be approximately 31% α-helix, 15% β-sheet, 23% turns and 31% disordered regions, using DichroWeb, Contin-LL method, dataset 3.[109–111] In the previous studies conducted in our group, the secondary structure of the GLP-1-Am monomer was found to be approximately constant over a wide range of pH values with only a minor change between pH 3 and 4.[13] As expected, structural changes of the incubated mixture were observed over time. The overall spectrum after 9 days of incubation of a sample containing a mixture of different chemical species (oligomers, monomer and fibrils), as was observed by SEC and SEM, is shown in **Figure 19B**. Interestingly, the spectrum of an isolated oligomeric species from mixture in **Figure 19B** has only a broad minimum around 200 nm corresponding to the disordered conformation (**Figure 19C**). In

contrast, a far-UV CD spectrum of solely fibrils (**Figure 19D**) shows a characteristic minimum around 220 nm, which reflects a large content of β-sheet.

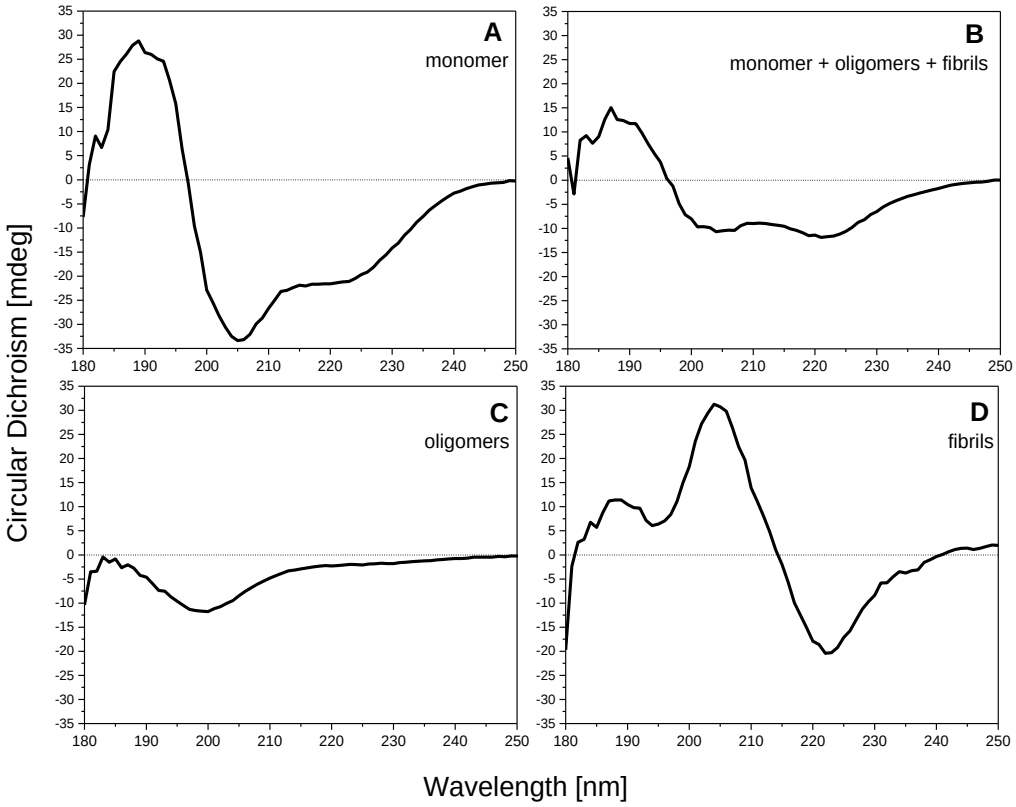

Figure 19: Far-UV CD spectra of different chemical species present in the aggregating mixture of GLP-1-Am at pH 8 in 25 mM sodium phosphate buffer. CD intensity is presented in millidegree units due to difficulties in the determination of the concentration of fibrils and oligomers. All samples were measured in a 0.1 cm pathlength cuvette. (**A**) GLP-1-Am monomer at 85 µM concentration, a freshly prepared sample. (**B**) GLP-1-Am (85 µM) after 9 days incubation at 37 °C with constant shaking at 80 rpm. (**C**) GLP-1-Am oligomers isolated from sample B using SEC. (**D**) Fibrils isolated (by centrifugation) from a sample prepared analogously to sample B. All spectra were recorded at 25 °C.

Interesting spectral features were also observed in the near-UV CD spectra (**Figure 20**). Whereas non-aggregated monomer does not have any signal in the near-UV CD region, fibrils show two sharp peaks at approximately 292 and 285 nm and a shoulder at around 280 nm. Since the near-UV spectral range in CD spectroscopy is associated with aromatic amino acid residues, a signal in this range can reveal structural information about the local environment of these residues. For the fibrils, the observed signal can be attributed mainly to the tryptophan residue (position 25 in the sequence) with a possible contribution from the phenylalanine (position 22). The appearance of the signal only in fibrillar structures can be explained by the fact that tryptophan residue is fixed in structure in this state restricting the rotation of its side chain. It is also possible that the signal is enhanced by exciton coupling of near-by tryptophan side chains from different peptide chains that are close in space in the amyloid fibril. Tryptophan exciton coupling usually has a characteristic pattern also in the far-UV region,[112] however, in the case

of fibrils this pattern may be hidden by a strong signal from the fibril secondary structure. A similar interaction was observed by CD spectroscopy in some tryptophan zipper motifs.[113,114] Thus, the observed signal can be considered to be an indicator of a stable tertiary structure. The fact that tryptophan residues are in a fixed environment agrees with the findings of some of the theoretical predictions of the aggregation (fibrillation) prone regions (**Chapter 1, Figure 10A, C**). The absence of a CD signal in the near-UV range for oligomers indicates free rotation of the tryptophan residue in these structures.

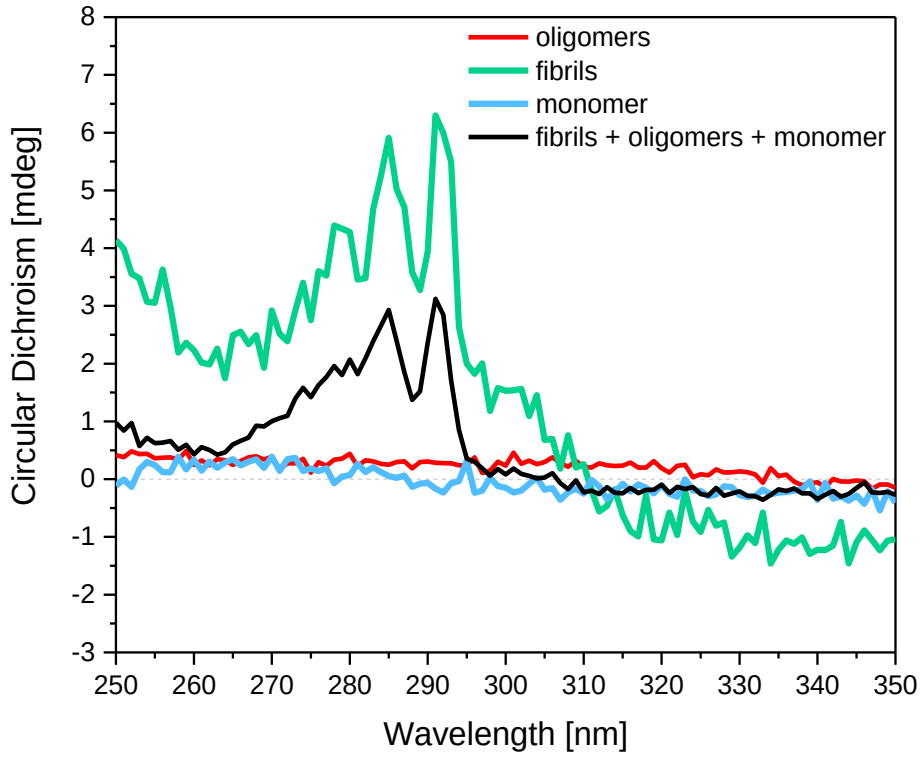

Figure 20: Near-UV CD spectra of the chemical species present in the aggregating mixture of GLP-1-Am at pH 8 in 25 mM sodium phosphate buffer. CD intensity is presented in millidegree units due to difficulties in the determination of the concentration of fibrils and oligomers. All samples were measured in a 0.2 cm pathlength cuvette. GLP-1-Am monomer at 85 µM concentration (blue line); GLP-1-Am (85 µM) after 9 days of incubation with continuous shaking at 80 rpm (black line); GLP-1-Am oligomers isolated from the incubated sample by SEC (red line); Fibrils isolated (by centrifugation) from a sample prepared analogously to the sample with the black spectrum (green line). All spectra were recorded at 25 °C.

Tryptophan fluorescence spectra are sensitive to the environment of the tryptophan residue giving information on its environment. Shift of the emission maxima (λ_{max}) can reveal the extent of tryptophan exposure to the solvent. The wavelength λ_{max} at 345 nm, **Figure 21**, observed for the peptide fibrils corresponds to tryptophans buried within a fibrillar structure. A significant red shift of λ_{max} to 360 nm observed for the oligomers indicates a higher exposure of tryptophan side chains to the solvent suggesting an unfolded structure of the oligomers (**Figure 21**). The value of λ_{max} of the oligomers is even higher than the value for the monomeric peptide which

may indicate a loss of the secondary structure present in the monomeric form, which can be seen by far-UV CD spectroscopy (**Figure 19A**).

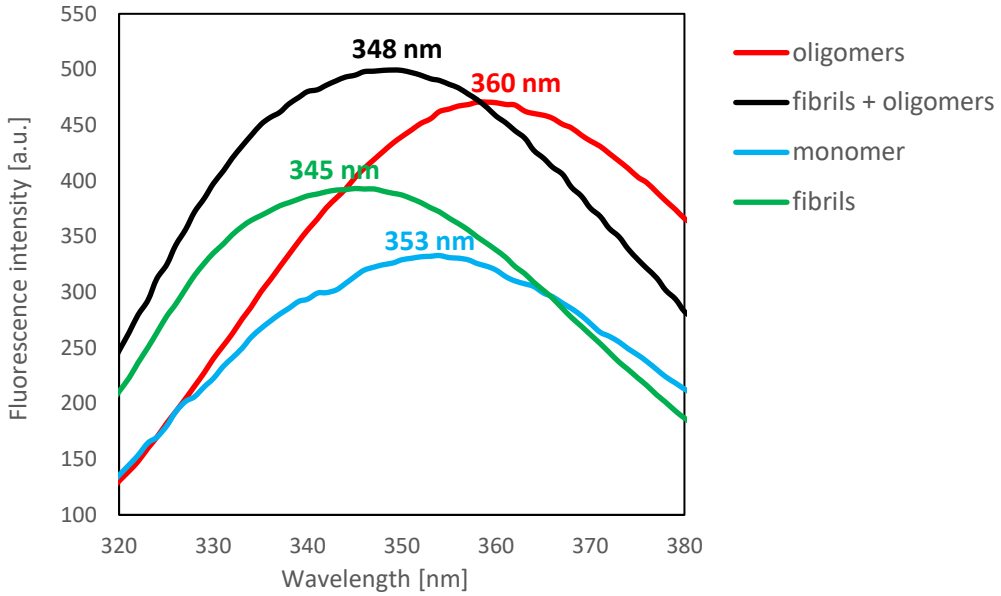

Figure 21: Emission spectra showing the maxima (λ_{max}) of the intrinsic tryptophan fluorescence. The lowest λ_{max} was observed for the folded structure of GLP-1-Am amyloid fibrils (green line), whereas the highest value for the unfolded oligomers (red line). All samples were measured in 25 mM sodium phosphate buffer at pH 8.

Binding of thioflavin T and 8-anilinonaphtalene-1-sulfonic acid

ThT and ANS are extrinsic fluorescent probes that can provide additional structural information about protein aggregates. ThT is known for its binding to the cross β-sheet structure present in amyloid fibrils.[8] Upon binding to amyloid fibrils, ThT has a strong fluorescence emission maximum at around 482 nm after excitation at 450 nm.[115] ANS binds to exposed hydrophobic patches present in some reported oligomeric species such as those formed by Aβ or islet amyloid polypeptide.[116] These oligomeric species are often believed to be the main cytotoxic species in the aggregation process.[117] Unbound ANS in solution weakly emits, after excitation at 350 nm, at around 530 nm. When bound to protein, its emission maximum is blue-shifted to approximately 470 nm and the emission intensity is greatly increased.[118]

Here, it was shown that small oligomers of GLP-1-Am do not bind ThT, neither do they bind ANS (**Figure 22**). Even though the emission maximum of intrinsic tryptophan fluorescence at 360 nm indicates an unfolded structure with exposed hydrophobic tryptophan residues, these oligomers are probably quite small, and therefore, do not have sufficient number of exposed hydrophobic residues to bind the ANS dye. The fact that oligomers do not bind ThT is in accordance with their structural characteristics as shown by far-UV CD with no evidence for any significant β-sheet structure.

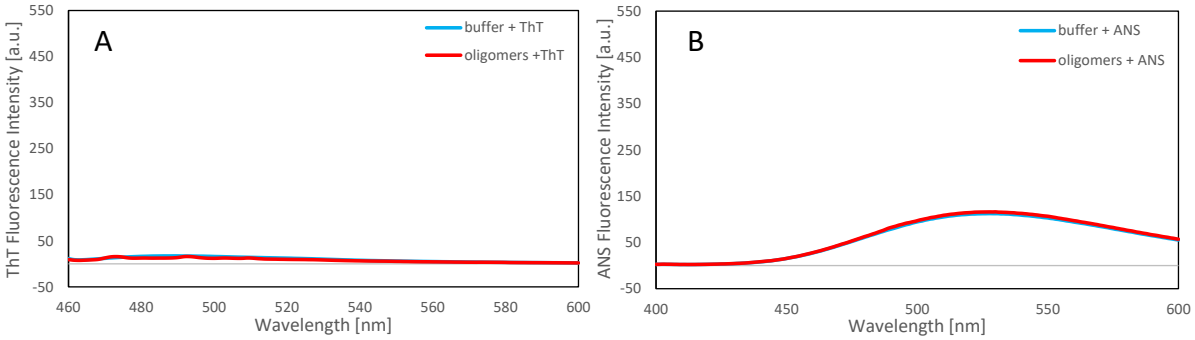

Figure 22: Fluorescence spectroscopy: ThT and ANS binding to oligomers. Oligomers isolated using SEC (5 µM) do not show detectable binding of ThT (50 µM concentration in the sample) (A), or ANS (250 µM concentration in the sample) (B). All samples were measured in 25 mM sodium phosphate buffer at pH 8 at room temperature.

3.6 The effect of 1% Tween® 20 on GLP-1-Am aggregation

Non-ionic surfactants such as Tween® 20 or Tween® 80 are known for their capabilities of preventing protein aggregation induced by various types of mechanical stress.[119] However, it has also been shown that addition of Tween® 20 to the solution of protein can increase the concentration of small protein aggregates. For example, Tween® 20 enhanced the formation of soluble aggregates of the recombinant human factor XIII, but prevented the formation of large insoluble aggregates.[120] A similar effect was observed for the anti-L-selectin antibody where the addition of Tween® 20 promoted dimerization but inhibited the formation of higher-order aggregates.[121] Further detection and characterization of the GLP-1-Am oligomers formed in the buffer with 1% Tween® 20 might, therefore, help us to explore the energy landscape of this peptide.

The propensity to form soluble oligomeric species was shown when GLP-1-Am was incubated in sodium phosphate buffer at pH 8 with the addition of 1% non-ionic surfactant Tween® 20 (v/v). After the addition of 1% Tween® 20 to 130 µM GLP-1-Am in phosphate buffer and 5 days of incubation at 37 °C, an intense well-defined peak corresponding to a large oligomer species was detected alongside the peak of the monomeric peptide (**Figure 23**). The elution volume of the oligomeric peak is approximately 11.9 mL which corresponds to the size of circa 86.8 kDa (≈ 26-mer). However, the presence of a surfactant may affect the elution profiles and the hydrodynamic radii of both the monomer and the oligomers. This may lead to earlier elution and an overestimation of the size of the species.

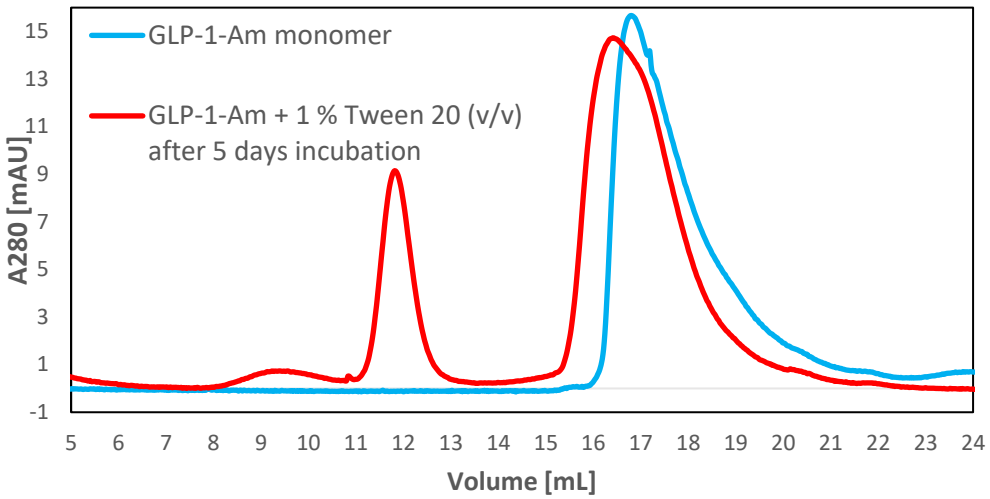

Figure 23: SEC of GLP-1-Am incubated in 1% Tween® 20. Elution chromatogram of 130 µM GLP-1-Am incubated in 25 mM sodium phosphate buffer at pH 8 with the addition of 1% Tween® 20 (v/v) for 5 days at 37 °C, 180 rpm rotation. Sample was analysed on a Superose 12 10/300 column run in 25 mM sodium phosphate buffer at pH 8 at room temperature.

3.7 Fibrils formation during aggregation of GLP-1-Am at pH 7–8

Samples of GLP-1-Am incubated for 10 days in 25 mM sodium phosphate buffer at pH 8 with continuous shaking at 80 rpm at 37 °C was analysed using SEM. From SEM images, it is apparent that amyloid fibrils are also formed under these condition (**Figure 24**), but probably not to the same extent as at other pH values, or for GLP-1. SEM images show some other aggregate-like species as well, however, it is very difficult to distinguish whether they are formed by the peptide or by buffer salts. SEM images of the pure phosphate buffer can be found in **Appendix B**.

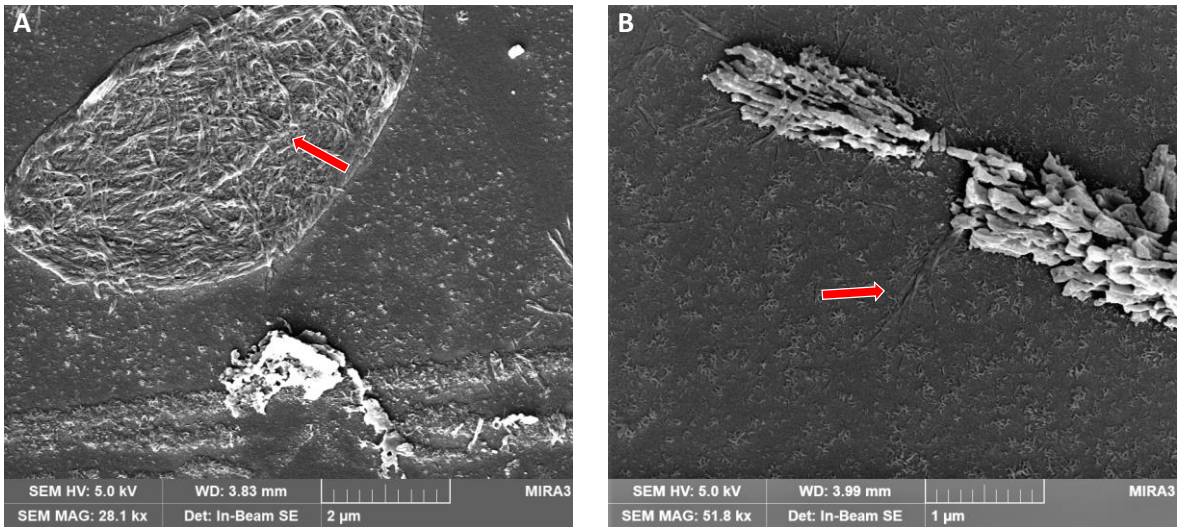

Figure 24: SEM images of GLP-1-Am aggregates. SEM images of GLP-1-Am after 10 days of incubation in 25 mM sodium phosphate buffer, pH 8, at 37 °C, with continuous agitation at 80 rpm. Amyloid fibrils are highlighted by red arrows. Images **A** and **B** are both of the same sample but have different magnifications.

3.8 Conclusions on the aggregation of GLP-1-Am at pH values between 7 and 8

GLP-1-Am shows a very slow fibrillation when incubated in 25 mM sodium phosphate buffer in the pH range of 7–8. The ThT fluorescence increases approximately linearly over the long lag phase. There is no rapid increase nor a growth phase observed that would indicate a fast elongation combined with a secondary nucleation phase. After 48 hours, small soluble oligomers were detected in the incubated samples. The amount of the oligomers gradually increased until all monomer was depleted. Based on the size-exclusion calibration curve, the size of the oligomers was determined to be in the range from 6.7 to 13 kDa corresponding to peptide dimer to tetramers. These small oligomers show a remarkable stability with respect to time and they are resistant to heat, sonication and addition of 20% isopropanol. Nevertheless, they probably slowly denature when incubated in 40% acetonitrile and during SDS-PAGE electrophoresis they denature completely. The structure of these small oligomeric species is highly disordered. SEM images of the partially aggregated GLP-1-Am samples showed that amyloid fibrils are present to some extent in addition to the oligomers. GLP-1-Am is also prone to form soluble oligomeric species when incubated with 1% non-ionic detergent Tween® 20 (v/v) in 25 mM sodium phosphate buffer at pH 8.

Chapter 4
GLP-1-Am aggregation above pH 8

In this Chapter the aggregation behaviour of GLP-1-Am in solution above pH 8 is investigated. All experiments in this Chapter were performed in 25 mM Tris buffer at pH 8.2 or 8.5 (as specified further in the text).

4.1 Large variance in aggregation kinetics

ThT aggregation assays of GLP-1-Am above pH 8 show large variation in kinetic parameters (lag times, *k*, *A*) and thus poor reproducibility between equivalent measurements. It can be estimated (**Figure 25 and 26**) that lag times are generally longer than 60 hours and that the aggregation profile is, at least at pH 8.5, sigmoidal, as shown for 75 µM GLP-1-Am at pH 8.5 and 8.2 (**Figure 25**). This is the greatest difference relative to the aggregation at pH 7 to 8 where the aggregation profiles are approximately linear over the same timescales measured. At pH 8.2, other peptide concentrations (150 µM, 125 µM, 50 µM, 25 µM) showed similar variation and lag times longer than 60 hours. Surprisingly, for high peptide concentrations (150 µM and 125 µM), often no fibrillation was observed over the time course studied (**Figure 26**).

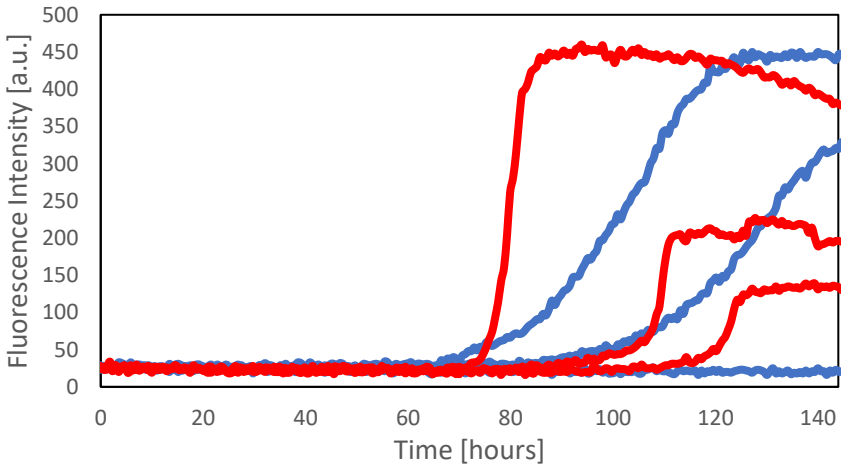

Figure 25: Irregularity and high variance in ThT aggregation profiles of GLP-1-Am at pH > 8. GLP-1-Am at 75 µM concentration at pH 8.2 in 25 mM Tris buffer in a triplicate (blue lines), pH 8.5 in 25 mM Tris buffer in triplicate (red lines). All samples were incubated in the same plate.

Figure 25 illustrates how the slope of the elongation and growth phase is steeper at pH 8.5 than at pH 8.2, where the increase in the fluorescence signal in the same region is more gradual and closer to aggregation behaviour observed in phosphate buffer between pH 7 and 8 (**Figure 11**). The steep increase in fluorescence in the elongation and growth phase is characteristic of

secondary nucleation processes that work as autocatalytic feedback loops.[99] The different slope of the aggregation curve in the elongation and growth phase at pH 8.2 and 8.5 may be caused by the extent of the secondary nucleation processes (secondary surface-catalysed nucleation and fragmentation) or even by the absence of those secondary processes at pH 8 in phosphate buffer (**Chapter 3**). Nevertheless, one must take into an account the possible buffer effects of Tris *versus* phosphate buffer. For example, data in **Appendix A, Figure A2** show a higher rate of fibrillation when GLP-1-Am was incubated in Tris buffer compared to the incubation in sodium phosphate buffer (both at pH 7.5). The observed decrease in fluorescence in the plateau phase at pH 8.5 (**Figure 25**) is most probably caused by ThT degradation at high pH.[122]

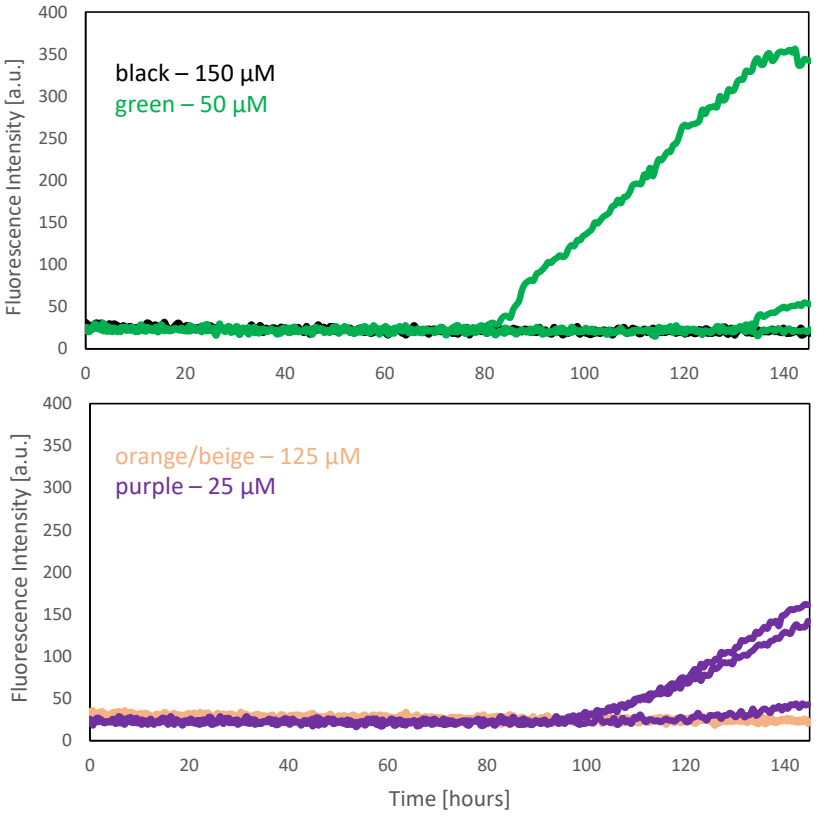

Figure 26: ThT aggregation profiles over a range of GLP-1-Am concentrations at pH 8.2. Samples were incubated at 37 °C in 25 mM Tris buffer at pH 8.2. Runs in triplicate are shown.

4.2 Oligomer formation

The samples were incubated at 37 °C and analysed by SEC (Superose 12 10/300) at 25 °C, always in the appropriate version of the Tris buffer. After 24 hours (and longer) of incubation at 37 °C, soluble oligomeric species were detected (**Figure 27**). The elution volumes of these oligomeric species significantly differed from the elution volumes of the oligomers detected in 25 mM sodium phosphate buffer with pH values between 7 and 8. In 25 mM Tris, pH 8.2, the

elution volumes of the oligomers were 12.2 mL (larger peak) and 14.1 mL (smaller peak), the elution volume of the monomeric peptide was 16.4 mL (**Figure 27A**). At pH 8.5, the elution volumes of the detected oligomers were 11.2 mL (larger peak), 11.8 mL and 13.0 mL (smaller peaks), the elution volume of the monomeric peptide was 15.5 mL (**Figure 27B**).

However, when the same samples (incubated at pH 8.2 or 8.5) were injected on a column using 25 mM sodium phosphate buffer with pH 8, as a mobile phase, the same elution profile as for the samples incubated at pH 8 sodium phosphate buffer (Chapter 3) was obtained (**Figure 12 and 27**). Moreover, in Tris buffer, the elution volume of the monomeric peptide is shifted as well. The constant shift in elution volumes (by about 1 mL) of all detected species is apparent even between pH 8.2 and pH 8.5 (both in Tris buffer). In this case, it is very probable that the detected species are of the same character. In addition, when these oligomers were run on on NativePAGE (non-denaturing electrophoresis), they were not resolved since they most probably run below the resolving range of 15 kDa. From these findings it can be assumed that the species formed at pH 8.2 and 8.5 in Tris buffer and those formed in phosphate buffer at pH 7–8 are likely to have the same size and that the difference in elution volumes is due to the elution buffer properties (e.g. the pH and ionic strength of the solution). Indeed, the ionic strength of 25 mM Tris (pH 8.5 and 8.2) and 25 mM sodium phosphate buffer (pH 8) differs greatly, which may play a role in the observed shift in elution volumes.[123]

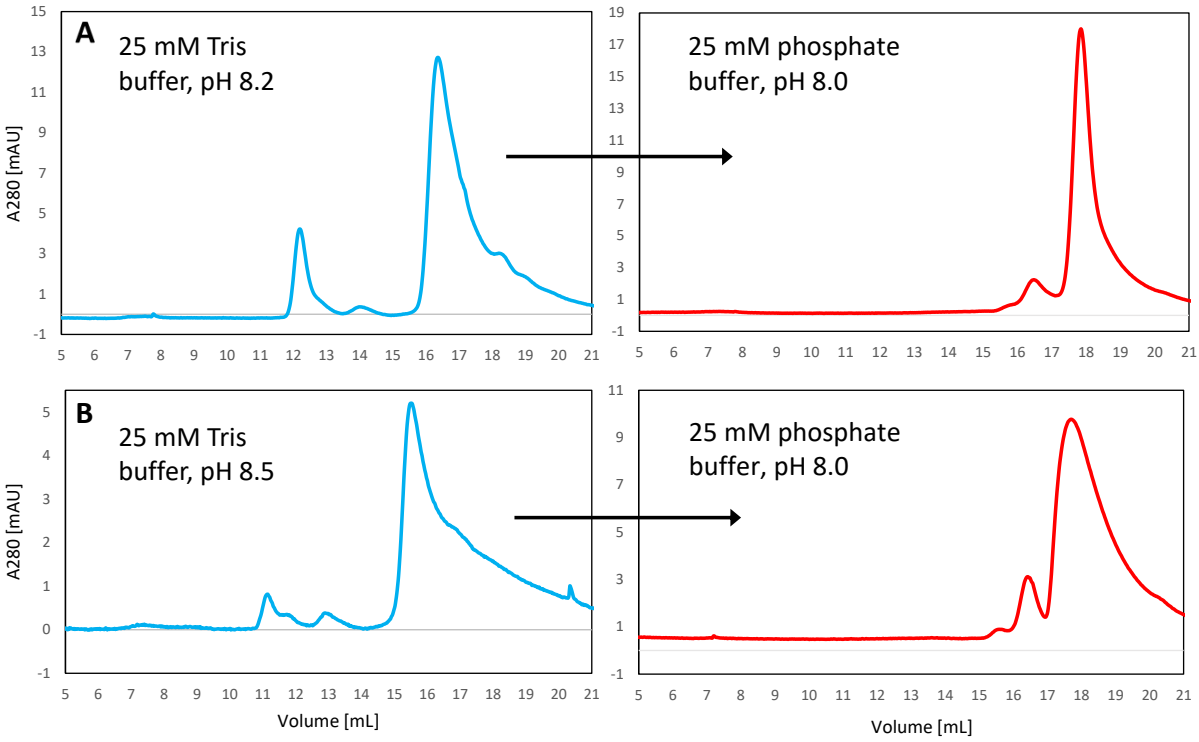

Figure 27: Shift in elution profiles of monomer and oligomers in different buffers. Same samples analysed on a Superose 12 10/300 in 25 mM Tris buffer at pH 8.2 (**A**, blue line), in 25 mM sodium phosphate buffer at pH 8 (red line), in Tris buffer at pH 8.5 (**B**, blue line), and in 25 mM sodium phosphate buffer at pH 8 (red line). The observed constant shift in elution volumes is believed to be due to a change in the ionic strength of the elution buffer. Incubation of samples was performed at 37 °C in Tris buffer and SEC analysis at 25 °C, always either in Tris buffer or in phosphate buffer, always at the appropriate pH.

4.3 Stability of oligomers formed at pH values above 8

The oligomeric peak with the elution volume of 11.2 mL (in 25 mM Tris, pH 8.5) was separated using SEC and subsequently the stability with respect to time and 30% ACN was tested and analysed by SEC (**Figure 28**). When the separated oligomeric fraction was incubated with 30% ACN for approximately 3 hours, the oligomer was partly denatured, presumably, to monomer. However, after this, new peaks with higher elution volumes than that of the monomer were detected, **Figure 28**. The new species may be either fragments of GLP-1-Am resulting from peptide degradation or differently folded monomers. Similarly to the oligomers formed in 25 mM sodium phosphate buffer at pH 8, the oligomers isolated in Tris buffer at higher pH values show remarkable stability with respect to time (**Figure 28**).

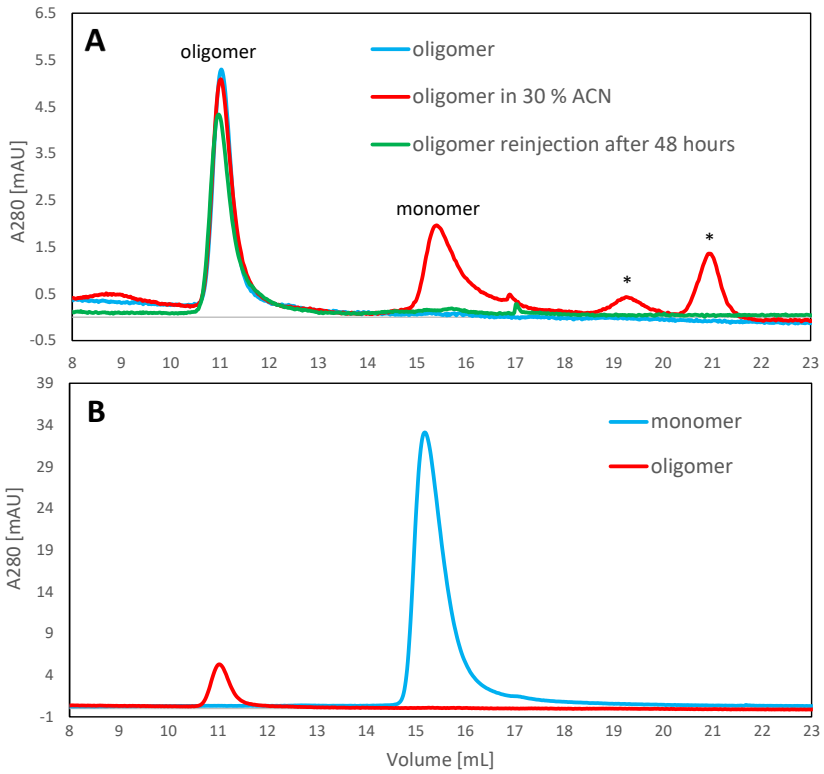

Figure 28: Stability of the oligomers formed in 25 mM Tris buffer at pH 8.5. Stability of the oligomer formed in 25 mM Tris buffer at pH 8.5. (**A**) The oligomer shows good stability with respect to time and can be partly denatured when incubated with 30% acetonitrile for approximately 3 hours. For ACN stability experiment, the volume of the injected sample was two times bigger (red line) than in previous injections (blue line, green line). (**B**) The retention volumes of the pure oligomer and of the monomer are shown for comparison.

4.4 Characterization of oligomers formed at pH 8.5

The structure of the oligomers was investigated using CD in the far- and near-UV range, and using intrinsic tryptophan fluorescence spectroscopy. The far-UV CD spectrum of the oligomers isolated using SEC (**Figure 29A**) shows only a broad minimum at 200 nm corresponding to the disordered structure. The spike (marked with *) at approximately 203 nm (blue line) is due to noise from the Tris buffer at this wavelength. There is no observable signal in the near-UV CD spectrum of oligomers in contrast to that of fibrils formed under these conditions, which show two positive bands at approximately 286 and 292 nm (**Figure 29B, D**). In the latter case, this signal comes most probably from the tryptophan residue which is rigidly fixed in the structure of fibrils. It is worth noting that the sign of the signal can reveal some information about the morphology of the fibrils (at least in the surroundings of tryptophan residue) when combined with molecular modelling.[114] Under different conditions a negative signal was observed at the same wavelengths as the positive signal mentioned previously (**Appendix C**). The far-UV CD spectrum of mature fibrils formed at pH 8.5 (**Figure 29C**)

shows subtle differences when compared to the fibrils formed at pH 8 (**Chapter 3, Figure 19D**). Nevertheless, the characteristic β-sheet structural motif can be still observed.

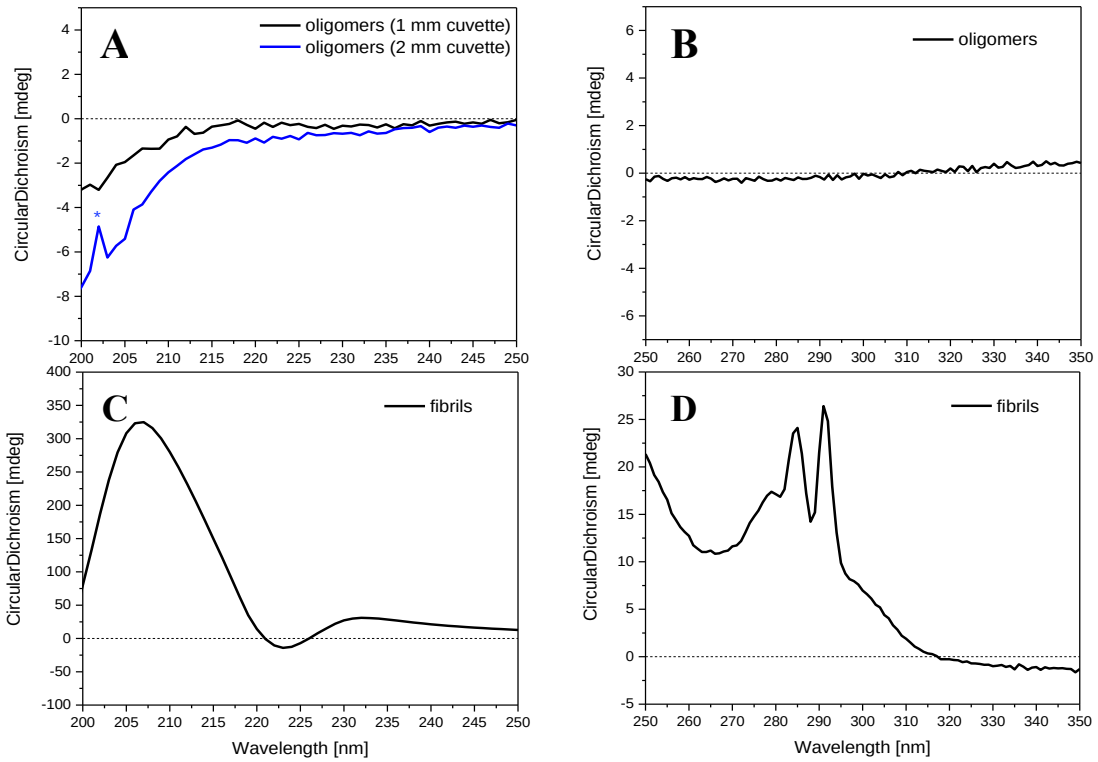

Figure 29: Far-UV and near-UV CD spectra of oligomers and fibrils incubated in 25 mM Tris buffer, pH 8.5. Far-UV CD spectrum of an isolated oligomer (**A**), near-UV CD spectrum of an isolated oligomer (**B**), far-UV CD spectrum of fibrils (**C**), near-UV CD spectrum of fibrils (**D**). Samples were incubated at 37 °C with continuous shaking at 180 rpm and measured at 25 °C. Intensity left in original millidegree units due to the difficulties in concentration determination of fibrils and oligomers.

Trends identical to those observed at pH 8 are also apparent in the tryptophan fluorescence emission spectra measured at pH 8.5 (**Figure 30**). The structure of the monomer does not significantly differ between pH 8 and 8.5 as can be seen from i) the value of λ_{max} (**Figure 30** and **Chapter 3, Figure 21**) and ii) the CD spectra of freshly prepared samples that were previously measured in our group.[13] The largest blue shift of λ_{max} to 344 nm can be seen for fibrillated GLP-1-Am as opposed to the λ_{max} of oligomers, which is shifted to 361 nm. This again indicates a largely unfolded structure of oligomers, which is in agreement with the results obtained for oligomers at pH 8 (**Chapter 3, Figure 21**).

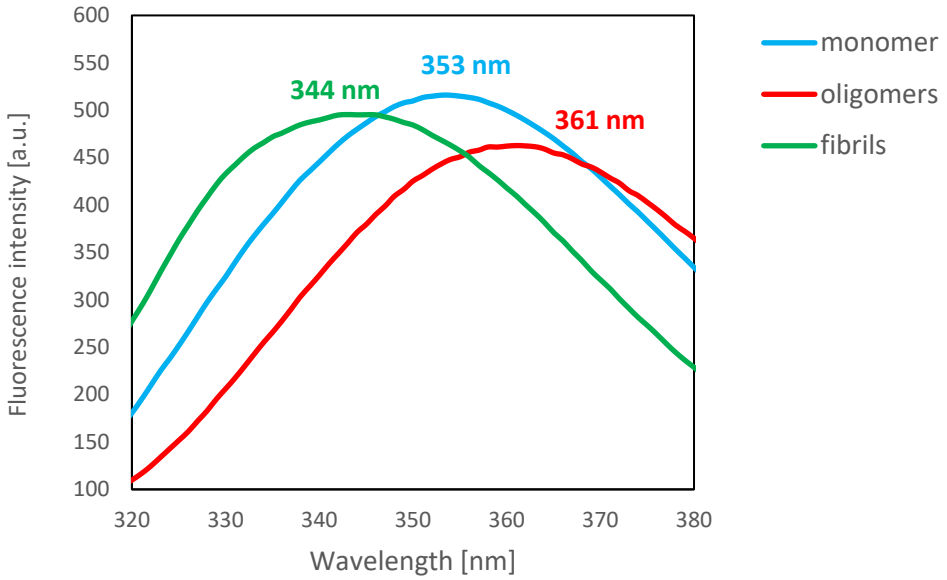

Figure 30: Emission maxima (λ_{max}) of the intrinsic tryptophan fluorescence at pH 8.5 in 25 mM Tris buffer. The lowest λ_{max} was observed for the folded structure of GLP-1-Am amyloid fibrils (green line) and the highest value for the largely unstructured oligomers (red line).

4.5 Conclusions on GLP-1-Am aggregation above pH 8

At pH values above 8, slow fibrillation with high variation in many aggregation parameters was observed. Under these conditions, aggregation lag times are generally longer than 60 hours and then fibrillation occurs. During the lag and elongation phase, formation of small soluble oligomers was detected. The oligomers are formed to a greater extent than at pH values from 7 to 8. This could explain the significant variance in the aggregation kinetics. The structural properties of oligomers formed at pH 8.5 in 25 mM Tris buffer are identical to the oligomers formed at pH values from 7 to 8 (Chapter 3).

Chapter 5
Discussion

This Discussion analyses and summarises results described in Chapter 3 and Chapter 4.

5.1 GLP-1 and GLP-1-Am show a minimum in aggregation propensity around their pI

GLP-1 aggregates over a wide range of pH values. However, the kinetic parameters associated with the aggregation reaction are highly pH dependent.[12] The same is true for the C-terminally amidated analogue of GLP-1, GLP-1-Am.[13]

Here, the aggregation of GLP-1-Am has been investigated in further detail, with the objective of detecting and characterising oligomeric species formed during the fibrillation. The lowest rate of GLP-1-Am fibrillation was observed between pH 7 and 8 in 25 mM sodium phosphate buffer. With the increasing value of pH the propensity to fibrillation increases again as shown in **Figure 31**. Nevertheless, the lag time under these conditions remains very long, about 60 hours or more. Another interesting difference is the change of the shape of the ThT aggregation curves even though the lag times did not significantly differ between different pH values. Whereas at pH 8, there is a rather gradual increase in fluorescence over the time scale of the measurement, at pH 8.5 a sigmoidal shape of the aggregation curve, with steep increase in fluorescence in the elongation and growth phase, was observed. At pH 8.2, the ThT curve shape is intermediate between those at pH 8 and 8.5.

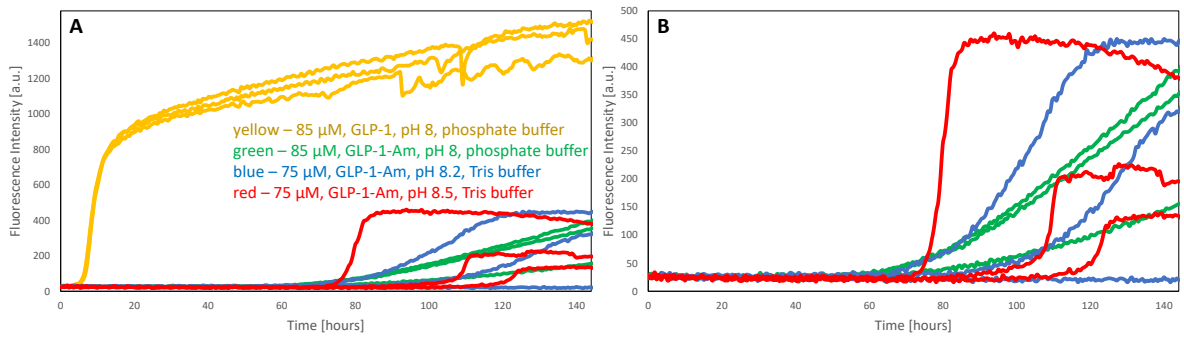

Figure 31: ThT aggregation profiles summary. ThT aggregation curves of GLP-1 and GLP-1-Am at 85 µM and 75 µM concentration at pH 8 (yellow and green), 8.2 (blue) and 8.5 (red) (**A**). Detail of GLP-1-Am aggregation (**B**).

The steep increase in fluorescence is generally due to secondary processes such as surface-catalysed secondary nucleation or fragmentation that work as autocatalytic loops.[99] A

shape of the aggregation curves different to sigmoidal may result from a different prevalence of these secondary processes or might even suggest a more complex aggregation pathway. However, it might also be the case that the aggregation propensity, especially at pH 8, is simply too low for the elongation and growth phases to be observed over the timescale of the experiment. It is not recommended to use very long incubation times (i.e. longer than one week) as this can be associated with many complications, e.g. peptide degradation, evaporation or possible bacterial contamination, that make it very challenging to study aggregation over time periods of this length.

One can also observe (**Figure 31**) that the maximal fluorescence amplitude at similar peptide concentrations and the same fluorescence gain is significantly lower for GLP-1-Am compared to the GLP-1, even when the stable plateau was reached for both peptides (and all monomeric peptide was depleted). Also, the lower fluorescence of the plateau, the longer the aggregation takes (**Figure 31B**).This suggests either lower binding of ThT to the GLP-1-Am fibrils at neutral and basic pH, for example due to the different morphology of fibrils, or a possible difference in the structure of bound ThT that affects its fluorescence, or the presence of a large amount of aggregates of a different type that do not bind ThT. Large clusters were apparent on the SEM image at pH 8 (**Chapter 3, Figure 24**), but it was difficult to distinguish whether they are peptide or whether they consist of salts from the buffer. SEM images of pure buffer can be found in **Appendix B**. It is also worth noting that at acidic pH the fluorescence amplitudes in the plateau phase in ThT assays are comparable for GLP-1-Am and GLP-1 at the same concentration.[13]

Therefore, we hypothesise that there may be a different aggregation process competing with the fibrillation process. This was already suggested for the unusual aggregation behaviour of GLP-1 at pH 7.5, where the lag time increases with the increasing peptide concentration, which is opposite to the usually observed trend in fibrillation processes following the nucleation-polymerization mechanism.[12] This difference was attributed to the formation of off-pathway oligomeric species together with a slow, unimolecular step of monomer conversion to a different monomeric form that forms on-pathway oligomers and eventually fibrils.[12] Similar types of off-pathway behaviour have been already reported for other proteins, e.g. for ribosomal protein S6[124] or immunoglobulin light chain where the decrease in fibrillation propensity with the increasing concentration was explained by dimer formation.[125] At pH 6.4, liraglutide (lipidated form of GLP-1) also shows more rapid fibrillation as the concentration decreases.[26] The presence of off-pathway species in the aggregation of both GLP-1 and GLP-1-Am is

consistent with the finding that at pH 8.2 high concentrations of GLP-1-Am did not show any or only a very slow rate of aggregation (**Chapter 4, Figure 26**).

One should also take into account that for pH 8, the 25 mM sodium phosphate buffer was used, whereas for pH 8.2 and 8.5 the 25 mM Tris buffer was used. Not only it is possible that the buffer itself leads to (de)stabilization of different species,[44–46] but the ionic strength of the buffers also differs greatly. For the 25 mM sodium phosphate buffer at pH 8 the ionic strength is 71 mM while for the 25 mM Tris buffer it is only 7 mM at pH 8.2 (at 37 °C) and 4 mM at pH 8.5 (at 37 °C). In other systems, it was shown that ionic strength can also significantly alter the aggregation behaviour.[27,28] A possible solution of this problem can be modulation of the ionic strength by addition of sodium chloride to keep the ionic strength constant at different values of pH. On the other hand, in this approach, the influence of the chloride anion (the Hofmeister effect) may appear as well.[54,58] Previous studies on GLP-1 conducted in our group showed that there is only a slight effect of the ionic strength on GLP-1 aggregation at pH 3.5 (when ionic strength was altered by addition of NaCl), more significant changes were observed at pH 8.2 when samples were incubated with 1% Tween® 80 in different concentrations of NaCl.[126]

Studying aggregation behaviour of GLP-1-Am at higher pH values than 8.5 may provide a better insight into its aggregation mechanism, however, at very basic pH values a higher propensity of peptides and proteins to deamidation has been observed,[24] which would largely complicate the description of the aggregation process by introducing multiple chemically different monomeric or oligomeric peptide species. Moreover, the rate of ThT hydroxylation (degradation) is significantly higher at high pH, which complicates the interpretation of ThT kinetic curves.[122] Therefore, studies at pH > 8.5 were not undertaken.

Whereas most peptides are most prone to aggregation close to their isoelectric point,[40,42] both GLP-1 and its amide show an aggregation minimum around their pI values as was shown here and in previous studies conducted by our group.[13] For GLP-1, the pI was measured to be 5.9 while GLP-1-Am has a pI around 6.8. The main difference between the two is that GLP-1-Am has a much broader minimum in aggregation propensity around its isoelectric point.[13] The aggregation of GLP-1-Am at neutral basic pH (i.e. 7–8.5) is much slower than at acidic pH (3.5–5.5)[13]. Nevertheless, even under these conditions GLP-1-Am eventually forms amyloid fibrils as was shown in this Thesis.

5.2 GLP-1-Am forms small soluble oligomers at pH from 7 to 8.5

At all studied pH values (from 7 to 8.5), small soluble oligomers were detected during the aggregation reaction. When analysed on an SEC column in the same phosphate elution buffer, the oligomeric species had the same elution volumes regardless of the incubation buffer (Tris *versus* phosphate buffer, **Chapter 3, Figure 12** and **Chapter 4, Figure 27**). Therefore, it can be assumed that the oligomeric species formed over the pH range 7–8.5 are of the same size.

However, samples incubated in Tris buffer (25 mM at pH 8.2 or 8.5) which were subsequently analysed on SEC using the a Tris buffer at the same pH (at the analysis temperature), a large shift in elution volumes (**Figure 27**) of both the monomer and the oligomeric species was observed compared with the elution in 25 mM phosphate buffer at pH 8. A similar shift was previously observed when these buffers were used for the SEC analysis of GLP-1.[12] It is important to note the different ionic strength of the elution buffers. For the phosphate buffer (25 mM at pH 8) the ionic strength was 71 mM whereas for the Tris buffer it was only 11 mM (pH 8.2, at 25 °C) and 7 mM (pH 8.5 at 25 °C). For other proteins analysed on a Superose 12 SEC column, it has been shown that the ionic strength significantly alters the elution profile.[123] A Tris buffer of such a low ionic strength (11 mM or 7 mM) is not ideal for elution since the possible electrostatic interactions between peptide molecules and the column matrix are not suppressed. To ensure ideal elution conditions, a weak salting-out electrolyte, such as sodium chloride, should be added to the buffer. Superose 12 has a residual negative charge and for pH values above the pI (of the eluted peptide) the peptide and the column matrix have the same charge. It leads to a repulsive electrostatic interaction and earlier elution (so called ion-exclusion effect).[123]

During the incubation of GLP-1 and GLP-1-Am in 25 mM sodium phosphate buffer at pH 8, only GLP-1-Am formed small soluble oligomers. Both GLP-1 and GLP-1-Am formed large insoluble aggregates (presumably fibrils) under these conditions. In the GLP-1 SEC, elution profiles, only a depletion of monomer was observed without detecting any other soluble species formed during the aggregation reaction.

These observations suggest that either GLP-1 is less prone to oligomerization or that the GLP-1 oligomers are less stable and therefore not detectable by SEC. Amidation of the C-terminus may stabilise the oligomeric structure by reducing unfavourable electrostatic interactions in the oligomer. The net charge of GLP-1-Am is approximately 0 at pH 8, whereas the net charge of GLP-1 is -1. The plot illustrating dependence of the net charge of GLP-1 and GLP-1-Am on pH with highlighted ionizable residues can be found in **Appendix D**. The fact that the

fibrillation of GLP-1 proceeds much faster than for GLP-1-Am may also contribute. If the monomer is already largely incorporated in the fibril structure (which generally is very stable), only a small fraction of monomers is available for oligomerisation. The main, and still unsolved, question is whether the oligomerisation observed by SEC is the reason for, or a consequence of, the low rate of fibrillation and the rather unusual aggregation profiles (**Figure 31**) of GLP-1-Am at pH 8, 8.2 and 8.5. The formation of the off-pathway oligomers is generally considered as the reason of slower aggregation kinetics since they limit the concentration of the monomer available for fibril formation. As the monomer gets depleted by fibrillation, off-pathway oligomers release monomers back into the solution to preserve the equilibrium a thus slow down the fibrillation process. Therefore, it is possible that observed oligomers are off-pathway products.

A pH-dependent oligomerisation has been reported in a similar system liraglutide, a lipidated derivative of GLP-1.[26,27] It was found that liraglutide forms either a 7-mer or a 13-mer depending on the pH. Liraglutide contains a fatty acid moiety (attached to GLP-1 at lysine 20) that was found to noticeably contribute to the stability of the oligomers.[127] In the case of GLP-1-Am, a simple amidation of the C-terminus may play a similar role as the fatty acid in liragluratide, and thus stabilise the oligomer by decreasing electrostatic repulsion. At pH 6.4, liraglutide shows a slower fibrillation rate at higher peptide concentrations as opposed to lower concentrations.[26] This is also in agreement with the behaviour observed for GLP-1-Am at pH 8.2 described here (**Chapter 4, Figure 26**).

At this pH, GLP-1-Am oligomerization was also observed when the peptide was incubated in 1% Tween® 20 (in 25 mM sodium phosphate buffer pH 8). The addition of 1% Tween® 20 slowed the formation of large insoluble aggregates but promoted oligomerisation (**Chapter 3, Figure 23**). This effect has been reported in the literature for other proteins as well.[120,121] It was suggested that Tween® 20 in a sufficiently large concentration may stabilise some intermediate states, and therefore shift the equilibrium of aggregation. It could also function similarly to the attached fatty acid in liraglutide, and form micelle-like self-assemblies of peptide monomers. The size of the observed oligomers in Tween® 20 (**Chapter 3, Figure 23**) has not been determined since Tween® 20 can alter the elution conditions on the SEC column and consequently the elution profile. A proper calibration of a SEC column under these conditions would be needed and it is worth reconsidering the choice of the elution buffer, e.g. buffer with addition of sodium chloride in order to increase the ionic strength of the eluent and suppress possible electrostatic and hydrophobic interactions.

5.3 GLP-1-Am oligomers are stable with respect to time, temperature and organic solvents

Over the range of pH values studied in this work (7–8.5) protein oligomers showed a remarkable stability with respect to time, temperature, sonication and addition of organic solvents (**Chapters 3** and **4, Figures 17** and **28**). The formation of these small oligomers is quite slow, at least at pH 8, where oligomers start to be detectable by SEC after 48 hours (**Figure 12**). At higher pH, the formation of oligomers seems to be faster, however, the exact kinetic parameters were not quantified. The oligomerisation rate may also be highly dependent on the peptide concentration.

The remarkably high observed stability suggests either that the oligomers are largely thermodynamically favoured or that their formation is irreversible. An irreversible formation can occur, for instance, if observed oligomers are chemically modified degradation products or covalently linked monomers. However, GLP-1-Am does not have any cysteine residues which excludes any linkage *via* disulphide bridges. Linkage via other residues (e.g. tyrosine) is possible but much less probable.[128,129] It was also shown that some modifications of the amino acids side chains can cause an elution shift on SEC, for example tryptophan oxidation.[130] Therefore, confirmation of the oligomer size by other methods is needed. On the other hand, the isolated oligomers were completely denatured during an SDS-PAGE (**Figure 18**) and a partial denaturation occurred during incubation with 30 or 40% acetonitrile in the solution (**Figure 17** and **28**). These results suggest a non-covalent character of the oligomers, but cannot fully exclude the possibility of chemical degradation of the peptide.

Very stable small peptide oligomers have already been reported in the literature. In the case of the Aβ peptide, α-synuclein or the islet amyloid polypeptide, formation of small, stable off-pathway (not forming fibrils) oligomers is promoted by addition of small organic molecules (e.g. polyphenols).[131,132] Irreversible or almost irreversible dimerization was observed in the Aβ peptide incubated under physiological conditions.[81,133] In some cases these oligomers were resistant to further fibrillation. Stable small oligomers of GLP-1 or GLP-1 analogues have been previously reported as well.[134,135]

It could be worth testing the stability of the already pre-formed oligomers of GLP-1-Am in acidic pH, since at acidic pH GLP-1-Am fibrillation is significantly faster. For liraglutide, the equilibrium of the oligomer formation was found to be fully reversible upon changes of pH.[27]

5.4 GLP-1-Am oligomers have disordered structure

Extracting structural information from the CD spectra of aggregating samples is not straightforward, since there are multiple species present, and each contributes to the overall spectrum, **Figure 19**. Moreover, the ratio of the species is changing during the aggregation process. To obtain more information, individual chemical species (monomer, oligomers, fibrils) were separated from the aggregating mixture and analysed in isolation.

Oligomeric species, isolated using SEC, formed both in phosphate buffer (pH 7–8) and in Tris buffer (pH 8.2 or 8.5) showed the same structural features. Far-UV CD spectra of the oligomeric species (**Chapter 3** and **4**, **Figure 19** and **29**) show only one broad minimum at around 200 nm corresponding to a highly disordered structure. The formation of these oligomers is, therefore, accompanied by a partial loss of the secondary structure present in the monomeric peptide. The oligomers (similarly to the monomer) do not show any signal in the near-UV CD spectra in contrast to the fibrils, which show two positive peaks at approximately 292 and 285 nm, and a shoulder at around 280 nm.

The structural information obtained from CD spectroscopy agrees with the findings from intrinsic tryptophan fluorescence emission spectra. Intrinsic tryptophan fluorescence maximum of oligomers showed a red-shift from 353 nm to 360–361 nm relative to the monomeric form, which indicates a greater exposure of the tryptophan residue to the solvent and thus a more unfolded structure. Despite the probably more exposed hydrophobic patches (e.g. tryptophan), binding of ANS to the oligomers was not observed. This can be explained by the fact, that these oligomers are too small to have a suitable cluster of exposed hydrophobic residues that would enable ANS binding. Oligomers also do not bind ThT which is in agreement with the absence of any β-sheet structure. This provides a possible explanation of why significantly lower ThT fluorescence is observed even in the plateau phase under certain conditions. In these cases, the aggregating samples could have contained oligomers (no ThT binding) and fibrils (binding ThT) even when they reached the equilibrium and therefore have a lower fluorescence signal than samples where all the monomer has converted into fibrils.

Potential toxicity of oligomers

The structure and the size of oligomers of amylogenic proteins and peptides detected during aggregation is diverse (from disordered to β-sheet) and it is difficult to predict their toxicity.[117] Generally, it has been observed that increased cell toxicity is linked with small hydrophobic residues on the surface of the oligomers as this may facilitate undesirable interactions with the

lipid bilayers of biological membranes.[1,83–85,136] However, these features were observed mainly in peptides and proteins responsible for neurodegenerative diseases and extrapolation of these findings to the oligomers of GLP-1-Am may not be justified. Nevertheless, the potential cytotoxicity of GLP-1-Am oligomers should be assessed.

5.5 Effect of oligomer formation on fibrillation

There are many questions arising from these results. How do the oligomers affect the fibrillation process? Are they an alternative form of aggregates coexisting with the fibrils or are they formed as an intermediate on the fibrillation pathway and subsequently misfold? Are oligomerisation and fibrillation dependent on each other? The exact role of these small soluble disordered aggregates in fibrillation requires further investigation but the current results give us a strong platform from which to investigate this further.

At pH 8.2 and 8.5, a very low fibrillation rate was observed at higher GLP-1-Am concentrations (150 µM, 125 µM), while at lower peptide concentrations fibrillation proceeds faster (**Figure 25 and 26**). Samples of all peptide concentrations contained small soluble oligomers (the exact fraction was not quantified). The observed concentration dependence of fibrillation is not consistent with a classical nucleation-polymerization mechanism, and, therefore, it is likely that oligomers affect fibrillation kinetics and that some of the oligomers formed are off-pathway. These findings can be further explored by seeded assays, where pre-formed oligomers are used as ‘seeds’, and/or by exact quantification of the fraction of oligomers formed for each peptide concentration.

Chapter 6
Conclusions and future work

6.1 Conclusions

In this work, the aggregation behaviour of a C-terminally amidated analogue of GLP-1, was investigated over the pH range 7–8.5. It was shown that between pH 7 and 8 the aggregation rate is low and fibrillation proceeds slowly compared to the non-amidated GLP-1 under the same conditions. Above pH 8, aggregation also has long lag times of over 60 hours. Generally, at pH above 8, there is a large variation in the kinetic parameters (lag times, *k*, *A*), and thus poor reproducibility between equivalent measurements. Interestingly, at high peptide concentrations (150 µM, 125 µM) samples do not show any significant fibrillation compared to that observed at lower concentrations, at least over the time range studied.

Over the studied pH range (7–8.5),formation of small soluble oligomers of GLP-1-Am was detected during aggregation. These oligomers were found to be highly stable with respect to time, temperature and sonication. However, they were partly denatured when incubated in 30% or 40% acetonitrile and completely denatured during an SDS-PAGE experiment. According to analytical SEC, the size of the oligomers formed is in the range from 6.7 kDa to 13 kDa corresponding to peptide dimers to tetramers. The structure of the oligomeric species is highly disordered. The oligomer formation was accompanied by loss of some of the secondary structure present in the monomer, as was shown by multiple probes. Intrinsic tryptophan fluorescence emission spectra also show higher exposure of the tryptophan residue to the solvent than in the monomeric structure (or in fibrils). This indicates that the structure of the oligomers is less tightly packed and that hydrophobic patches are more accessible to the solvent. It was also shown that the oligomers do not bind ThT or ANS fluorescent dyes. This is probably caused by their small size and the absence of any β-sheet structure. GLP-1-Am oligomers usually coexist in an equilibrium with the monomer and fibrils (and possibly other insoluble aggregates); however, they do not dissociate or further aggregate when separated from other species. Formation of soluble oligomers was also detected when GLP-1-Am samples were incubated in phosphate buffer at pH 8 with addition of 1% (v/v) Tween® 20. The size and structure of these oligomers appears to be different from those observed in the absence of Tween® 20 and will be subject to further research.

Elucidation of the exact role of the small soluble species in the fibrillation process certainly requires further investigation. The fact that peptide fibrillation is suppressed at higher peptide concentrations (at pH 8.2 and 8.5) and that these samples contain a high percentage of oligomers and monomers could imply that oligomerisation and fibrillation rates are mutually dependent and off-pathway species play a significant role under these conditions.

6.2 Future work

First, it is essential to confirm the size of the oligomeric species by a more precise method, e.g. native mass spectrometry. It would also be useful to test the oligomeric samples using liquid chromatography-mass spectrometry. This could definitely exclude a covalent linkage of the oligomers and reveal any potential chemical degradation of the peptide that might precede the formation of oligomers.

It is also worth investigating whether this type of oligomeric species can also form at acidic pH and whether a pre-formed oligomer would be stable under such conditions. The aggregation of GLP-1-Am has been studied at low pH by ThT assay[13], but no SEC analysis to detect or quantify oligomers has been performed. Incubation of samples with the addition of a small percentage of organic solvent or at a higher temperature can also shift the equilibrium between fibrils and oligomers. Therefore, it is also needed to quantify the percentage of oligomers formed under different conditions (peptide concentration, ionic strength etc.) in order to better understand what role they play in the fibrillation process. Seeded assays with pre-formed oligomers can also help with examining the role of oligomers in aggregation or any effect they may have.

An interesting question arises from the results of this work regarding the remarkable stability of the oligomers. What is the reason of the stability of such small oligomers? Can they dissociate back into the monomers, or can they form some type of higher-order aggregates? What is the role of the amidation in the stabilisation of these oligomers?

Many studies have highlighted the cytotoxicity of oligomeric species.[82–85,136] Since various analogues of GLP-1 are used as therapeutic drugs, the threat of potential toxicity should be carefully examined. It should also be investigated whether oligomerization does indeed inhibit the binding of the peptide to the GLP-1 receptor as is expected.

Chapter 7
References

(1) Chiti, F.; Dobson, C. M. Protein Misfolding, Amyloid Formation, and Human Disease: A Summary of Progress Over the Last Decade. *Annu. Rev. Biochem.* **2017**, *86* (1), 27–68. https://doi.org/10.1146/annurev-biochem-061516-045115.

(2) Dobson, C. M.; Knowles, T. P. J.; Vendruscolo, M. The Amyloid Phenomenon and Its Significance in Biology and Medicine. *Cold Spring Harb. Perspect. Biol.* **2019**, a033878. https://doi.org/10.1101/cshperspect.a033878.

(3) Paslawski, W.; Lorenzen, N.; Otzen, D. E. *Protein Amyloid Aggregation*; Eliezer, D., Ed.; Methods in Molecular Biology; Springer New York: New York, NY, 2016; Vol. 1345. https://doi.org/10.1007/978-1-4939-2978-8.

(4) Thal, D. R.; Walter, J.; Saido, T. C.; Fändrich, M. Neuropathology and Biochemistry of Aβ and Its Aggregates in Alzheimer's Disease. *Acta Neuropathologica*. February 23, 2015, pp 167–182. https://doi.org/10.1007/s00401-014-1375-y.

(5) Benilova, I.; Karran, E.; De Strooper, B. The Toxic Aβ Oligomer and Alzheimer's Disease: An Emperor in Need of Clothes. *Nat. Neurosci.* **2012**, *15* (3), 349–357. https://doi.org/10.1038/nn.3028.

(6) Zapadka, K. L.; Becher, F. J.; Gomes dos Santos, A. L.; Jackson, S. E. Factors Affecting the Physical Stability (Aggregation) of Peptide Therapeutics. *Interface Focus* **2017**, *7* (6), 20170030. https://doi.org/10.1098/rsfs.2017.0030.

(7) Chiti, F.; Dobson, C. M. Protein Misfolding, Amyloid Formation, and Human Disease: A Summary of Progress Over the Last Decade. *Annu. Rev. Biochem.* **2017**, *86* (1), 27–68. https://doi.org/10.1146/annurev-biochem-061516-045115.

(8) Gade Malmos, K.; Blancas-Mejia, L. M.; Weber, B.; Buchner, J.; Ramirez-Alvarado, M.; Naiki, H.; Otzen, D. ThT 101: A Primer on the Use of Thioflavin T to Investigate Amyloid Formation. *Amyloid* **2017**, *24* (1), 1–16. https://doi.org/10.1080/13506129.2017.1304905.

(9) Kaspar, A. A.; Reichert, J. M. Future Directions for Peptide Therapeutics Development. *Drug Discov. Today* **2013**, *18* (17–18), 807–817. https://doi.org/10.1016/j.drudis.2013.05.011.

(10) Fosgerau, K.; Hoffmann, T. Peptide Therapeutics: Current Status and Future Directions. *Drug Discov. Today* **2015**, *20* (1), 122–128. https://doi.org/10.1016/j.drudis.2014.10.003.

(11) Lau, J. L.; Dunn, M. K. Therapeutic Peptides: Historical Perspectives, Current Development Trends, and Future Directions. *Bioorg. Med. Chem.* **2018**, *26* (10), 2700–2707. https://doi.org/10.1016/j.bmc.2017.06.052.

(12) Zapadka, K. L.; Becher, F. J.; Uddin, S.; Varley, P. G.; Bishop, S.; Gomes dos Santos, A. L.; Jackson, S. E. A pH-Induced Switch in Human Glucagon-Like Peptide-1 Aggregation Kinetics. *J. Am. Chem. Soc.* **2016**, *138* (50), 16259–16265. https://doi.org/10.1021/jacs.6b05025.

(13) Becher, F. J.; Santos, A.; Jackson, S. E. The Influence of C-Terminal Amidation on the Physical Stability of GLP-1.*Unpublished work*.

(14) Glaesner, W.; Millican, R. L.; Mark, A.; Vick, A. M. GLP-1 Analog Fusion Proteins. US 7.452,966 B2, 2008.

(15) Sheridan, C. Proof of Concept for Next-Generation Nanoparticle Drugs in Humans. *Nat. Biotechnol.* **2012**, *30*, 471.

(16) Steidler, L.; Rottiers, P.; Coulie, B. Actobiotics™ as a Novel Method for Cytokine Delivery: The Interleukin-10 Case. In *Annals of the New York Academy of Sciences*; 2009; Vol. 1182, pp 135–145. https://doi.org/10.1111/j.1749-6632.2009.05067.x.

(17) Wakankar, A. A.; Borchardt, R. T. Formulation Considerations for Proteins Susceptible to Asparagine Deamidation and Aspartate Isomerization. *Journal of Pharmaceutical Sciences*. Elsevier November 1, 2006, pp 2321–2336. https://doi.org/10.1002/jps.20740.

(18) Torosantucci, R.; Schöneich, C.; Jiskoot, W. Oxidation of Therapeutic Proteins and Peptides: Structural and Biological Consequences. *Pharm. Res.* **2014**, *31* (3), 541–553. https://doi.org/10.1007/s11095-013-1199-9.

(19) Ji, J. A.; Zhang, B.; Cheng, W.; Wang, Y. J. Methionine, Tryptophan, and Histidine Oxidation in a Model Protein, PTH: Mechanisms and Stabilization. *J. Pharm. Sci.* **2009**, *98* (12), 4485–4500. https://doi.org/10.1002/jps.21746.

(20) Wang, W. Instability, Stabilization, and Formulation of Liquid Protein Pharmaceuticals. *International Journal of Pharmaceutics*. August 1999, pp 129–188. https://doi.org/10.1016/S0378-5173(99)00152-0.

(21) Bao, W.; Holt, L. J.; Prince, R. D.; Jones, G. X.; Aravindhan, K.; Szapacs, M.; Barbour, A. M.; Jolivette, L. J.; Lepore, J. J.; Willette, R. N.; et al. Novel Fusion of GLP-1 with a Domain Antibody to Serum Albumin Prolongs Protection against Myocardial Ischemia/Reperfusion Injury in the Rat. *Cardiovasc. Diabetol.* **2013**, *12* (1), 148. https://doi.org/10.1186/1475-2840-12-148.

(22) Houston, M. E.; Campbell, A. P.; Lix, B.; Kay, C. M.; Sykes, B. D.; Hodges, R. S. Lactam Bridge Stabilization of α-Helices: The Role of Hydrophobicity in Controlling Dimeric versus Monomeric α-Helices. *Biochemistry* **1996**, *35* (31), 10041–10050. https://doi.org/10.1021/bi952757m.

(23) Sim, S.; Kim, Y.; Kim, T.; Lim, S.; Lee, M. Directional Assembly of α-Helical Peptides Induced by Cyclization. *J. Am. Chem. Soc.* **2012**, *134* (50), 20270–20272. https://doi.org/10.1021/ja3098756.

(24) Knudsen, L. B. Liraglutide: The Therapeutic Promise from Animal Models. *Int. J. Clin. Pract.* **2010**, *64* (SUPPL. 167), 4–11. https://doi.org/10.1111/j.1742-1241.2010.02499.x.

(25) Gilroy, C. A.; Luginbuhl, K. M.; Chilkoti, A. Controlled Release of Biologics for the Treatment of Type 2 Diabetes. *J. Control. Release* **2016**, *240*, 151–164. https://doi.org/10.1016/j.jconrel.2015.12.002.

(26) Bothe, J. R.; Andrews, A.; Smith, K. J.; Joyce, L. A.; Krishnamachari, Y.; Kashi, S. Peptide Oligomerization Memory Effects and Their Impact on the Physical Stability of the GLP-1 Agonist Liraglutide. *Mol. Pharm.* **2019**, *16* (5), 2153–2161. https://doi.org/10.1021/acs.molpharmaceut.9b00106.

(27) Wang, Y.; Lomakin, A.; Kanai, S.; Alex, R.; Benedek, G. B. Transformation of Oligomers of Lipidated Peptide Induced by Change in pH. *Mol. Pharm.* **2015**, *12* (2), 411–419. https://doi.org/10.1021/mp500519s.

(28) Rezaei-Ghaleh, N.; Amininasab, M.; Kumar, S.; Walter, J.; Zweckstetter, M. Phosphorylation Modifies the Molecular Stability of β-Amyloid Deposits. *Nat. Commun.* **2016**, *7* (1), 11359. https://doi.org/10.1038/ncomms11359.

(29) Rezaei-Ghaleh, N.; Kumar, S.; Walter, J.; Zweckstetter, M. Phosphorylation Interferes with Maturation of Amyloid-β Fibrillar Structure in the N-Terminus. *J. Biol. Chem.* **2016**, *291* (31), 16059–16067. https://doi.org/10.1074/jbc.M116.728956.

(30) Osaki, D.; Hiramatsu, H. Citrullination and Deamidation Affect Aggregation Properties

of Amyloid β -Proteins. *Amyloid* **2016**, *23* (4), 234–241. https://doi.org/10.1080/13506129.2016.1240076.

(31) Guivernau, B.; Bonet, J.; Valls-Comamala, V.; Bosch-Morató, M.; Godoy, J. A.; Inestrosa, N. C.; Perálvarez-Marín, A.; Fernández-Busquets, X.; Andreu, D.; Oliva, B.; et al. Amyloid-β Peptide Nitrotyrosination Stabilizes Oligomers and Enhances NMDAR-Mediated Toxicity. *J. Neurosci.* **2016**, *36* (46), 11693–11703. https://doi.org/10.1523/JNEUROSCI.1081-16.2016.

(32) Xiang, W.; Schlachetzki, J. C. M.; Helling, S.; Bussmann, J. C.; Berlinghof, M.; Schäffer, T. E.; Marcus, K.; Winkler, J.; Klucken, J.; Becker, C. M. Oxidative Stress-Induced Posttranslational Modifications of Alpha-Synuclein: Specific Modification of Alpha-Synuclein by 4-Hydroxy-2-Nonenal Increases Dopaminergic Toxicity. *Mol. Cell. Neurosci.* **2013**, *54*, 71–83. https://doi.org/10.1016/j.mcn.2013.01.004.

(33) Bae, E.-J.; Ho, D.-H.; Park, E.; Jung, J. W.; Cho, K.; Hong, J. H.; Lee, H.-J.; Kim, K. P.; Lee, S.-J. Lipid Peroxidation Product 4-Hydroxy-2-Nonenal Promotes Seeding-Capable Oligomer Formation and Cell-to-Cell Transfer of α-Synuclein. *Antioxid. Redox Signal.* **2013**, *18* (7), 770–783. https://doi.org/10.1089/ars.2011.4429.

(34) Fernandez-Escamilla, A.-M.; Rousseau, F.; Schymkowitz, J.; Serrano, L. Prediction of Sequence-Dependent and Mutational Effects on the Aggregation of Peptides and Proteins. *Nat. Biotechnol.* **2004**, *22* (10), 1302–1306. https://doi.org/10.1038/nbt1012.

(35) Galzitskaya, O. V.; Garbuzynskiy, S. O.; Lobanov, M. Y. Prediction of Amyloidogenic and Disordered Regions in Protein Chains. *PLoS Comput. Biol.* **2006**, *2* (12), e177. https://doi.org/10.1371/journal.pcbi.0020177.

(36) Trovato, A.; Seno, F.; Tosatto, S. C. E. The PASTA Server for Protein Aggregation Prediction. *Protein Eng. Des. Sel.* **2007**, *20* (10), 521–523. https://doi.org/10.1093/protein/gzm042.

(37) Conchillo-Solé, O.; de Groot, N. S.; Avilés, F. X.; Vendrell, J.; Daura, X.; Ventura, S. AGGRESCAN: A Server for the Prediction and Evaluation of "Hot Spots" of Aggregation in Polypeptides. *BMC Bioinformatics* **2007**, *8* (1), 65. https://doi.org/10.1186/1471-2105-8-65.

(38) Sormanni, P.; Aprile, F. A.; Vendruscolo, M. The CamSol Method of Rational Design of Protein Mutants with Enhanced Solubility. *J. Mol. Biol.* **2015**, *427* (2), 478–490. https://doi.org/10.1016/j.jmb.2014.09.026.

(39) Thompson, M. J.; Sievers, S. A.; Karanicolas, J.; Ivanova, M. I.; Baker, D.; Eisenberg, D. The 3D Profile Method for Identifying Fibril-Forming Segments of Proteins. *Proc. Natl. Acad. Sci.* **2006**, *103* (11), 4074–4078. https://doi.org/10.1073/pnas.0511295103.

(40) Marshall, K. E.; Morris, K. L.; Charlton, D.; O'Reilly, N.; Lewis, L.; Walden, H.; Serpell, L. C. Hydrophobic, Aromatic, and Electrostatic Interactions Play a Central Role in Amyloid Fibril Formation and Stability. *Biochemistry* **2011**, *50* (12), 2061–2071. https://doi.org/10.1021/bi101936c.

(41) Kamihira, M.; Oshiro, Y.; Tuzi, S.; Nosaka, A. Y.; Saitô, H.; Naito, A. Effect of Electrostatic Interaction on Fibril Formation of Human Calcitonin as Studied by High Resolution Solid State 13C NMR. *J. Biol. Chem.* **2003**, *278* (5), 2859–2865. https://doi.org/10.1074/jbc.M205285200.

(42) Schmittschmitt, J. P.; Scholtz, J. M. The Role of Protein Stability, Solubility, and Net Charge in Amyloid Fibril Formation. *Protein Sci.* **2009**, *12* (10), 2374–2378. https://doi.org/10.1110/ps.03152903.

(43) Krebs, M. R. H.; Domike, K. R.; Donald, A. M. Protein Aggregation: More than Just Fibrils. *Biochem. Soc. Trans.* **2009**, *37* (4), 682–686.

https://doi.org/10.1042/BST0370682.

(44) Manning, M. C.; Chou, D. K.; Murphy, B. M.; Payne, R. W.; Katayama, D. S. Stability of Protein Pharmaceuticals: An Update. *Pharm. Res.* **2010**, *27* (4), 544–575. https://doi.org/10.1007/s11095-009-0045-6.

(45) Mezzasalma, T. M.; Kranz, J. K.; Chan, W.; Struble, G. T.; Schalk-Hihi, C.; Deckman, I. C.; Springer, B. A.; Todd, M. J. Enhancing Recombinant Protein Quality and Yield by Protein Stability Profiling. *J. Biomol. Screen.* **2007**, *12* (3), 418–428. https://doi.org/10.1177/1087057106297984.

(46) Fayos, R.; Pons, M.; Millet, O. On the Origin of the Thermostabilization of Proteins Induced by Sodium Phosphate. *J. Am. Chem. Soc.* **2005**, *127* (27), 9690–9691. https://doi.org/10.1021/ja051352e.

(47) Kameoka, D.; Masuzaki, E.; Ueda, T.; Imoto, T. Effect of Buffer Species on the Unfolding and the Aggregation of Humanized IgG. *J. Biochem.* **2007**, *142* (3), 383–391. https://doi.org/10.1093/jb/mvm145.

(48) Chen, B.; Bautista, R.; Yu, K.; Zapata, G. A.; Mulkerrin, M. G.; Chamow, S. M. Influence of Histidine on the Stability and Physical Properties of a Fully Human Antibody in Aqueous and Solid Forms. *Pharm. Res.* **2003**, *20* (12), 1952–1960. https://doi.org/10.1023/B:PHAM.0000008042.15988.c0.

(49) Katayama, D. S.; Nayar, R.; Chou, D. K.; Valente, J. J.; Cooper, J.; Henry, C. S.; Vander Velde, D. G.; Villarete, L.; Liu, C. P.; Manning, M. C. Effect of Buffer Species on the Thermally Induced Aggregation of Interferon-Tau. *J. Pharm. Sci.* **2006**, *95* (6), 1212–1226. https://doi.org/10.1002/jps.20471.

(50) Arakava, T.; Philo, J. S.; Kita, Y. Kinetic and Thermodynamic Analysis of Thermal Unfolding of Recombinant Erythropoietin. *Biosci. Biotechnol. Biochem.* **2001**, *65* (6), 1321–1327. https://doi.org/10.1271/bbb.65.1321.

(51) Bottomley, S. P.; Tew, D. J. The Citrate Ion Increases the Conformational Stability of A1-Antitrypsin. *Biochim. Biophys. Acta - Protein Struct. Mol. Enzymol.* **2000**, *1481* (1), 11–17. https://doi.org/10.1016/S0167-4838(00)00118-7.

(52) Raibekas, A. A.; Bures, E. J.; Siska, C. C.; Kohno, T.; Latypov, R. F.; Kerwin, B. A. Anion Binding and Controlled Aggregation of Human Interleukin-1 Receptor Antagonist. *Biochemistry* **2005**, *44* (29), 9871–9879. https://doi.org/10.1021/bi050388g.

(53) Marek, P. J.; Patsalo, V.; Green, D. F.; Raleigh, D. P. Ionic Strength Effects on Amyloid Formation by Amylin Are a Complicated Interplay among Debye Screening, Ion Selectivity, and Hofmeister Effects. *Biochemistry* **2012**, *51* (43), 8478–8490. https://doi.org/10.1021/bi300574r.

(54) Lo Nostro, P.; Ninham, B. W. Hofmeister Phenomena: An Update on Ion Specificity in Biology. *Chem. Rev.* **2012**, *112* (4), 2286–2322. https://doi.org/10.1021/cr200271j.

(55) Hasecke, F.; Miti, T.; Perez, C.; Barton, J.; Schölzel, D.; Gremer, L.; Grüning, C. S. R.; Matthews, G.; Meisl, G.; Knowles, T. P. J.; et al. Origin of Metastable Oligomers and Their Effects on Amyloid Fibril Self-Assembly. *Chem. Sci.* **2018**, *9* (27), 5937–5948. https://doi.org/10.1039/C8SC01479E.

(56) Miti, T.; Mulaj, M.; Schmit, J. D.; Muschol, M. Stable, Metastable, and Kinetically Trapped Amyloid Aggregate Phases. *Biomacromolecules* **2015**, *16* (1), 326–335. https://doi.org/10.1021/bm501521r.

(57) Hofmeister, F. Zur Lehre von Der Wirkung Der Salze. *Arch. für Exp. Pathol. und Pharmakologie* **1888**, *25* (1), 1–30. https://doi.org/10.1007/BF01838161.

(58) Gurau, M. C.; Lim, S.-M.; Castellana, E. T.; Albertorio, F.; Kataoka, S.; Cremer, P. S. On the Mechanism of the Hofmeister Effect. *J. Am. Chem. Soc.* **2004**, *126* (34), 10522–

10523. https://doi.org/10.1021/ja047715c.

(59) Klement, K.; Wieligmann, K.; Meinhardt, J.; Hortschansky, P.; Richter, W.; Fändrich, M. Effect of Different Salt Ions on the Propensity of Aggregation and on the Structure of Alzheimer's Aβ(1-40) Amyloid Fibrils. *J. Mol. Biol.* **2007**, *373* (5), 1321–1333. https://doi.org/10.1016/j.jmb.2007.08.068.

(60) Jain, S.; Udgaonkar, J. B. Salt-Induced Modulation of the Pathway of Amyloid Fibril Formation by the Mouse Prion Protein. *Biochemistry* **2010**, *49* (35), 7615–7624. https://doi.org/10.1021/bi100745j.

(61) Wang, W.; Roberts, C. J. Non-Arrhenius Protein Aggregation. *AAPS J.* **2013**, *15* (3), 840–851. https://doi.org/10.1208/s12248-013-9485-3.

(62) Batzli, K. M.; Love, B. J. Agitation of Amyloid Proteins to Speed Aggregation Measured by ThT Fluorescence: A Call for Standardization. *Mater. Sci. Eng. C* **2015**, *48*, 359–364. https://doi.org/10.1016/j.msec.2014.09.015.

(63) Thomas, C. R.; Geer, D. Effects of Shear on Proteins in Solution. *Biotechnol. Lett.* **2011**, *33* (3), 443–456. https://doi.org/10.1007/s10529-010-0469-4.

(64) Hamilton-Brown, P.; Bekard, I.; Ducker, W. A.; Dunstan, D. E. How Does Shear Affect Aβ Fibrillogenesis? *J. Phys. Chem. B* **2008**, *112* (51), 16249–16252. https://doi.org/10.1021/jp805257n.

(65) O'Nuallain, B.; Williams, A. D.; Westermark, P.; Wetzel, R. Seeding Specificity in Amyloid Growth Induced by Heterologous Fibrils. *J. Biol. Chem.* **2004**, *279* (17), 17490–17499. https://doi.org/10.1074/jbc.M311300200.

(66) Blancas-Mejía, L. M.; Misra, P.; Ramirez-Alvarado, M. Differences in Protein Concentration Dependence for Nucleation and Elongation in Light Chain Amyloid Formation. *Biochemistry* **2017**, *56* (5), 757–766. https://doi.org/10.1021/acs.biochem.6b01043.

(67) Ramirez-Alvarado, M.; Kelly, J. W.; Dobson, C. M. *Protein Misfolding Diseases: Current and Emerging Principles and Therapies*; John Wiley & Sons, 2010.

(68) Chen, S. W.; Drakulic, S.; Deas, E.; Ouberai, M.; Aprile, F. A.; Arranz, R.; Ness, S.; Roodveldt, C.; Guilliams, T.; De-Genst, E. J.; et al. Structural Characterization of Toxic Oligomers That Are Kinetically Trapped during α-Synuclein Fibril Formation. *Proc. Natl. Acad. Sci.* **2015**, *112* (16), E1994–E2003. https://doi.org/10.1073/pnas.1421204112.

(69) Carrió, M.; González-Montalbán, N.; Vera, A.; Villaverde, A.; Ventura, S. Amyloid-like Properties of Bacterial Inclusion Bodies. *J. Mol. Biol.* **2005**, *347* (5), 1025–1037. https://doi.org/10.1016/j.jmb.2005.02.030.

(70) Fowler, D. M.; Koulov, A. V.; Alory-Jost, C.; Marks, M. S.; Balch, W. E.; Kelly, J. W. Functional Amyloid Formation within Mammalian Tissue. *PLoS Biol.* **2005**, *4* (1), e6. https://doi.org/10.1371/journal.pbio.0040006.

(71) Maji, S. K.; Perrin, M. H.; Sawaya, M. R.; Jessberger, S.; Vadodaria, K.; Rissman, R. A.; Singru, P. S.; Nilsson, K. P. R.; Simon, R.; Schubert, D.; et al. Functional Amyloids As Natural Storage of Peptide Hormones in Pituitary Secretory Granules. *Science.* **2009**, *325* (5938), 328–332. https://doi.org/10.1126/science.1173155.

(72) Fowler, D. M.; Koulov, A. V.; Balch, W. E.; Kelly, J. W. Functional Amyloid – from Bacteria to Humans. *Trends Biochem. Sci.* **2007**, *32* (5), 217–224. https://doi.org/10.1016/j.tibs.2007.03.003.

(73) Eisenberg, D. S.; Sawaya, M. R. Structural Studies of Amyloid Proteins at the Molecular Level. *Annu. Rev. Biochem.* **2017**, *86* (1), 69–95. https://doi.org/10.1146/annurev-biochem-061516-045104.

(74) Wasmer, C.; Lange, A.; Van Melckebeke, H.; Siemer, A. B.; Riek, R.; Meier, B. H. Amyloid Fibrils of the HET-s(218-289) Prion Form a β Solenoid with a Triangular Hydrophobic Core. *Science.* **2008**, *319* (5869), 1523–1526. https://doi.org/10.1126/science.1151839.

(75) Paravastu, A. K.; Leapman, R. D.; Yau, W.-M.; Tycko, R. Molecular Structural Basis for Polymorphism in Alzheimer's -Amyloid Fibrils. *Proc. Natl. Acad. Sci.* **2008**, *105* (47), 18349–18354. https://doi.org/10.1073/pnas.0806270105.

(76) Fitzpatrick, A. W. P.; Debelouchina, G. T.; Bayro, M. J.; Clare, D. K.; Caporini, M. A.; Bajaj, V. S.; Jaroniec, C. P.; Wang, L.; Ladizhansky, V.; Muller, S. A.; et al. Atomic Structure and Hierarchical Assembly of a Cross- Amyloid Fibril. *Proc. Natl. Acad. Sci.* **2013**, *110* (14), 5468–5473. https://doi.org/10.1073/pnas.1219476110.

(77) Xiao, Y.; Ma, B.; McElheny, D.; Parthasarathy, S.; Long, F.; Hoshi, M.; Nussinov, R.; Ishii, Y. Aβ(1–42) Fibril Structure Illuminates Self-Recognition and Replication of Amyloid in Alzheimer's Disease. *Nat. Struct. Mol. Biol.* **2015**, *22* (6), 499–505. https://doi.org/10.1038/nsmb.2991.

(78) Cohen, S. I. A.; Linse, S.; Luheshi, L. M.; Hellstrand, E.; White, D. A.; Rajah, L.; Otzen, D. E.; Vendruscolo, M.; Dobson, C. M.; Knowles, T. P. J. Proliferation of Amyloid- 42 Aggregates Occurs through a Secondary Nucleation Mechanism. *Proc. Natl. Acad. Sci.* **2013**, *110* (24), 9758–9763. https://doi.org/10.1073/pnas.1218402110.

(79) Meisl, G.; Yang, X.; Hellstrand, E.; Frohm, B.; Kirkegaard, J. B.; Cohen, S. I. A.; Dobson, C. M.; Linse, S.; Knowles, T. P. J. Differences in Nucleation Behavior Underlie the Contrasting Aggregation Kinetics of the Aβ40 and Aβ42 Peptides. *Proc. Natl. Acad. Sci.* **2014**, *111* (26), 9384–9389. https://doi.org/10.1073/pnas.1401564111.

(80) Chen, S. W.; Drakulic, S.; Deas, E.; Ouberai, M.; Aprile, F. A.; Arranz, R.; Ness, S.; Roodveldt, C.; Guilliams, T.; De-Genst, E. J.; et al. Structural Characterization of Toxic Oligomers That Are Kinetically Trapped during α-Synuclein Fibril Formation. *Proc. Natl. Acad. Sci.* **2015**, *112* (16), E1994–E2003. https://doi.org/10.1073/pnas.1421204112.

(81) Nick, M.; Wu, Y.; Schmidt, N. W.; Prusiner, S. B.; Stöhr, J.; DeGrado, W. F. A Long-Lived Aβ Oligomer Resistant to Fibrillization. *Biopolymers* **2018**, *109* (8), e23096. https://doi.org/10.1002/bip.23096.

(82) Vivoli Vega, M.; Cascella, R.; Chen, S. W.; Fusco, G.; De Simone, A.; Dobson, C. M.; Cecchi, C.; Chiti, F. The Toxicity of Misfolded Protein Oligomers Is Independent of Their Secondary Structure. *ACS Chem. Biol.* **2019**, *14* (7), 1593–1600. https://doi.org/10.1021/acschembio.9b00324.

(83) Bolognesi, B.; Kumita, J. R.; Barros, T. P.; Esbjorner, E. K.; Luheshi, L. M.; Crowther, D. C.; Wilson, M. R.; Dobson, C. M.; Favrin, G.; Yerbury, J. J. ANS Binding Reveals Common Features of Cytotoxic Amyloid Species. *ACS Chem. Biol.* **2010**, *5* (8), 735–740. https://doi.org/10.1021/cb1001203.

(84) Campioni, S.; Mannini, B.; Zampagni, M.; Pensalfini, A.; Parrini, C.; Evangelisti, E.; Relini, A.; Stefani, M.; Dobson, C. M.; Cecchi, C.; et al. A Causative Link between the Structure of Aberrant Protein Oligomers and Their Toxicity. *Nat. Chem. Biol.* **2010**, *6* (2), 140–147. https://doi.org/10.1038/nchembio.283.

(85) Krishnan, R.; Goodman, J. L.; Mukhopadhyay, S.; Pacheco, C. D.; Lemke, E. A.; Deniz, A. A.; Lindquist, S. Conserved Features of Intermediates in Amyloid Assembly Determine Their Benign or Toxic States. *Proc. Natl. Acad. Sci.* **2012**, *109* (28), 11172–11177. https://doi.org/10.1073/pnas.1209527109.

(86) Fu, Z.; Aucoin, D.; Davis, J.; Van Nostrand, W. E.; Smith, S. O. Mechanism of Nucleated

Conformational Conversion of Aβ42. *Biochemistry* **2015**, *54* (27), 4197–4207. https://doi.org/10.1021/acs.biochem.5b00467.

(87) O'Nuallain, B.; Freir, D. B.; Nicoll, A. J.; Risse, E.; Ferguson, N.; Herron, C. E.; Collinge, J.; Walsh, D. M. Amyloid -Protein Dimers Rapidly Form Stable Synaptotoxic Protofibrils. *J. Neurosci.* **2010**, *30* (43), 14411–14419. https://doi.org/10.1523/JNEUROSCI.3537-10.2010.

(88) Bitan, G.; Kirkitadze, M. D.; Lomakin, A.; Vollers, S. S.; Benedek, G. B.; Teplow, D. B. Amyloid -Protein (A) Assembly: A 40 and A 42 Oligomerize through Distinct Pathways. *Proc. Natl. Acad. Sci.* **2003**, *100* (1), 330–335. https://doi.org/10.1073/pnas.222681699.

(89) Chimon, S.; Shaibat, M. A.; Jones, C. R.; Calero, D. C.; Aizezi, B.; Ishii, Y. Evidence of Fibril-like β-Sheet Structures in a Neurotoxic Amyloid Intermediate of Alzheimer's β-Amyloid. *Nat. Struct. Mol. Biol.* **2007**, *14* (12), 1157–1164. https://doi.org/10.1038/nsmb1345.

(90) Matsumura, S.; Shinoda, K.; Yamada, M.; Yokojima, S.; Inoue, M.; Ohnishi, T.; Shimada, T.; Kikuchi, K.; Masui, D.; Hashimoto, S.; et al. Two Distinct Amyloid β-Protein (Aβ) Assembly Pathways Leading to Oligomers and Fibrils Identified by Combined Fluorescence Correlation Spectroscopy, Morphology, and Toxicity Analyses. *J. Biol. Chem.* **2011**, *286* (13), 11555–11562. https://doi.org/10.1074/jbc.M110.181313.

(91) Naiki, H.; Higuchi, K.; Hosokawa, M.; Takeda, T. Fluorometric Determination of Amyloid Fibrils in Vitro Using the Fluorescent Dye, Thioflavine T. *Anal. Biochem.* **1989**, *177* (2), 244–249. https://doi.org/10.1016/0003-2697(89)90046-8.

(92) Knowles, T. P. J.; Waudby, C. A.; Devlin, G. L.; Cohen, S. I. A.; Aguzzi, A.; Vendruscolo, M.; Terentjev, E. M.; Welland, M. E.; Dobson, C. M. An Analytical Solution to the Kinetics of Breakable Filament Assembly. *Science (80-.).* **2009**, *326* (5959), 1533–1537. https://doi.org/10.1126/science.1178250.

(93) Ferrone, F. Analysis of Protein Aggregation Kinetics. *Methods Enzymol.* **1999**, *309*, 256–274. https://doi.org/10.1016/S0076-6879(99)09019-9.

(94) Morris, A. M.; Watzky, M. A.; Finke, R. G. Protein Aggregation Kinetics, Mechanism, and Curve-Fitting: A Review of the Literature. *Biochim. Biophys. Acta - Proteins Proteomics* **2009**, *1794* (3), 375–397. https://doi.org/10.1016/j.bbapap.2008.10.016.

(95) Arosio, P.; Knowles, T. P. J.; Linse, S. On the Lag Phase in Amyloid Fibril Formation. *Phys. Chem. Chem. Phys.* **2015**, *17* (12), 7606–7618. https://doi.org/10.1039/C4CP05563B.

(96) Nielsen, L.; Khurana, R.; Coats, A.; Frokjaer, S.; Brange, J.; Vyas, S.; Uversky, V. N.; Fink, A. L. Effect of Environmental Factors on the Kinetics of Insulin Fibril Formation: Elucidation of the Molecular Mechanism. *Biochemistry* **2001**, *40* (20), 6036–6046. https://doi.org/10.1021/bi002555c.

(97) Buell, A. K.; Galvagnion, C.; Gaspar, R.; Sparr, E.; Vendruscolo, M.; Knowles, T. P. J.; Linse, S.; Dobson, C. M. Solution Conditions Determine the Relative Importance of Nucleation and Growth Processes in -Synuclein Aggregation. *Proc. Natl. Acad. Sci.* **2014**, *111* (21), 7671–7676. https://doi.org/10.1073/pnas.1315346111.

(98) Törnquist, M.; Michaels, T. C. T.; Sanagavarapu, K.; Yang, X.; Meisl, G.; Cohen, S. I. A.; Knowles, T. P. J.; Linse, S. Secondary Nucleation in Amyloid Formation. *Chem. Commun.* **2018**, *54* (63), 8667–8684. https://doi.org/10.1039/c8cc02204f.

(99) Michaels, T. C. T.; Šarić, A.; Habchi, J.; Chia, S.; Meisl, G.; Vendruscolo, M.; Dobson, C. M.; Knowles, T. P. J. Chemical Kinetics for Bridging Molecular Mechanisms and Macroscopic Measurements of Amyloid Fibril Formation. *Annu. Rev. Phys. Chem.* **2018**,

69 (1), 273–298. https://doi.org/10.1146/annurev-physchem-050317-021322.

(100) Galvagnion, C.; Buell, A. K.; Meisl, G.; Michaels, T. C. T.; Vendruscolo, M.; Knowles, T. P. J.; Dobson, C. M. Lipid Vesicles Trigger α-Synuclein Aggregation by Stimulating Primary Nucleation. *Nat. Chem. Biol.* **2015**, *11* (3), 229–234. https://doi.org/10.1038/nchembio.1750.

(101) Wegner, A.; Savko, P. Fragmentation of Actin Filaments. *Biochemistry* **1982**, *21* (8), 1909–1913. https://doi.org/10.1021/bi00537a032.

(102) Aguzzi, A.; Calella, A. M. Prions: Protein Aggregation and Infectious Diseases. *Physiol. Rev.* **2009**, *89* (4), 1105–1152. https://doi.org/10.1152/physrev.00006.2009.

(103) Hokenson, M. J.; Brandt, D.; King, M.; Greene, S.; Faris, M.; Oberg, K.; Cheatham, W. W.; Gelber, C.; Leone-Bay, A. Glucagon-Like Peptide 1 (GLP-1) Pharmaceutical Formulations. US 2008/0260838 A1, 2008.

(104) Graaf, C. de; Donnelly, D.; Wootten, D.; Lau, J.; Sexton, P. M.; Miller, L. J.; Ahn, J.-M.; Liao, J.; Fletcher, M. M.; Yang, D.; et al. Glucagon-Like Peptide-1 and Its Class B G Protein–Coupled Receptors: A Long March to Therapeutic Successes. *Pharmacol. Rev.* **2016**, *68* (4), 954–1013. https://doi.org/10.1124/pr.115.011395.

(105) Holst, J. J. The Physiology of Glucagon-like Peptide 1. *Physiological Reviews*. October 2007, pp 1409–1439. https://doi.org/10.1152/physrev.00034.2006.

(106) Drucker, D. J. The Biology of Incretin Hormones. *Cell Metab.* **2006**, *3* (3), 153–165. https://doi.org/10.1016/j.cmet.2006.01.004.

(107) Lau, J.; Bloch, P.; Schäffer, L.; Pettersson, I.; Spetzler, J.; Kofoed, J.; Madsen, K.; Knudsen, L. B.; McGuire, J.; Steensgaard, D. B.; et al. Discovery of the Once-Weekly Glucagon-Like Peptide-1 (GLP-1) Analogue Semaglutide. *J. Med. Chem.* **2015**, *58* (18), 7370–7380. https://doi.org/10.1021/acs.jmedchem.5b00726.

(108) Cardamone, M.; Puri, N. K. Spectrofluorimetric Assessment of the Surface Hydrophobicity of Proteins. *Biochem. J.* **1992**, *282* (2), 589–593. https://doi.org/10.1042/bj2820589.

(109) Whitmore, L.; Wallace, B. A. DICHROWEB, an Online Server for Protein Secondary Structure Analyses from Circular Dichroism Spectroscopic Data. *Nucleic Acids Res.* **2004**, *32* (Web Server), W668–W673. https://doi.org/10.1093/nar/gkh371.

(110) Whitmore, L.; Wallace, B. A. Protein Secondary Structure Analyses from Circular Dichroism Spectroscopy: Methods and Reference Databases. *Biopolymers* **2008**, *89* (5), 392–400. https://doi.org/10.1002/bip.20853.

(111) Sreerama, N.; Woody, R. W. Estimation of Protein Secondary Structure from Circular Dichroism Spectra: Comparison of CONTIN, SELCON, and CDSSTR Methods with an Expanded Reference Set. *Anal. Biochem.* **2000**, *287* (2), 252–260. https://doi.org/10.1006/abio.2000.4880.

(112) Cochran, A. G.; Skelton, N. J.; Starovasnik, M. A. Tryptophan Zippers: Stable, Monomeric -Hairpins. *Proc. Natl. Acad. Sci.* **2001**, *98* (10), 5578–5583. https://doi.org/10.1073/pnas.091100898.

(113) Wu, L.; McElheny, D.; Huang, R.; Keiderling, T. A. Role of Tryptophan−Tryptophan Interactions in Trpzip β-Hairpin Formation, Structure, and Stability. *Biochemistry* **2009**, *48* (43), 10362–10371. https://doi.org/10.1021/bi901249d.

(114) Huang, R.; Wu, L.; McElheny, D.; Bouř, P.; Roy, A.; Keiderling, T. A. Cross-Strand Coupling and Site-Specific Unfolding Thermodynamics of a Trpzip β-Hairpin Peptide Using 13 C Isotopic Labeling and IR Spectroscopy. *J. Phys. Chem. B* **2009**, *113* (16), 5661–5674. https://doi.org/10.1021/jp9014299.

(115) Biancalana, M.; Koide, S. Molecular Mechanism of Thioflavin-T Binding to Amyloid

Fibrils. *Biochim. Biophys. Acta - Proteins Proteomics* **2010**, *1804* (7), 1405–1412. https://doi.org/10.1016/j.bbapap.2010.04.001.

(116) Younan, N. D.; Viles, J. H. A Comparison of Three Fluorophores for the Detection of Amyloid Fibers and Prefibrillar Oligomeric Assemblies. ThT (Thioflavin T); ANS (1-Anilinonaphthalene-8-Sulfonic Acid); and BisANS (4,4′-Dianilino-1,1′-Binaphthyl-5,5′-Disulfonic Acid). *Biochemistry* **2015**, *54* (28), 4297–4306. https://doi.org/10.1021/acs.biochem.5b00309.

(117) Vivoli Vega, M.; Cascella, R.; Chen, S. W.; Fusco, G.; De Simone, A.; Dobson, C. M.; Cecchi, C.; Chiti, F. The Toxicity of Misfolded Protein Oligomers Is Independent of Their Secondary Structure. *ACS Chem. Biol.* **2019**, acschembio.9b00324. https://doi.org/10.1021/acschembio.9b00324.

(118) Stryer, L. The Interaction of a Naphthalene Dye with Apomyoglobin and Apohemoglobin. *J. Mol. Biol.* **1965**, *13* (2), 482–495. https://doi.org/10.1016/S0022-2836(65)80111-5.

(119) Khan, T. A.; Mahler, H.-C.; Kishore, R. S. K. Key Interactions of Surfactants in Therapeutic Protein Formulations: A Review. *Eur. J. Pharm. Biopharm.* **2015**, *97*, 60–67. https://doi.org/10.1016/j.ejpb.2015.09.016.

(120) Krielgaard, L.; Jones, L. S.; Randolph, T. W.; Frokjaer, S.; Flink, J. M.; Manning, M. C.; Carpenter, J. F. Effect of Tween 20 on Freeze-Thawing- and Agitation-Induced Aggregation of Recombinant Human Factor XIII. *J. Pharm. Sci.* **1998**, *87* (12), 1597–1603. https://doi.org/10.1021/js980126i.

(121) Jones, L. S.; Randolph, T. W.; Kohnert, U.; Papadimitriou, A.; Winter, G.; Hagmann, M.; Manning, M. C.; Carpenter, J. F. The Effects of Tween 20 and Sucrose on the Stability of Anti-L-Selectin during Lyophilization and Reconstitution. *J. Pharm. Sci.* **2001**, *90* (10), 1466–1477. https://doi.org/10.1002/jps.1098.

(122) Foderà, V.; Groenning, M.; Vetri, V.; Librizzi, F.; Spagnolo, S.; Cornett, C.; Olsen, L.; van de Weert, M.; Leone, M. Thioflavin T Hydroxylation at Basic pH and Its Effect on Amyloid Fibril Detection. *J. Phys. Chem. B* **2008**, *112* (47), 15174–15181. https://doi.org/10.1021/jp805560c.

(123) Golovchenko, N. P.; Kataeva, I. A.; Akimenko, V. K. Analysis of pH-Dependent Protein Interactions with Gel Filtration Medium. *J. Chromatogr. A* **1992**, *591* (1–2), 121–128. https://doi.org/10.1016/0021-9673(92)80229-N.

(124) Deva, T.; Lorenzen, N.; Vad, B. S.; Petersen, S. V; Thørgersen, I.; Enghild, J. J.; Kristensen, T.; Otzen, D. E. Off-Pathway Aggregation Can Inhibit Fibrillation at High Protein Concentrations. *Biochim. Biophys. Acta - Proteins Proteomics* **2013**, *1834* (3), 677–687. https://doi.org/10.1016/j.bbapap.2012.12.020.

(125) Souillac, P. O.; Uversky, V. N.; Fink, A. L. Structural Transformations of Oligomeric Intermediates in the Fibrillation of the Immunoglobulin Light Chain LEN. *Biochemistry* **2003**, *42* (26), 8094–8104. https://doi.org/10.1021/bi034652m.

(126) Zapadka, K. L. Understanding the Mechanism of Aggregation and Amyloid Fibril Formation of Glucagon-like Peptide-1, University of Cambridge, 2016.

(127) Frederiksen, T. M.; Sønderby, P.; Ryberg, L. A.; Harris, P.; Bukrinski, J. T.; Scharff-Poulsen, A. M.; Elf-Lind, M. N.; Peters, G. H. Oligomerization of a Glucagon-like Peptide 1 Analog: Bridging Experiment and Simulations. *Biophys. J.* **2015**, *109* (6), 1202–1213. https://doi.org/10.1016/j.bpj.2015.07.051.

(128) Malencik, D. A.; Anderson, S. R. Dityrosine as a Product of Oxidative Stress and Fluorescent Probe. *Amino Acids* **2003**, *25* (3–4), 233–247. https://doi.org/10.1007/s00726-003-0014-z.

(129) Fricano, A.; Librizzi, F.; Rao, E.; Alfano, C.; Vetri, V. Blue Autofluorescence in Protein Aggregates “Lighted on” by UV Induced Oxidation. *Biochim. Biophys. Acta - Proteins Proteomics* **2019**. https://doi.org/10.1016/j.bbapap.2019.07.011.

(130) Yang, J.; Wang, S.; Liu, J.; Raghani, A. Determination of Tryptophan Oxidation of Monoclonal Antibody by Reversed Phase High Performance Liquid Chromatography. *J. Chromatogr. A* **2007**, *1156* (1–2), 174–182. https://doi.org/10.1016/j.chroma.2007.01.140.

(131) Nedumpully-Govindan, P.; Kakinen, A.; Pilkington, E. H.; Davis, T. P.; Chun Ke, P.; Ding, F. Stabilizing Off-Pathway Oligomers by Polyphenol Nanoassemblies for IAPP Aggregation Inhibition. *Sci. Rep.* **2016**, *6* (1), 19463. https://doi.org/10.1038/srep19463.

(132) Ehrnhoefer, D. E.; Bieschke, J.; Boeddrich, A.; Herbst, M.; Masino, L.; Lurz, R.; Engemann, S.; Pastore, A.; Wanker, E. E. EGCG Redirects Amyloidogenic Polypeptides into Unstructured, off-Pathway Oligomers. *Nat. Struct. Mol. Biol.* **2008**, *15* (6), 558–566. https://doi.org/10.1038/nsmb.1437.

(133) Kuo, Y.-M.; Webster, S.; Emmerling, M. R.; De Lima, N.; Roher, A. E. Irreversible Dimerization/Tetramerization and Post-Translational Modifications Inhibit Proteolytic Degradation of Aβ Peptides of Alzheimer’s Disease. *Biochim. Biophys. Acta - Mol. Basis Dis.* **1998**, *1406* (3), 291–298. https://doi.org/10.1016/S0925-4439(98)00014-3.

(134) Takeuchi, M.; Okamoto, M.; Okamoto, R.; Kinoshita, H.; Yamaguchi, Y.; Watanabe, N. Discovery of a Long-Acting Glucagon-like Peptide-1 Analog with Enhanced Aggregation Propensity. *Peptides* **2018**, *102* (December 2017), 8–15. https://doi.org/10.1016/j.peptides.2018.01.014.

(135) Chang, X.; Keller, D.; O’Donoghue, S. I.; Led, J. J. NMR Studies of the Aggregation of Glucagon-like Peptide-1: Formation of a Symmetric Helical Dimer. *FEBS Lett.* **2002**, *515* (1–3), 165–170. https://doi.org/10.1016/S0014-5793(02)02466-3.

(136) Mannini, B.; Mulvihill, E.; Sgromo, C.; Cascella, R.; Khodarahmi, R.; Ramazzotti, M.; Dobson, C. M.; Cecchi, C.; Chiti, F. Toxicity of Protein Oligomers Is Rationalized by a Function Combining Size and Surface Hydrophobicity. *ACS Chem. Biol.* **2014**, *9* (10), 2309–2317. https://doi.org/10.1021/cb500505m.

Appendix A
Aggregation of GLP-1-Am at pH 7 (7.1), 7.5 and 3

A.1 GLP-1-Am ThT aggregation profiles at pH 3 and 7

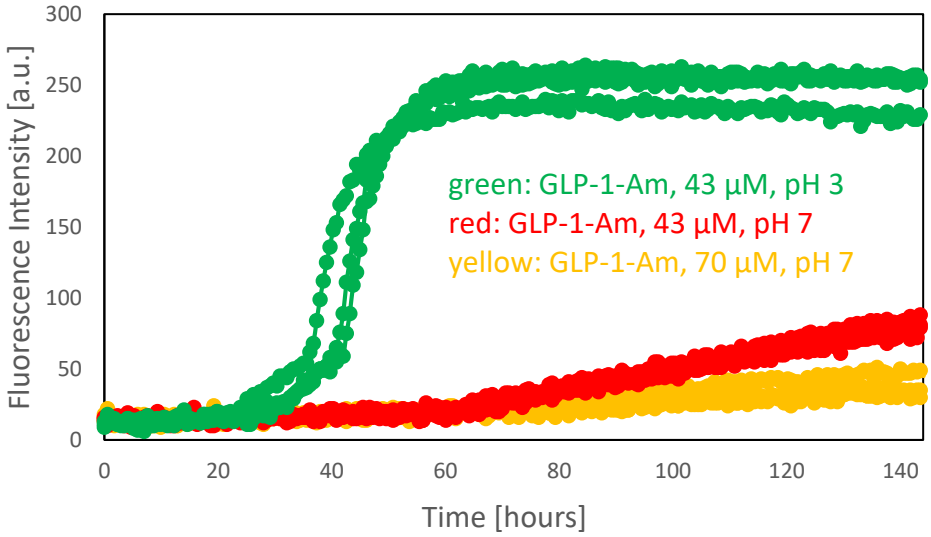

Figure A1: GLP-1-Am ThT aggregation profiles at pH 7 and 3. GLP-1-Am samples of 70 and 43 µM concentration were incubated at 37 °C in 25 mM sodium phosphate buffer at pH 7 and 3, respectively. Runs were done in triplicates.

A.2 GLP-1-Am ThT aggregation profiles at pH 7.5

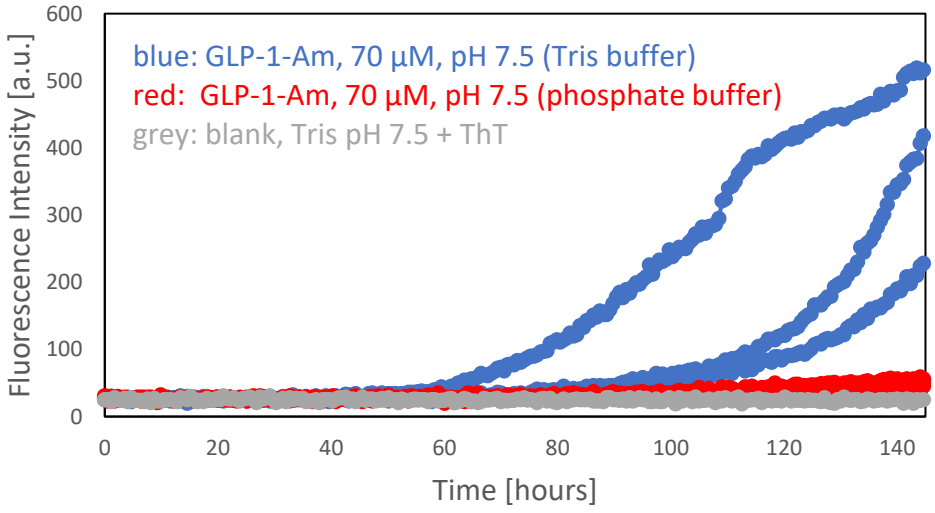

Figure A2: GLP-1-Am ThT aggregation profiles in 25 mM Tris (blue) and phosphate buffer (red) at pH 7.5. GLP-1-Am samples of 70 µM concentration were incubated at 37 °C in the respective buffer. Runs were done in triplicates.

A.3 Comparison of GLP-1 and GLP-1-Am ThT aggregation profiles at pH 7

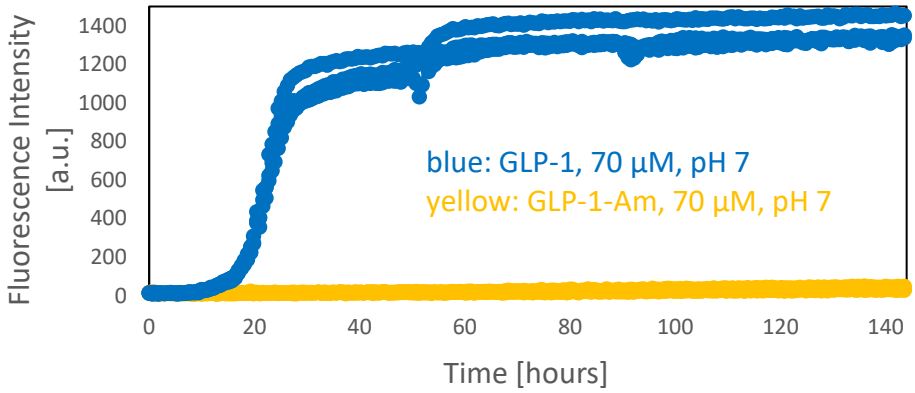

Figure A3: GLP-1-Am and GLP-1 ThT aggregation profiles in 25 mM sodium phosphate buffer at pH 7. GLP-1-Am samples of 70 µM concentration were incubated at 37 °C in the buffer. Runs were done in triplicates.

A.4 SEC analysis of GLP-1-Am incubated at pH 7.1

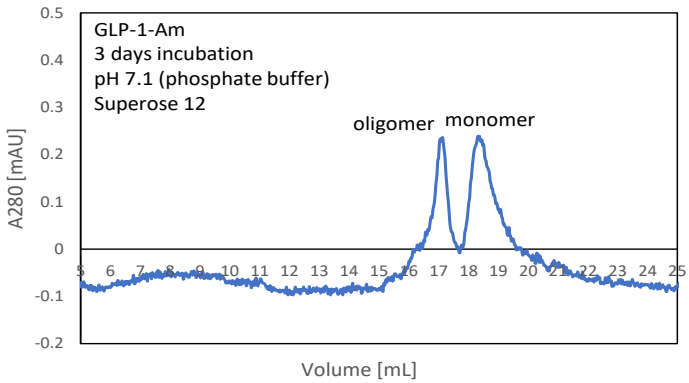

Figure A4: SEC chromatogram of GLP-1-Am at pH 7.1. 40 µM GLP-1-Am after a 3-day incubation in 25 mM phosphate buffer, pH 7.1, at 37 °C with continuous shaking at 80 rpm. Run on a Superose 12 10/300 SEC column.

A.5 SEC analysis of GLP-1-Am incubated at pH 7.5

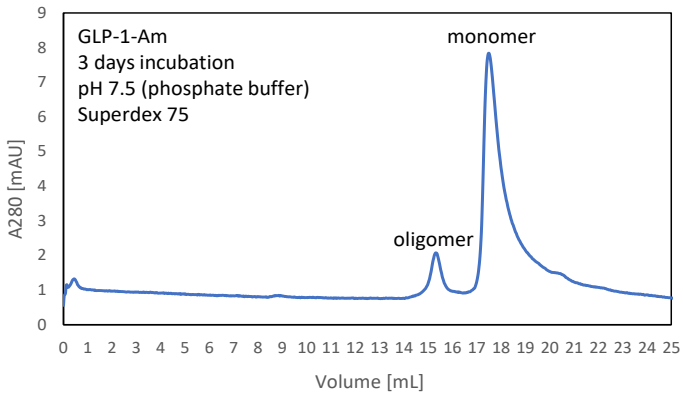

Figure A5: SEC chromatogram of GLP-1-Am at pH 7.5. 85 µM GLP-1-Am after a 3-day incubation in 25 mM phosphate buffer, pH 7.5, at 37 °C with continuous shaking at 80 rpm. Run on a Superdex 75 10/300 SEC column.

Appendix B
SEM images of sodium phosphate buffer

B.1 SEM images of sodium phosphate buffer

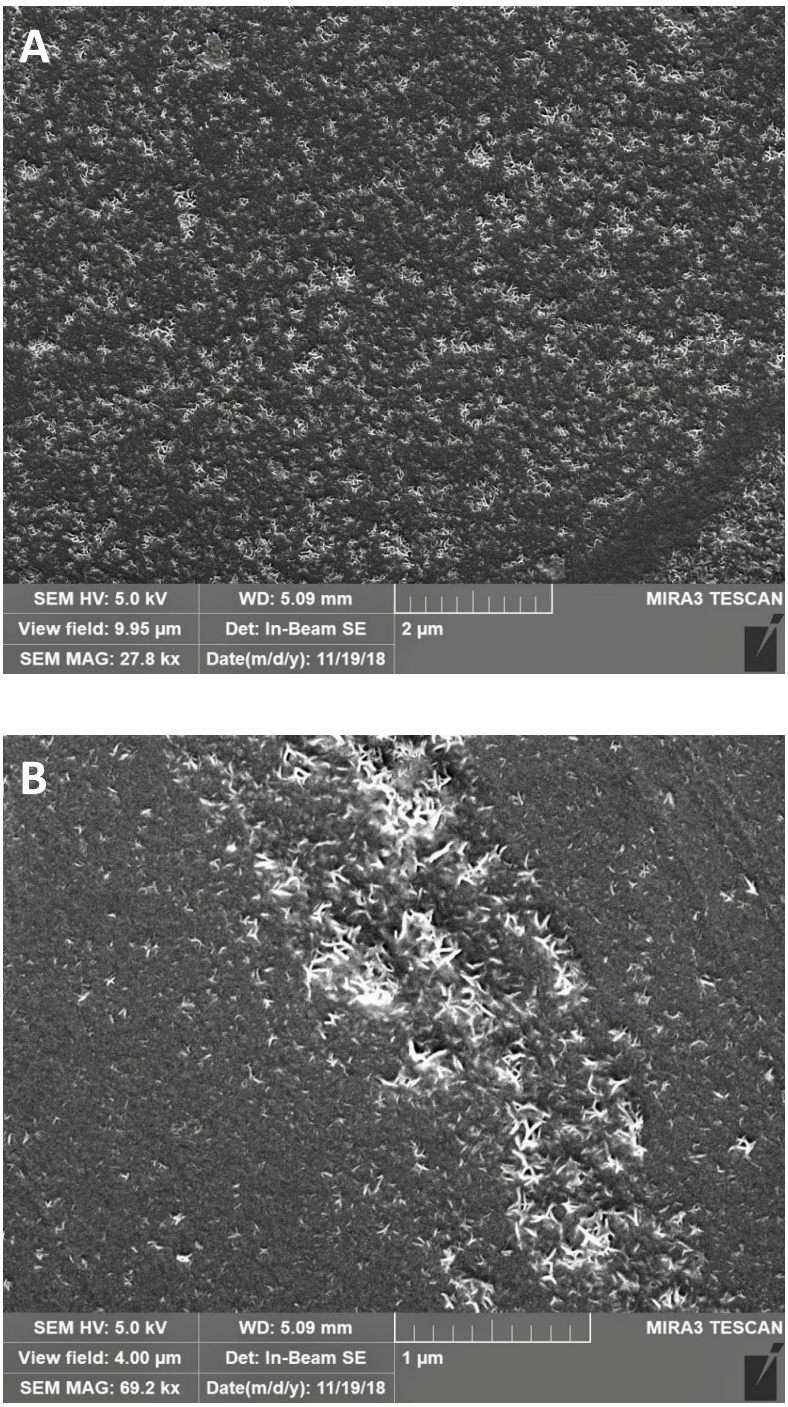

Figure B1: SEM images of sodium phosphate buffer only. Sodium phosphate buffer 25 mM at pH 4, samples for SEM prepared analogously to the samples containing peptide. A, B are images of the same sample with different magnification. Both images were taken by Frederik Becher.

Appendix C
Far- and near-UV CD spectra of GLP-1-Am in different aggregated states

C.1 Far- and near-UV CD spectra of GLP-1-Am in different aggregated states at pH 3 in citric buffer.

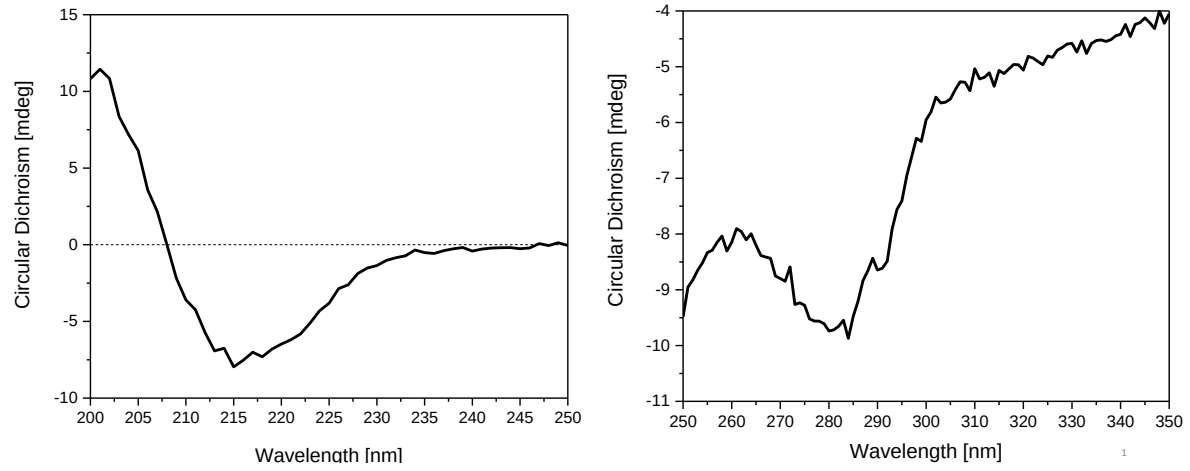

Figure: C1: GLP-1-Am fibrils incubated in 25 mM citric buffer at pH 3. Intensities left in original millidegree units due to the difficulties in concentration determination of fibrils and potential oligomers. Far-UV CD spectrum (left) measured in a 0.1 cm pathlength cuvette, near-UV CD spectrum (right) measured in a 1 cm pathlength cuvette.

C.2 Far- and near-UV CD spectra of GLP-1-Am in different aggregated states at pH 3 in sodium phosphate buffer.

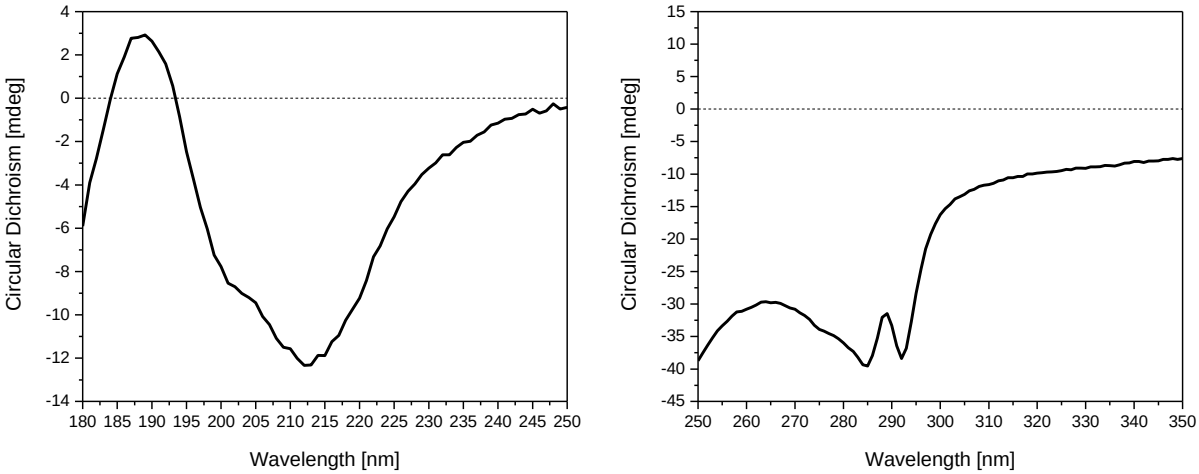

Figure C2: GLP-1-Am fibrils in 25 mM phosphate buffer at pH 3. Intensities left in original millidegree units due to the difficulties in concentration determination of fibrils and potential oligomers. Far-UV CD spectrum (left) measured in a 0.01 cm pathlength cuvette, near-UV CD spectrum (right) measured in a 0.2 cm pathlength cuvette.

Appendix D
Ionizable GLP-1-Am residues and a net charge

D.1 Ionizable GLP-1-Am residues and dependence of the net charge of GLP-1 and GLP-1-Am on pH value

GLP-1-Am sequence and ionizable residues

NH_2-HAEGTFTSDVSSYLEGQAAKEFIAWLVKGRG-*$CONH_2$*

Potentially positively charged residues are shown in red; potentially negatively charged residues shown in blue.

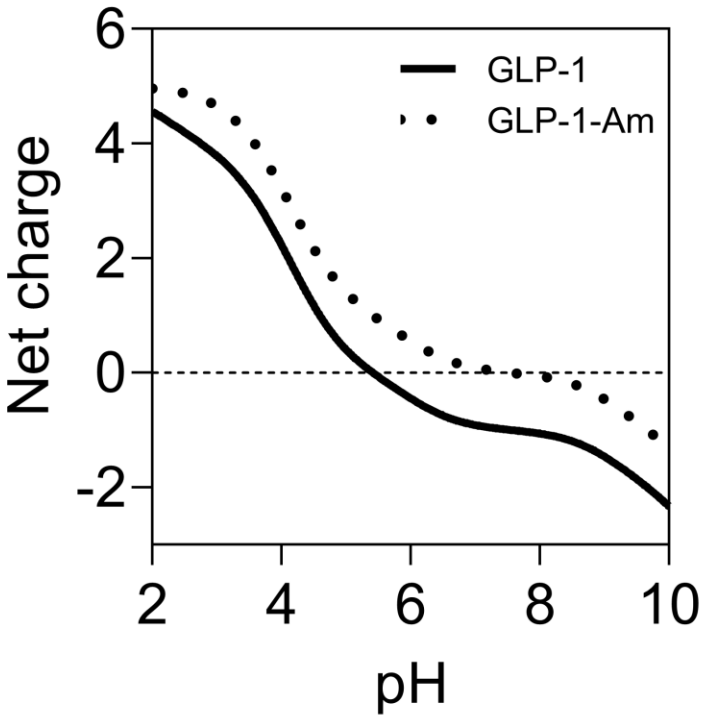

Figure D1: Dependence of GLP-1 and GLP-1-Am net charge on pH value. Figure taken from (Becher 2019).[13]